

Research Article

Evaluation of an Inverse Molecular Design Docking Algorithm for the computer aided molecular drug design of a QMMMIDD motif peptide targeted active pharmaco-agent (MalasmoruponaqTM™) against the gram positive bacteria Staphylococcus aureus for the dual deactivations of antimicrobial activity of the insect defensin from Anopheles gambiae and Ebola viruses: Understanding the Relativistic Generalization of Density Functional Theory (DFT) and Completing It in Practice

Grigoriadis Ioannis^{1*}

¹Department of Biogenetoligandorol TMligandorolTMQMMIDDD/QPRPICA/MACHNOT/

QIICDNNNDCA ADMET/QIICDNNNDCA Stations, Greece

²Department Of Wams For Pharmaceutical Biotechnology, Department Of Computer Drug Discovery Science Biogenetoligandoroltmiligandoroltm (Recoring Pharmacophoric Merging Qmmmiddd Algorithm), Biogenea Sa, Greece

Abstract

Computational molecular design is a useful tool in modern drug discovery. Virtual screening is an approach that docks and then scores individual members of compound libraries. In contrast to this forward approach, inverse approaches construct compounds from fragments, such that the computed affinity, or a combination of relevant properties, is optimized. Drug discovery and development involves a complicated three-dimensional highly correlated, many-body dynamical molecular system, and an intense, lengthy, interdisciplinary scientific endeavor which is often no intuitive even for highly trained researchers [1]. Small Molecule Drugs are indispensable for the treatment and cure of deleterious infectious diseases. There has been a plethora of new Malaria and Ebola infectious diseases short linear motif elements protein and DNA/RNA targets being discovered. Hence, ideal small molecule quantum thinking drugs are always in great demand. We have recently developed a new inverse approach combining human spatial reasoning and AI design insight to our BiogenetoligandorolTMligandorolTM novel drug design technologies based on the most promising lead compounds and dead-end eliminated Docking Algorithms by employing a hybrid classical/quantum mechanical physical potential function. In an attempt to increase the antimicrobial activity of the insect defensin from Anopheles gambiae, which is active against Staphylococcus aureus at low concentration, hybrid defensins were designed by

combining conserved sequence regions and variable regions of insect defensins. The three-dimensional structure of Anopheles gambiae defensin and five hybrids were determined by NMR and molecular modeling. Here, we have discovered for the first time an in-silico predicted and computer-aided molecular designed Inverse Molecular

***Corresponding Author:** Grigoriadis Ioannis, Biogenetoligandorol_tm_Ligandorol_tm_qmmidd/QPRPICA/MACHNOTQIICDNNNDCA ADMET/QIICDNNNDCA Stations, Greece, Tel: +306936592686; E-mail : jgrigoriadis@biogenea.gr

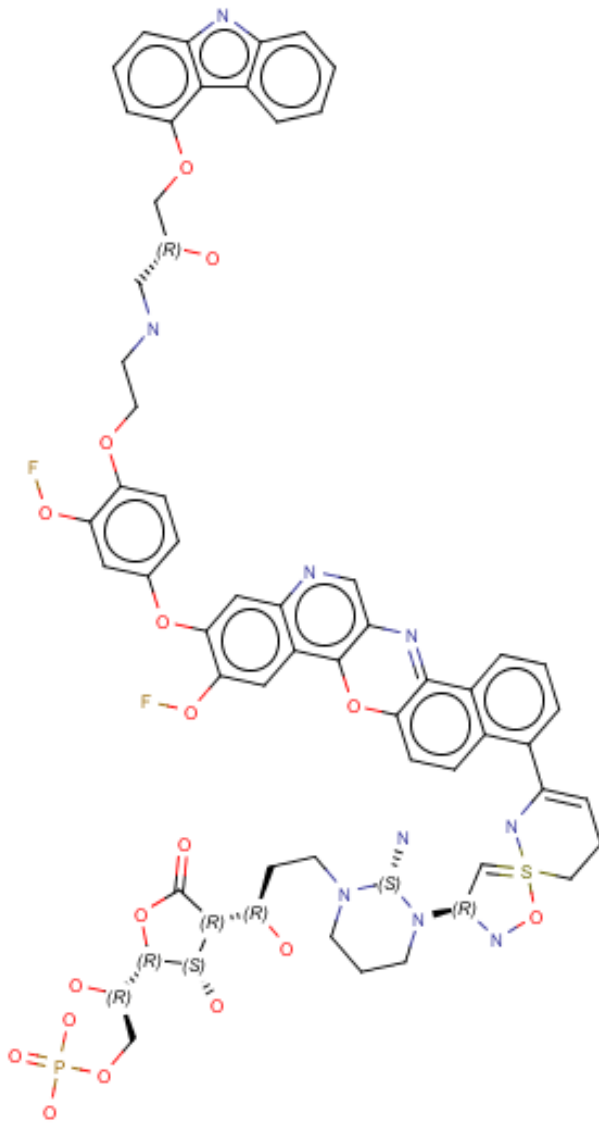
Sub Date: July 3rd 2019, **Acc Date:** July 11th 2019, **Pub Date:** July 16th 2019

Citation: Grigoriadis I (2019) Evaluation of an Inverse Molecular Design Docking Algorithm for the computer aided molecular drug design of a QMMMIDD motif peptide targeted active pharmaco-agent (MalasmoruponaqTM™) against the gram positive bacteria Staphylococcus aureus for the dual deactivations of antimicrobial activity of the insect defensin from Anopheles gambiae and Ebola viruses: Understanding the Relativistic Generalization of Density Functional Theory (DFT) and Completing It in Practice. Int J Drug Disc 3: 016

Copyright: © 2019 Grigoriadis I. This is an open access article distributed under the terms of the Creative Commons Attribution License, which permits unrestricted use, distribution, and reproduction in any medium, provided the original author and source are credited.

Design Docking Algorithm in a Model Binding Site offering the potential to usher in a new paradigm for engineering an In silico predicted and computer-aided molecular designed structure of peptide mimetic active pharmaco-agent (MalasmoruponaqTM™): 7,{{4,(2,[(2R),3,(42,2,3,4,4 a,4b,5,6,7,8,decahydro,9λ⁴,carbazol,4,yloxy),2,hydroxypropyl]amino}ethoxy},3,oxocyclohexyl]oxy},19,[(42Z),1,[(2R),2,[(2S),2,amino,3,[(3R),3,hydroxy,3,[(3R,4S,5R),4,hydroxy,5,[(42R),1,hydroxy,2,[(oxophosph

o),λ³,oxy]ethyl],2,oxooxolan,3,yl]propyl],1,3,diazinan,1,yl],2,(hydroxy amino)ethylidene],5,6,dihydro,4H,1λ⁴,2,thiazin,3,yl],2λ³,oxa,10λ⁴,13λ⁴,diazapentacyclo[12.8.0.0^{3,12}.0^{4,9}.0^{15,20}]docosa,1,9,10,12,13,pentaen,6, one dihydrofluoride against the gram positive bacteria *Staphylococcus aureus* for the depletion of its antibacterial defensin DEF-AAA for the dual deactivations of antimicrobial activity of the insect defensin from *Anopheles gambiae* and Ebola viruses.



2D MalasmoruponaqTM™ QMMMIDDD miracle molecule.

Keywords: Anopheles Gambiae; Inverse Molecular; Design Docking Algorithm; Computer Aided Molecular Drug Design; Motif Peptide; Pharmaco-Agent; Relativistic; Generalization of Density Functional Theory (DFT)

Introduction

To meet the challenges of ideal drugs, an efficient method of drug development is demanding and more applied technologies Machine

Learning and Computer Vision Systems have to be introduced for Phenotype Data Acquisition and Analysis Direct quantum process tomography via measuring sequential weak values of incompatible observables Docking Algorithms. The process of the alchemical perturbation (AP) methods and QM-MMM in silico computer-aided drug discovery is typically challenging, costly, time consuming, and requires consideration of different computational aspects since it has historically been limited by the lack of validated molecular algorithmic sequences, consensus targets and of high-throughput machine learning based screening methods. It is considered as a linear, consecutive process that initiates with interactive molecular dynamics in virtual targets and small molecule lead discovery approaches including training machines to learn potential free energy functions, combining strict alchemical perturbation methods with the Poisson-Boltzmann or generalized Born biomolecular conformational heuristic samplings, surface area continuum solvation (MM/PBSA and MM/GBSA) and protein-MalasmoruponaqTM™ligand binding methods with fused pharmacophoric reaction discoveries using “on-the-magic-fly” quantum chemistry, and transport hadamard dynamics with computational exhausted automation technologies to generate real-time Quantum Mechanics MD simulations of flexible 3D hyper-structures, followed by fragment lead based FBDD/LBDD optimization and pre-clinical in vitro and in vivo studies to determine if such selected compounds satisfy a number of pre-set criteria for initiating clinical trial developments. Malaria, a form of *P.falcifarum*, is a mosquito-borne infectious disease that affects humans and other animals which is often occurred. Mefloquine is an anti-malarial synthetic chemoprotective molecule with anti-malarial activity and selectively inhibits the lactate dehydrogenase molecular mechanism. Glycolysis is the major bio-molecular pathway for ATP production in the malaria parasite *Plasmodium falciparum* and its inhibition is needed for cell survival. Malaria, one of the most distressing diseases, is caused by the parasitic protozoan *Plasmodium falciparum*. It takes away millions of lives with the rate increasing each growing year. According to WHO’s Factsheet on the World Malaria Report 2013, 1.2 billion people out of a total of an estimated 3.4 billion are at a high risk of malaria. Malaria is highly prevalent in sub-Saharan Africa where 90% of all malaria deaths occur (WHO 2013). A lot of research has been going on in the field of malarial therapeutics. This method predicted controlled quantum small molecule SMILES teleportations with an arbitrator for secure quantum channels via quantum dots inside protein cavities Docking Interactions using experimentally known intraspecies and interspecies Docking Interactions and filtered proteins on several parameters, such as cellular location and cellular function for Supercritical entanglement in local systems to the area law for quantum mechanical Docking Algorithm to confirm the practicality of the predictions. In this study, a complete protein interaction network Neutron Diffraction in Transmission Mode Implementation between human host and *Plasmodium falciparum* has been developed by inte-

gration of experimental and computational BiogenetoligandorolTM’s Semi-empirical methods, which are less accurate methods that use experimental results to avoid the solution of some terms that appear in the ab initio methods. BiogenetoligandorolTM’s uses the accuracy of electric charges plays an important role in protein-MalasmoruponaqTM™ligand docking, which is why QM-MM calculations are incorporated into docking procedures. Fixed charges of MalasmoruponaqTM™ligands obtained from force-field parameterization are replaced by QM-MM calculations in the protein-MalasmoruponaqTM™ligand complex, treating only the MalasmoruponaqTM™ligand as the quantum region. BiogenetoligandorolTM’s uses the QM-MIDD quantum thinking approach that provides unprecedented accuracy in fragment MalasmoruponaqTM™ligand based structure-based binding-energy calculations that enable formalistic application of QM methodologies to noncovalent hyper geometric and intra topology meta-Docking Interactions in complex systems as large as protein-MalasmoruponaqTM™ligand druggable complexes and conformational ensembles. AgamOBP20 is one of a limited subset of OBPs that it is preferentially expressed in female mosquitoes and its expression is regulated by blood feeding and by the day/night light cycles that correlate with blood-feeding behavior. Analysis of AgamOBP20 in solution reveals that the apo-protein exhibits significant conformational heterogeneity but the binding of odorant molecules results in a significant conformational change, which is accompanied by a reduction in the conformational flexibility present in the protein. Crystal structures of the free and bound states reveal a novel pathway for entrance and exit of odorant molecules into the central-binding pocket, and that the conformational changes associated with ligand binding are a result of rigid body domain motions in α -helices 1, 4, and 5, which act as lids to the binding pocket. The eventual aim of this computer-aided in silico drug design study is to design an efficient multi-pharmacophoric drug molecule against the Malaria target by adapting machine general-purpose earning techniques using inverse probability of censoring weighting Docking Algorithms for the accurate algebraic topology predictions of small molecules in machine learning based scoring and virtual screening techniques. Various tubulin mitotic small molecule inhibitors such as benzimidazole, dinitroanilines which interact within Malarial P. and EBOV protein proteins and hinder the infection process have been fragmented, re-cored and merged into a MalasmoruponaqTM™’s larger druggable scaffold by using Absolute Binding Free Energy Computational Scoring Calculations of Protein-MalasmoruponaqTM™ligand Docking Interactions for the constructions of exact representations of quantum many-body systems with Force-momentum-based Langevin dynamic self-guided deep neural networks as a rapid sampling inverse docking method that approaches the canonical neuronal version of Grover’s quantum algorithm. Finally, the MalasmoruponaqTM™ molecule is computationally designed by using some of Electronic Nose Quantum Noosphere Improved Quantum Artificial Fish Docking Algorithmic Applications to Distributed Net-

work quantum classifiers which has exhibited better binding affinity than the other FDA anti-malarial molecules which can be considered as a novel drug molecule candidate. In this study, we have discovered for the first time an in-silico predicted and computer-aided molecular designed Inverse Molecular Design Docking Algorithm in a Model Binding Site as an In silico predicted and computer-aided molecular designed structure of peptide mimetic active pharmaco-agent (MalasmoruponaqTM™): 7,[[4,(2,{{(2R),3,(42,2,3,4,4a,4b,5,6,7,8,decahydro, 9λ⁴,carbazol,4,yloxy)},2,hydroxypropyl]amino}ethoxy],3,oxocyclohexyl]oxy],19 ,[(42Z),1,[(2R),2,[(2S),2,amino,3,[(3R),3,3,[(3R,4S,5R),4,hydroxy,5,[(42R),1,hydroxy,2,[(oxophospho),λ³,oxy]ethyl],2,oxooxolan,3,yl]propyl],1,3, diazinan,1,yl],2,(hydroxyamino) ethylidene],5,6, dihydro, 4H,1λ⁴, 2, thiazin,3,yl] 2λ³,oxa,10λ⁴,13λ⁴, diazapentacyclo [12.8.0³,12,0⁴,9,0¹⁵,20] docosa,1,9,10,12,13,pentaen,6,one dihydrofluoride against the gram positive bacteria *Staphylococcus aureus* for the depletion of its antibacterial defensin DEF-AAA for the deactivation of antimicrobial activity of the insect defensin from *Anopheles gambiae*. To determine the number of binding sites, a proof of concept docking study employing a widely- accepted validation tool called GEMDOCK (Generic Evolutionary Method for molecular docking), is used to compare MalasmopuronaqTM with the other FDA drugs approved for use against Malaria. The results are impressive. Comparison against other FDA approved drugs proves l14122871974,78905 - fold times higher. To accomplish these challenges, several multidisciplinary BiogenetoligandorolTM's Ab initio methods, where the solution of the Schrodinger equation is obtained from first principles of quantum chemistry using rigorous mathematical approximations, and without using empirical data approaches have been integrated for the process of drug development; collectively these approaches would form the basis of BiogenetoligandorolTM's Wavefunction based methods, which are based on obtaining the wave function of the anti-malarial rational drug design system [2]. With the advent of genomics, proteomics, bioinformatics and technologies like crystallography, NMR, the structures of more and more protein targets are integrated into the BiogenetoligandorolTM's Density functional based methods, that consist in the study of the properties of the system through its electronic density, but avoiding the explicit determination of the electronic wave function. The MalasmopuronaqTM QMMP small molecule binds to the crystal structures with some of 190800000379.40 Docking Fitness Scoring Values within the PfNDH2 protein and for the first time within Apo-, NADH, bound states/binding domains. The PfNDH2 targeted MalasmopuronaqTM QMMP small molecule inhibitor exhibits excellent docking potency against the PfNDH2 protein and for the first time within Apo-, NADH-bound states/binding domains via a potential allosteric mechanism and agonistically increases the conformational adaptation to different odorants that have important implications in the selection and development of reagents targeted at disrupting normal OBP function.

Material and Methods

Softwares

All softwares were open acces, except the academic version of Biogenetoligandorol TM (2018.19) obtained from (Biogenetoligandorol TM, BiogeneaSA, Greece) [4,6,8-12]. Biogenetoligandorol TM protocol [3,5,7,8-12,13]. The complex structure was applied with the CHARMM-Polar-H force field in the BiogenetoligandorolTM 2016 [3,4,7,6,8-13,15,18,21]. The typed structure was then exported and used as the basis for mutagenesis. Using a Perl script specific to BiogenetoligandorolTM, we mutated the hybrid CDR residues to all 20 genetically encoded amino acids and calculated both the ΔΔEbinding and ΔΔEstability values, which resulted in 1400 mutations [24,25,28,29,51,52,76,71,72,73,78]. BiogenetoligandorolTM biologics suite protocol: The complex structure was prepared by using the Protein Preparation Wizard tool [48, 49,69-73] within the BiogenetoligandorolTM, BiogeneaSA, Greece 2018-3 [33]. The titratable residues were protonated in accordance with their environment by using BiogenetoligandorolTM_Ka [50, 51,52,76,71,72,73,78] and were typed with the OPLS3 [52] force field, and the structure was subsequently minimised. Because optimization of the wider environment of a mutation may result in the unwarranted acceptance of large side chains, two separate mutagenesis experiments were performed. One experiment used a 0.0 Å optimization distance, that is, only the mutated residue, and one also minimised any residues within 5.0 Å. By using both optimization criteria and taking a consensus of accepted mutations, it was possible to avoid selection of residues that sterically disrupted the local protein environment whilst identifying those that required only a small structural rearrangement to enter a conformation, thereby leading to improved binding affinity [52,76,71,72,73,78].

Genome-Wide Drug-Target Prediction, Dataset and QSAR Study

Using FP-2 (PF3D7_1115700) and FP-3 (PF3D7_1115400) [78-112,113,115,118,119,122] as query sequences, seven plasmodial protein homologs together with three human homologs were retrieved from the PlasmoDB version 9.31 [78-112,113,115,118,119,122] and NCBI [74,78-112,113,115,118,119,122] databases, respectively as described earlier [50,78-112,113,115,118,119,122] A set of 341 molecules with inhibitory activity for plasmodial proteases was selected from the CanSAR database 7(<https://cansar.icr.ac.uk/>) based on their molecular weight and IC50. This was converted to pIC50 for the QSAR analysis. The set of these molecules NAG:L:701, NAG:L:702, BMA:L:703, MAN:L:704, MAN:L:705, MAN:L:706, MAN:L:707, interacting chains: K, L, N was randomly distributed to a training set of 240 compounds NAG:D:701 (NAG-NAG-BMA-MAN-MAN-MAN-MAN)-POLYMER+ NAG:D:702+ BMA:D:703 + MAN:D:704+

MAN:D:705+ MAN:D:706+ MAN:D:707(70% of the data) and a test set of 131 NAG:H:701 (NAG-NAG-BMA-MAN-MAN-MAN-MAN)-POLYMER+ NAG:H:702+ BMA:H:703+ MAN:H:704+ MAN:H:705+ MAN:H:706+ MAN:H:707 compounds (32% of the data). cathepsin L (Cat-L) like plasmodial proteases is the presence of an N-terminal signalling (non-structural) RNA+ION starting with C (composite ligand, containing Cytidine Monophosphate)C-G-C-A-U-G-C-G-MG Composite ligand consists of C:C:1, G:C:2, C:C:3, A:C:4, U:C:5, G:C:6, C:C:7, G:C:8, MG:C:9. Interacting chains: A, B peptide sequence (~150 amino acids), which is responsible for targeting them into the food vacuole in 4IOD (malarial clp b2 atpase/hsp101 protein). SO4 (sulfate) SO4-A-201 Interacting chains: A. For each of the plasmodial proteins, this segment was chopped off, and the remaining prodomain portion-catalytic domain saved into a Fasta file (Additional file 1) in 3L27 (polymerase cofactor vp35). As guided by the partial zymogen complex crystal structure of Cat-K [PDB: 1BY8], ~21 amino acids (N-terminal) were also chopped off from the human cathepsin prodomain sequences V-M-GLU-50, V-S-GLU-50, V-M-GLU-51, V-S-GLN-54, V-S-HIS-80, V-M-GLU-144, V-M-ALA-145, V-S-ASN-146, V-M-ASP-226, V-S-ASP-226, V-M-ALA-227. Together, these sequences were used in the rest of the study, and are referred as “partial zymogen” or “prodomain-catalytic domain” sequences interchangeably in the manuscript [78-112,113,115,118,119,122]. Position details of the PRF (queuine) PRF-A-290 Interacting chains: A prodomain and PRF-B-290 Interacting chains: B catalytic portions per protein are listed in Additional file 4. To determine the conservation of the PRF-C-290 Interacting chains: C prodomain-catalytic portion, multiple sequence alignment (MSA) 4DGH (sulfate permease family protein) was performed using Profile Multiple Alignment with predicted Local Structures and 3D constraints (PROMALS3D) web server [75] with default parameters except PSI-BLAST Expect value which was adjusted to 0.0001, and the alignment output visualized using JalView [76]. The GOL (Glycerol) GOL-A-608 Interacting chains: A training set has been subjected to the Partial Least Square (PLS) 8. In absence of an experimentally validated inhibitor with a biological activity of LMTK3 protein in the different databases, the construction of QSAR model based on the biological activity of these inhibitors cannot take place [78-112,113,115,118,119,122,127] and NCBI [74,78-112,113,115,118,119,122] databases, respectively as described earlier [50,78-112,113,115,118,119,122]. Genome-wide anti-malarial drug-in 6IOT target ION CA (calcium ion) CA-A-502 Interacting chains: ADocking Interactions were predicted using DockThor. DockThor takes four networks as input: chemical-protein association (matrix R), off-target (matrix Q), chemical-chemical similarity, protein-protein similarity networks, The chemical-protein associations were obtained by integrating three resources: 1) publicly available databases, ChEMBL [53] (v23.1) and Drug Bank [54] (v5.5.10), 2) four data sets from recent publications about kinase

assays [55-58], and 3) protein structure-based off-target prediction from previous step. From ChEMBL, inhibition assays having IC50 ≤ 10 μM was regarded as active associations s78-112,113,115,118,119,122] and NCBI [74,78-112,113,115,118,119,122] databases, respectively as described earlier, [50,78-112,113,115,118,119,122]. Those with suboptimal confidence scores (i.e. confidence < 9) were excluded. From Drug Bank, drug-CA-B-502 Interacting chains: B target, drug-2BH1 (general secretion pathway protein 1 general secretion pat...), drug-G9D (SureCN12750328), G9D-A-1, Interacting chains: A, and drug-transporter associations were collected for the generation of the Hydrophobic Docking Interactions of the 2 MalasmoruponaqTM™ binding site(s) in 3ZML (glutathione s-transferase e2) GSH (Glutathione)GSH-A-1222 Interacting chains: A. The data sets from kinase assays are available in different types of activity measurement. Christmann-Franck et al. collected chemical-kinase assays from multiple past publications and presented the activity standardization protocol, which assumed an activity with Ki ≤ 5 μM is active [55,74,78-112,113,115,118,119,122]. If the original publication presented percent inhibition (or percent remaining activity) at a given compound concentration, Ki was calculated as follows:

$$\text{control} = (\text{TestCompoundSignal} - \text{PositiveControlSignal}) / (\text{NegativeControlSignal} - \text{PositiveControlSignal}) \times 100$$

$$\text{response} = \text{background} + \text{signal} - \text{background} + (Kd - 1) / \text{dose} - 1$$

$$y = A + B - A1 + (Cx)DKi = \text{concentration} \times (100 - \% \text{inhibition}) \% \text{inhibition}$$

$$\min_{U,V} U, V \geq 0 \sum_{i,j} (i,j) w(R(i,j) + Q(i,j) - U(i,:) \otimes V(j,:))$$

$$T)^2 + \alpha(\|U\|^2 + \|V\|^2) + \beta \text{tr}(UT(DC-C)U) + \gamma \text{tr}(VT(DT-T)V)$$

$$P(i,j) = UUP(i,:) \cdot VUP(j,:) T \text{FoldChange} = \{ES/ER, if ES > ER - ER/ES, if ES < ER\}$$

$$q = (prank) \times N(1)$$

Here, w is the confidence weight on the observed and predicted off-target associations which indicate the reliability of the assigned probability of true association; α is the regularization parameter to prevent overfitting; β is the importance parameter for chemical-chemical similarity, γ is the importance parameter for protein-protein similarity, and tr(A) is the trace of matrix A [90-110,121,123,127]. The predicted score for the ith chemical to bind the jth protein can be calculated by $P(i,j) = UUP(i,:) \cdot VTUP(j,:)$, where UUP and VUP are the low-rank matrices U and V after completion of the updates. Different from original winOCCF [33], Q in DockThor is the predicted off-target network instead of a fixed imputation value within MalasmoruponaqTM™ binding site(s) in 3ZML (glutathione s-transferase e2). GSH (Glutathione)GSH-A-1222 Interacting chains: A. More details on the optimization algorithm of Eq (1) are published elsewhere [90-110,121,123,127], where ES and ER are the mean log2 mRNA probe levels for a given gene in cell lines found in the sensitive and resistant groups, respectively [89,90-110,121,123,127] to demonstrate the hydrogen Bonds

from the MalasmoruponaqTM™ binding site(s) in 3EBH (m1 family aminopeptidase): ION MG (magnesium ion) MG-A-7 Interacting chains: A. A false discovery rate (FDR)-adjusted p-value (q-value) is computed with a null hypothesis of no difference between “sensitive” and “resistant” groups for the generation of the Metal Complexes MalasmoruponaqTM™ binding site(s) in 3EBH (m1 family aminopeptidase): ION MG (magnesium ion) MG-A-7 Interacting chains: A. The q-value is calculated according to the following formula: $q = (\text{rank}/N) \times N$ where rank is the rank of the p-value and N is the number of conducted tests. Gene set over-representative analysis was carried out using Protein-Ligand Interaction Profiler [60-89,90-110,121,123,127] in the Water Bridges of the MalasmoruponaqTM™ binding site(s) in 3EBH (m1 family aminopeptidase): ION MG (magnesium ion) MG-A-7 Interacting chains: A. Using Molecular Evolutionary Genetic Analysis (MEGA) version 5.2 software [87,89,90-110,121,123,127], the evolutionary relationship of plasmodial proteases and human cathepsins was evaluated with the following preferences; Maximum Likelihood (statistical method) and Nearest-Neighbor-Interchange (NNI) as the tree inference option the hydrogen Bonds from the MalasmoruponaqTM™ binding site(s) in 3EBH (m1 family aminopeptidase): ION MG (magnesium ion) MG-A-7 Interacting chains: A. A total of 9 H-S-ASP-65, H-M-GLN-67, H-S-THR-206, V-M-VAL-199, V-M-ARG-202, V-S-ARG-202, V-M-LEU-203, V-M-THR-206, V-S-THR-206 amino acid substitution models were calculated for both complete (100%) and partial (95%) deletion and the best three models based on Bayesian Information Criterion (BIC) were selected. For each selected IHP-B-210 Composite ligand consists of IHP:B:210, NA:B:211. Interacting chains: B model, the corresponding gamma (G) evolutionary distance correction value was selected to build different phylogenetic trees and comparison was made to determine robustness of dendrogram construction process [90-110,121,123,127]. 4IOD (malarial clp b2 atpase/hsp101 protein). SO4 (sulfate) SO4-A-201 Interacting chains: A was included in the tree calculations as outgroup.

Physicochemical Properties, Motif Analysis, Homology Modelling and Structure Validation

Using an ad hoc Python and Biopython script, the amino acid composition and physicochemical properties, namely molecular weight (Mr), isoelectric point (pI), aromaticity, instability index, aliphatic index and grand average of hydropathy index (GRAVY) of the proteins were determined [60-89,90-110,121,123,127]. Multiple Em for Motif Elicitation (MEME) standalone suite version 4.10.2 [57,58,59,60-89,90-102,03,104,107,108,110,121,123,127] was used to identify the composition and distribution of protein motifs within partial zymogen sequences of the hydrogen Bonds from the MalasmoruponaqTM™ binding site(s) in 3EBH (m1 family aminopeptidase): ON MG (magnesium ion) MG-A-7 Interacting chains: A. A Fasta file (Additional file 1-4) containing sequence information of the different proteins was parsed to MEME software with analysis preferences set as; -nostatus -time 18,000 -maxsize 16,000 -

mod zoops -nmotifs X -minw 6 -maxw 50 in the hydrophobic Docking Interactions of the MalasmoruponaqTM™ binding site(s) in 3EBH (m1 family aminopeptidase): ION MG (magnesium ion) MG-A-7 Interacting chains: A. The variable X (a whole number from 1) was varied until no more unique motifs were assessable as determined by Motif Alignment Search Tool (MAST) [87,89,90,95,96,97] for the profiling of the hydrogen Bonds of the MalasmoruponaqTM™ binding site(s) in 3EBH (m1 family aminopeptidase): ON MG (magnesium ion) MG-A-7 Interacting chains: A. A heat map showing motif distribution was generated using an in house Python script. PyMOL was used to map the different motifs onto the protein structures.

Homology Modelling And Structure Validation and Prodomain-Catalytic Domain Interaction Studies and Short Inhibitor Peptide Design

MODELLER version 9.18 + was used to build homology models of the inhibitor complex of all proteins except for Cat-K which has already a crystal structure. Using a combination of templates, high quality prodomain-catalytic domain complexes of the plasmodial proteases as well as cathepsins (Cat-L and Cat-S) were calculated by MODELLER with refinement set to very slow. Additional file 4 shows the details of templates selected for each protein model. For the plasmodial proteases, the crystallographic structure of procathepsin L1 from *Fasciola hepatica* [PDB: 2O6X] was used as it had the highest similarity with most target sequences (30–38%) and high resolution of 1.40 Å. However, it lacked the arm (β-hairpin) region while the nose residues were missing. To overcome these challenges, Cat-K [PDB: 1BY8] together with FP-2 [PDB: 2OUL] (for FP-2, VP-2, KP-2, BP-2 and YP-2) and FP-3 [3BWK] (for FP-3, VP-3, KP-3 and CP-2) were additionally used. For Cat-L and Cat-S, only two templates were used [PDB: 1BY8 and 2O6X]. For each protein, 100 models were calculated and ranked according to normalized discrete optimized protein energy (Z-DOPE) score [81] of the generated hydrogen Bonds MalasmoruponaqTM™ binding site(s) in 4F1K (thrombospondin related anonymous protein). selected ligands: CL MalasmoruponaqTM™ Small Molecule EDO (Ethylene Glycol) EDO-A-305 Interacting chains: A.. The top three models per protein were further validated using ProSA [82], Verify3D [83], QMEAN [84] and PROCHECK [85] and the best quality model selected Water Bridges: MalasmoruponaqTM™ binding site(s) in 4F1K (thrombospondin related anonymous protein). selected ligands: CL MalasmoruponaqTM™ Small Molecule EDO (Ethylene Glycol) EDO-A-305 Interacting chains: A.. To determine the prodomain inhibitory mechanism, residue Docking Interactions between prodomain and catalytic domain of plasmodial and human partial zymogen complexes were evaluated using the Protein Interaction Calculator (PIC) web server [86]. The interaction energy of identified residues was evaluated using the amino acid interaction (INTAA) web server [87] Hydrogen Bonds from the MalasmoruponaqTM™ binding site(s) in 4F1K (thrombospondin related anonymous protein). selected ligands: CL MalasmoruponaqTM™

Small Molecule EDO (Ethylene Glycol) EDO-A-305 Interacting chains: A.. PyMOL was used to visualize the resulting Docking Interactions. For each protein, prodomain segment interacting with the catalytic domain's active pocket residues was identified and extracted into a Fasta file. From the interaction energies, residues within these inhibitory segments forming strong contacts with subsite residues were identified. Based on the identified hot spot residues, the next objective was to design short peptide(s) exhibiting the native prodomain effect whilst showing selectivity on human cathepsins hydrogen Bonds from the MalasmoruponaqTM™ binding site(s) in 4F1K (thrombospondin related anonymous protein). selected ligands: CL MalasmoruponaqTM™ Small Molecule EDO (Ethylene Glycol) EDO-A-305 Interacting chains: A. The conservation of prodomain inhibitory segments for all the proteins, and separately of only the plasmodial proteases, was determined using WebLogo server [88]. Peptides of varying lengths and composition based on amino acid conservation forming contacts with subsite residues of the water Bridges from the MalasmoruponaqTM™ binding site(s) in 4F1K (thrombospondin related anonymous protein). selected ligands: CL MalasmoruponaqTM™ Small Molecule EDO (Ethylene Glycol) EDO-A-305 Interacting chains: A.. In order to evaluate the interaction of selected peptides on the catalytic domains, the prodomain segments of all proteins were chopped using PyMOL. Blind docking simulation runs of selected peptides were then performed on these sets of catalytic domains by CABS-dock protein-peptide docking tool [89] using the default parameters Hydrogen Bonds from the MalasmoruponaqTM™ binding site(s) in 4F1K (thrombospondin related anonymous protein). selected ligands: CL MalasmoruponaqTM™ Small Molecule EDO (Ethylene Glycol) EDO-A-305 Interacting chains: A.. To confirm the reliability of the results, docking experiments were repeated using catalytic domains of the same proteins that had been modelled and used in previous studies [50]. Binding affinity (ΔG) and dissociation constant (Kd) for each protein-peptide complex was then evaluated using PROtein binDIng enerGY prediction (PRODIGY) web server [90].

Sequence Analysis and Docking Studies of PfDHHCs

Using various databases like the PlasmoDB, PiroplasmaDB, and UniProt, we extracted DHHC sequences of different organisms including *Plasmodium falciparum*, *Plasmodium berghei*, *Toxoplasma gondii*, *Babesia bovis*, *Theileria parva*, *Cryptosporidium muris*, and *Eimeria tenella*. This data exploration was done using different apicomplexan specific databases including plasmodium genomics resource database (PlasmoDB) 13, toxoplasma genomics resource database (ToxoDB) 14, piroplasma genomics resource database (PiroplasmaDB) 15, and UniProt 16 for fetching other organism specific protein sequences. Using PlasmoDB, putative DHHC gene sequences in *P. falciparum* (PfDHHC) were annotated and extracted based on conserved domain architecture as receptors for the performance of the Docking Studies with MalasmoruponaqTM™ binding site(s) in 4F1K (thrombospondin related

anonymous protein), selected ligands: CL MalasmoruponaqTM™ Small Molecule EDO (Ethylene Glycol) EDO-A-305 Interacting chains: A, and in the MalasmoruponaqTM™ binding site(s) in 4F1K (thrombospondin related anonymous protein). selected ligands: CL MalasmoruponaqTM™ Small Molecule EDO (Ethylene Glycol) EDO-A-305 Interacting chains: A.. The domain architecture of protein sequences was assessed via SMART, Batch and INTERPRO online servers [81,82,83,86,88,89,90-110,119,121,122]. We performed multiple sequence alignment (MSA) of the 12 annotated PfDHHCs using MUSCLE algorithm (implemented in jalview software, Elixir,UK, <https://elixir-europe.org>) [101,102,103,107,109,110]. These 12 PfDHHCs along with PAT sequences from six other organisms namely closer members *P. berghei* and *T. gondii*, and distant members of Apicomplexa namely *B. bovis*, *T. parva*, *C. muris*, and *E. tenella* were further used to construct a neighbor joining (NJ) tree of the Hydrogen Bonds from the MalasmoruponaqTM™ binding site(s) in 4F1K (thrombospondin related anonymous protein), selected ligands: CL MalasmoruponaqTM™ Small Molecule EDO (Ethylene Glycol) EDO-A-305 Interacting chains: A. The indexing and integration of obtained data sets were carried out using XDS (Pilatus) [95,96,97,98,100-113] for the generation of the Hydrogen Bonds from the MalasmoruponaqTM™ binding site(s) in 4F1K (thrombospondin related anonymous protein). selected ligands: CL MalasmoruponaqTM™ Small Molecule EDO (Ethylene Glycol) EDO-A-305 Interacting chains: A.. The scaling, merging and calculating of structural factor amplitudes were executed using programs TRUNCATE47 and SCALA48 from CCP4 software [11,112,114,121]. Crystal structures were constructed by molecular replacement using Phaser50 with RnCCT (PDB: 3HL4) and free MalasmoruponaqTM_937d73c677_1 (PDB: 4ZCT) as search models, followed by model building in Coot51 in the Salt Bridges from the MalasmoruponaqTM™ binding site(s) in 4F1K (thrombospondin related anonymous protein). selected ligands: CL MalasmoruponaqTM™ Small Molecule EDO (Ethylene Glycol) EDO-A-305 Interacting chains: A.. The structure refinements were done using REFMAC 5.8.007352,53 and PHENIX 1.9.169254. Molecular graphics representations were created using PyMol55. All the MalasmoruponaqTM™ ligand structures were created using PRODRG server [56,92,94,95,98] Crystal diffraction data and final refinement statistics were summarized in Table 3. The bootstrap consensus tree inferred from 500 replicates finally represented the evolutionary history of the taxa analyzed using mega7 software (Pennsylvania State University, University Park, PA, USA) 20. The evolutionary distances were computed using the Day off matrix based method and are in the units of the number of amino acid substitutions per site in the Hydrophobic Docking Interactions of the 2 MalasmoruponaqTM™ binding site(s) in 1V0P (cell division control protein 2 homolog). MalasmoruponaqTM™ Small Molecule PVB (purvalanol B)PVB-A-1287 Interacting chains: A. The sequences of 12 PfDHHCs were obtained from PlasmoDB and their structural models were constructed using the I,TASSER web server using template as

HsDHHC20 (PDB code: 2BML)[81,83,88,89,94,95]. Using modrefiner software (University of Michigan, Ann Arbor, MI, USA), the structures were further refined for docking with substrate palmitic acid (PA) and a known inhibitor of palmitoylation, 2,BMP 22. Quality validation of the resultant models was done with RAMPAGE as prepared for the performance of the Hydrophobic Docking Interactions of the 2 MalasmoruponaqTM™ binding site(s) in 1V0P (cell division control protein 2 homolog). MalasmoruponaqTM™ Small MoleculePVB (purvalanol B)PVB-A-1287 Interacting chains: A. The theoretical models were visualized with pymol Molecular Graphics System (Schrodinger, LLC, New York, NY, USA), version 1.7.4 23. The MalasmoruponaqTM_937d73c677_1 and RnCCT catalytic domains share 44% sequence identity23 and high structural similarity for the illustration of the Hydrophobic Docking Interactions of the in 3UM6 (bifunctional dihydrofolate reductase-thymidylate synthase (Figure. 4). This especially holds for the core region of the conserved α/β Rossmann fold indicated by a dashed circle in Figure. 4b, that hosts the inner part of the active site accommodating DockThor for the demonstrations of the Hydrophobic Docking Interactions within the 3UM6 (bifunctional dihydrofolate reductase-thymidylate synthase. This region, defined by residues 618–760 in Malasmoruponaq TM_937d73c677_1 displays an all-atom RMSD value of 0.73fÅ with the respective region of the RnCCT structure complexed with Malasmoruponaq TM_341139 20. DockThor is found in the same zig-zag position in both MalasmoruponaqTM_937d73c677_1 and RnCCT co-structures with only the two methylene groups of this MalasmoruponaqTM™ligand adopting different conformations. The interaction network of DockThor is also largely similar to the Hydrophobic Docking Interactions of the in 3UM6 (bifunctional dihydrofolate reductase-thymidylate synthase (Figure. 4c). The differences in the catalytic site concern the residues V625, Y626, Q636 and V759 of MalasmoruponaqTM_937d73c677_1 corresponding to hydrophobic residues I84, F85, A95 and I200 of RnCCT, respectively (Figure. 4d). A notable structural difference involves Q636 side chain that enables a direct interaction with the ribose 3fOH moiety in MalasmoruponaqTM_937d73c677_1, whereas a similar contact in RnCCT is established by an ordered water molecule next to A95. Y626 and Q636 constitute the wall of the active site cavity around the hole for the ribose moiety of the MalasmoruponaqTM™ligands and its Hydrophobic Docking Interactions of the MalasmoruponaqTM™ fragmented compounds binding site(s) in 3UM6 (bifunctional dihydrofolate reductase-thymidylate synthase),(cycloguanil)1CY-A-609 Interacting chains: A. Both residues display conformational changes during the course of catalysis (Figure. 3e). The position corresponding to Y626 is strictly reserved for aromatic (Y/F) residues in the HxGH nucleotidyltransferase enzyme super family because the edge-on orientation of the aromatic side chain secures the parallel conformation and hydrogen bond contacts of the two histidines from the HxGH motif, critical for their proper catalytic function in 3UM6 (bifunctional dihydrofolate reductase-thymidylate synthase (Supplementary Figure. 5).

In a nucleotide-bound form, Q636 forms a hydrogen bridge to Y626, enabled by the phenolic OH group of the latter that is additionally present as compared to its RnCCT surrogate F85. In order to evaluate the impact of these residue changes, we engineered a Y626F/Q636A double mutant in MalasmoruponaqTM_937d73c677_1 (528–795) to mimic the RnCCT enzyme hydrogen Bonds from the MalasmoruponaqTM™ binding site(s) in 4F1K (thrombospondin related anonymous protein). selected ligands: CL MalasmoruponaqTM™ Small Molecule EDO (Ethylene Glycol) EDO-A-305 Interacting chains: A. This construct displayed a six-fold attenuated catalytic rate together with an unaltered KM,CTP value compared to MalasmoruponaqTM_937d73c677_1 (528–795) (Table 1). Thermodynamic analysis revealed unaltered CTP affinity of the mutant with a slightly increased favorable binding enthalpy counter balanced by a larger entropic penalty in the MalasmoruponaqTM™ binding site(s) in 4YWI. MalasmoruponaqTM™ Small Molecule EDO (Ethylene Glycol) EDO-A-302Interacting chains: A (Table 2). A modest effect of the residue substitutions was uncovered by the analysis of DockThor binding experiments. A somewhat tighter binding of DockThor was observed in the case of the Malasmoruponaq TM_341139 mimicking construct Malasmoruponaq TM_937d73c677_1 (528-795) Y626F/Q636A, accompanied by a decrease of both the favorable enthalpy and the unfavorable entropy components in the the MalasmoruponaqTM™ binding site(s) in 4YWI. MalasmoruponaqTM™ Small Molecule EDO (Ethylene Glycol)EDO-A-302 Interacting chains: A (Table 2). The differences observed for DockThor binding to Malasmoruponaq TM_937d73c677_1 or to the MalasmoruponaqTM_341139 mimicking construct may be interpreted by a slightly more constrained DockThor interaction in the wild-type MalasmoruponaqTM_937d73c677_1 enzyme water Bridges from MalasmoruponaqTM™ binding site(s) in 4YWI, MalasmoruponaqTM™ Small Molecule. This is also supported by the reduced flexibility of the nucleotide binding pocket in the MalasmoruponaqTM_341139-MalasmoruponaqTM_937d73c677_1 structure in comparison to the MalasmoruponaqTM_341139 -RnCCT structure (PDB: 3HL4), as suggested by B-factor values. Chemical structure of MalasmoruponaqTM_341139_2,BMP was downloaded from BiogenetoligandolTM database in SDF format, converted to standard PDB format and energy minimized using Chem3D Pro 12.0. Molecular docking was performed by using DockThor/GemDock24 to rationalize the activity of PA and 2,BMP against all 12 PfDHHCs. As per the already established 2,BMP binding pocket in PfDHHC homologue, HsDHHC20 (PDB ID: 6BML), we ensured that the active site residues were covered while constructing the virtual grid for docking. Incorporating the predicted MalasmoruponaqTM™ligand binding groove, a virtual 3D grid of mean (20 Å) × mean (20 Å) × mean (20 Å) with varying x, y, z coordinates of the center of energy was constructed for individual PfDHHCs through the Autogrid module of Protein-Ligand Interaction Profiler (PLIP) Tools24 Hydrogen Bonds from the MalasmoruponaqTM™ binding site(s) in 4YWI. MalasmoruponaqTM™ Small Molecule. We performed molecular docking studies using DockThor/GemDock with

compounds to rationalize its activity [Figure.25-67]. The top, ranked conformations of compound within the protein catalytic pocket were selected based on the lowest free binding energies of the hydrogen Bonds from the MalasmoruponaqTM™ binding site(s) in 4YWI. MalasmoruponaqTM™ Small Molecule Hydrogen Bonds from the MalasmoruponaqTM™ binding site(s) in 4YWI. MalasmoruponaqTM™ Small Molecule Ethylene Glycol) EDO-A-302 Interacting chains: A. The stable conformations were visualized for polar contacts like

hydrogen bonds. Top scoring docked conformations of the scaffold were selected based on the most negative free binding energies and visualized for polar contacts with the amino acid residues of Malasmoruponaq TM_937d73c677_1 ,12 51 hydrogen Bonds from the MalasmoruponaqTM™ binding site(s) in 4F1K (thrombospondin related anonymous protein). selected ligands: CL MalasmoruponaqTM™ Small Molecule EDO (Ethylene Glycol) EDO-A-305 by using pymol Molecular Graphics System.

Table1. Predicted High Energy MsMs Spectrum (40V), [M+H]+Peak Table and Fragment Structures Fragment IDs are shown in red. Corresponding scores for each fragment are in blue. Spectra Peaks and Possible Matching Fragments for N1([C@H]2C=[S@@J3(ON2)NC(=CCC3)[C@H]2CCC[C@@H]3[C@H]2CC[C@H]2C3=Nc3c(O2)c2c(nc3)cc(c(c2)OF)Oc2cc(c(OCCNC[C@H](COc3c4c5c([nH]c4ccc3)cccc5)O)cc2)OF)[C@H](N(CC[C@H]([C@@H]2[C@H]([C@@H](OC2=O)[C@@H](COP(=O)(O)O)O)O)CCC1)N

96.96852159	2.011347253	167
98.98417166	2.608625364	147
110.9841717	3.484688479	4
140.9947363	1.824866633	146
184.0756904	5.071068956	49
201.0158657	1.431013595	349
283.1441043	3.335371951	32
409.1558118	1.397975749	31 23
586.1784184	2.414940867	204
689.2854018	1.625305733	304
814.3046815	3.125531909	203
1060.357164	1.402674563	73 184
1062.372814	1.313193147	78 77
1063.443203	1.768410064	138
1078.367729	1.846996658	69
1122.393943	1.646301832	94
1187.459247	1.371806632	170
1189.474898	4.10473638	174 173
1191.490548	2.383004119	179 178
1207.485462	4.112312868	171
1241.446313	2.483930129	207 187
1251.45065	1.480559602	102
1251.45065	1.480559602	19
1259.456878	1.80571918	370
1261.472528	1.704715126	369
1269.441228	5.477741368	186 189 99 182 208
1269.461215	1.951095938	100
1269.461215	1.951095938	17
1287.451793	21.33770976	190 183 220 98 188 181 141 373
1288.435808	1.657557791	209 308

1305.462357	10.38914282	0
<i>energy1</i>		
96.96852159	3.13685149	167
98.98417166	4.536207808	147
100.0869237	2.165330475	3
140.9947363	1.807170326	146
184.0756904	4.121648365	49
240.1019051	1.799133463	43
283.1441043	13.36892362	32
302.1710473	1.983961668	6
382.1373778	6.418964597	10 7 8 9
400.1479425	2.303862095	2
759.2624824	2.404351063	198
799.2937825	1.799130751	237
801.3094326	2.352792101	201
802.3046815	1.996342903	254
803.3250826	2.317886434	200
804.3203316	1.933258541	202
1007.416989	3.142769765	108
1019.416989	3.357121574	114
1045.432639	1.904313076	140
1104.383379	2.997884778	95
1122.393943	2.497610752	94
1189.474898	3.65096062	174 173
1191.490548	2.255081838	178 179
1207.485462	2.220533706	171
1251.45065	2.879752492	102
1251.45065	2.879752492	19
1269.441228	4.808897166	99 186 182 189 208
1269.461215	2.269575042	100
1269.461215	2.269575042	17
1272.440894	2.172720077	218
1287.451793	6.247635875	98 190 141 181 183 188 220 373
<i>energy2</i>		
15.02292652	2.024186651	159
41.00219107	1.877381678	148
45.0334912	2.153370689	144
57.0334912	4.556355438	383
87.04405588	3.148287495	357
103.0389705	2.38133697	350
110.9841717	7.2143607	4

156.0807757	3.74900067	88
184.0756904	8.189437653	49
184.0768332	1.589698678	34
203.0914	2.46575231	104
283.1441043	2.063950961	32
359.0837898	6.030301946	295
570.1835038	2.061989067	293
778.30671	2.173506422	110
780.3223601	5.937500521	70
838.3642249	1.92755647	139
861.2926927	2.295510225	28
980.3908335	4.007442961	71
982.4064836	6.681838214	72
987.3044002	1.821423611	39
1044.382236	1.817691384	18 101
1058.341514	2.516430692	68
1062.372814	4.216562265	78 77
1066.367729	2.446963494	63
1104.383379	2.722246012	95
1165.474898	1.736198487	155
1187.459247	2.381554251	170
1191.490548	3.559315283	178 179
1269.441228	2.082901879	99 189 182 186 208
1287.451793	2.169946922	220 373 98 141 188 181 190 183

Table2. (Docking Fitness MalasmoruponaqTM™_VS_FDAs_Numerical Data of QMMMD BiogenetoligandorolTMligandorolTM (Recoring Pharmacophoric Merging QMMMD Algorithm), By QMMMD data of MalasmopuronaqTM small molecule binds to the PfNDH2 crystal structures with some of 190800000379.40 Docking Fitness Scoring Values within Apo-, NADH-, bound MalasmopuronaqTMstates»/binding domains. Laboratory № 519896 of 02.02.18

MalasmoruponaqTM™_VS_FDAs_	Docking_Fitness_Scoring_Analysis_cav2erb_PEU_
Mefloquine	1621.04
Atovaquone	1613.41
Proguanil	1319.04
Quinidine	694.196
Quinine	1325.55
MalasmorupomaqTM	190800000379.40

Table 3. Mechanical properties of the PfNDH2 targeted MalasmoruponaqTM small molecule inhibitor exhibits excellent docking potency against the PfNDH2 protein and for the first time within Apo-, NADH-bound «MalasmoruponaqTMstates» /binding domains via a potential allosteric mechanism. (Docking Fitness MalasmoruponaqTM™_VS_FDAs_Numerical Data of QM MMID BiogenetoligandorolTMligandorolTM (Recoring Pharmacophoric Merging QM MMIDDD Algorithm) Laboratory № 519896 of 02.02.19) Docking complete MalasmoruponaqTM Docking fitness = $1.908e+011$.

<i>Amodiaquine</i>	-11.05
<i>Artemethr</i>	537.074
<i>Artesunate</i>	638.957
<i>Proguanil</i>	1313.58
<i>Pyrimethamine</i>	1211.52
<i>Quinine</i>	921.469
<i>Doxycycline</i>	1418.29
<i>Chloroquine</i>	1127.56
<i>Mefloquine</i>	1468.75
<i>MalasmoruponaqTM</i>	$1.908e+011$

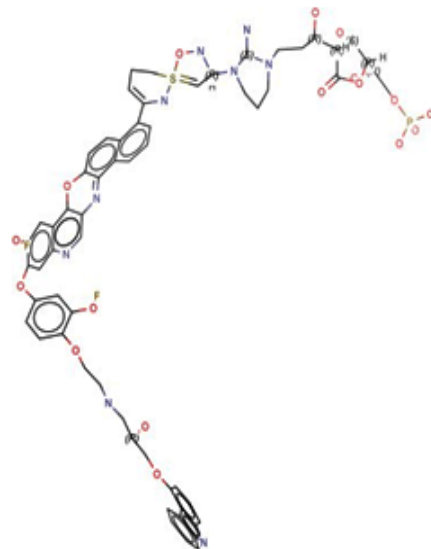


Figure 2: 3D structure of the MalasmoruponaqTM™

Data Set Curation and DATA Set Preparation and Descriptor Selection

Chemical structures of the curated data set in the SMILES format were converted into the .mol format and further optimized using Gaussian 09 (Frisch et al., 2009[13]) to obtain low energy conformation. Geometrical optimization of all chemical structures were achieved by semi-empirical Austin Model 1 (AM1) level followed by density functional theory (DFT) computation using the Becke's three-parameter hybrid method with the Lee-Yang-Parr correlation functional (B3LYP) together with the 6-31 g(d) level. The optimized structures were used for calculation of the first set of thirteen quantum chemical descriptors using an in-house developed script: the mean absolute atomic charge (Qm), total energy (Etotal), total dipole moment (μ), highest occupied molecular orbital energy (HOMO), lowest unoccupied molecular orbital energy (LUMO), energy difference of HOMO and LUMO (HOMO-LUMOGap), electron affinity (EA), ionization potential (IP), Mulliken electronegativity (χ), hardness (η), softness (S), electrophilic index (ω_i), and electrophilicity (ω).

Generation of QSAR Model

We used the Partial Least Square (PLS) as a statistical analysis method to establish a linear correlation between the subset of descriptors and bioactivities to derive predictive models. These models were established on a training set (240 molecules), and tested by test set (101 molecules) [110,121,123,127]. The module QuaSAR-Model in BiogenetoligandorolTM was used to construct the QSAR PLS model 8. QSAR models were separately developed according to the three different scaffolds using MLR method implemented in Protein-Ligand Interaction Profiler (PLIP) Tools according to the equation (1). $Y = B_0 + \Sigma B_n X_n$ (1) where Y is the pEC1.5 values of compounds, B0 is the intercept and Bn are the regression coefficient of descriptors Xn. Both maps are at near-atomic resolution, varying from 3–3.6 Å in the trans-membrane (TM) and core regions to 5–8 Å in the periphery (Figure. 14-22). X-ray co-structures of MalasmoruponaqTM_341139-MalasmoruponaqTM_937d73c677_1, MalasmoruponaqTM_ligand_9cd1e4c09f_MalasmoruponaqTM_937d73c677_1, MalasmoruponaqTM_Ligand_9cd1e4c09f_MalasmoruponaqTM_937d73c677_1 and Cho-MalasmoruponaqTM_937d73c677_1 monomers. Complexes with (a) DockThor(PDB: 4ZCS) at 2.45 Å resolution, (b) CMP (PDB: 4ZCP) at 1.98 Å resolution, (c) MalasmoruponaqTM_ligand_0c92b908ca_1 (PDB: 4ZCR) at 1.80 Å resolution and (d) Cho (PDB: 4ZCQ) at 1.92 Å resolution. In all cases only one monomer of a dimer is presented. The MalasmoruponaqTM™ligands (MalasmoruponaqTM_341139, MalasmoruponaqTM_937d73c677_1, MalasmoruponaqTM_ligand_0c92b908ca_1 and MalasmoruponaqTM_ligand_0323350cd7_1) are shown in sticks with electron density

around them [110,121,123,127].

Model Building and Refinement Validation Molecular Modelling

The QSAR model obtained has been validated in two steps. The first step through internal validation by allowing the calculation of the cross correlation coefficient (q2), using the LOO (cross validation Leave-One-Out). The second step through external validation used to evaluate the prediction set activities and calculating the numerical model parameters in the MalasmoruponaqTM Hydrogen Bonds from generated in 3UM6 (bifunctional dihydrofolate reductase-thymidylate synthase. For the better understanding of the binding and Docking Interactions of our compounds to 3UM6, we conducted 1 μs molecular dynamics (MD) simulations for the most potent compounds MalasmoruponaqTM_341139-MalasmoruponaqTM_937d73c677_1, MalasmoruponaqTM_937d73c677_1, MalasmoruponaqTM_Ligand_9cd1e4c09f_MalasmoruponaqTM_937d73c677_1 and Cho-MalasmoruponaqTM_937d73c677_1 (for full raw data see Supplementary Materials) for the generation of the MalasmoruponaqTM Hydrophobic Docking Interactions in 3UM6 (bifunctional dihydrofolate reductase-thymidylate synthase. Throughout the simulations, the 7-chloro-9H-pyrimido[4,5-b]indole scaffold of both MalasmoruponaqTM™ligands exhibits stable Docking Interactions with the backbone of the hinge residues Asp133 and Val135 (Figure 20), while the halogen-substituted third aromatic ring of the scaffold is pointing towards the hydrophobic region I of the kinase for the generation of the MalasmoruponaqTM Hydrophobic Docking Interactions of the in 3UM6 (bifunctional dihydrofolate reductase-thymidylate synthase. Leave-one-out cross validation (BiogenetoligandorolTM's) was employed to validate the predictive ability of constructed model. For small data sets of less than 50 compounds, BiogenetoligandorolTM's represents a reliable method for QSAR model validation (Gramatica, 2007[16]; Hawkins, 2004[19]). The BiogenetoligandorolTM's method was performed by removing one sample from the data set and used it as the testing set, while the remaining were used to build the QSAR model (Roy et al., 2015[43]) for the generation of the MalasmoruponaqTM Hydrophobic Docking Interactions in 3UM6 (bifunctional dihydrofolate reductase-thymidylate synthase. This cycle was repeated until every sample in the data set was used as the testing set. Furthermore, two statistical parameters were used to measure the predictive performance of the constructed QSAR models i.e., the squared correlation coefficient (R2) and root mean square error (RMSE) (Prachayasittikul et al., 2017[41]) for the generation of the Hydrophobic Docking Interactions of the in 3UM6 (bifunctional dihydrofolate reductase-thymidylate synthase. Peptides aimed at mimicking the inhibitory

prodomain segment were designed and tested based on the identified prodomain-catalytic domain interaction fingerprint (Figure. 8) for the generation of the MalasmoruponaqTM Hydrophobic Docking Interactions in 6 MalasmoruponaqTM™ binding site(s) in 3UM6 (bifunctional dihydrofolate reductase-thymidylate synthase), 1CY (cycloguanil)1CY-A-609 Interacting chains: A. Initially, a 22-mer peptide (peptide 1J=NRGDLSFEEFKKKYLNKLF, Peptide 1NRGDSLSEEFKKKYLNKLF, 2LTYHEFKKNKYLSRSSL, 3MTFEEFKQKYLTLKSKD, 4EFKKKYLTLSK, 5EFKKKYLTLSK) based on the conservation of the prodomain segments responsible for the inhibitory mechanism for all the proteases studied was selected for docking against the catalytic domains of individual proteins using the CABS-dock webserver (Figure.9) for the generation of the Hydrophobic Docking Interactions of the 2 MalasmoruponaqTM™ binding site(s) in 1V0P (cell division control protein 2 homolog). MalasmoruponaqTM™ Small Molecule PVB (purvalanol B) PVB-A-1287 Interacting chains: A.

Drug-Protein Docking Interactions, Drug Profiles, Protein Profiles

Let C be a drug (or a drug candidate compound) and let P be a target protein (or a target candidate protein). We represent a drug-protein pair (C,P) as a high dimensional feature vector $\mathbf{f}(C,P)$ and present a linear function, $f(C,P)=w^T\mathbf{f}(C,P)$, whose output is used to predict whether a (C,P) is an interacting pair or not. The weight vector w is estimated such that each drug-protein pair is correctly classified into the interaction class (positive class) or non-interaction class (negative class) based on the training set. An advantage of the linear model is that one can interpret features effective for predictions from learned models. Since each element in $\mathbf{f}(C,P)$ corresponds to an element of w , effective features can be selected by extracting highly weighted features. However, the performance of the linear model depends heavily on the feature vector design. We represent each MalasmoruponaqTM™ drug-protein pair as a high dimension feature vector by taking the tensor product of MalasmoruponaqTM™ drug profile and malaria's protein profile. The representation is similar to that in previous studies [15, 16]. The profile of a C is defined as a D -dimension binary vector:

$$\mathbf{f}(P)=(p_1,p_2,\dots,p_{D_f})^T \mathbf{f}(C,P)=(c_1p_1,c_1p_2,\dots,c_1p_{D_f},c_2p_1,\dots,c_{D_p}p_1,\dots,c_{D_p}p_{D_f})^T. LR(w)=\sum_{i=1}^n \sum_{j=1}^m \log(1+\exp(-y_{ij}w^T\mathbf{f}(C_i,P_j))). L1-LR(w)=\sum_{i=1}^n \sum_{j=1}^m \log(1+\exp(-y_{ij}w^T\mathbf{f}(C_i,P_j))+C||w||_1),$$

$$dLR(w)=\sum_{i=1}^n \sum_{j=1}^m -y_{ij} \frac{\partial}{\partial w} d(C_i, P_j) \exp(-y_{ij}w^T\mathbf{f}(C_i, P_j)) \frac{1}{1+\exp(-y_{ij}w^T\mathbf{f}(C_i, P_j))},$$

$$LR(w)^T RD \times D \int f(C_i, P_j) = LR(w)$$

$$1LR(w), \\ 2LR(w), \dots, \\ D \times D \int LR(w) T.$$

$\mathbf{f}(C)=(c_1,c_2,\dots,c_D)^T$, where $c_i \in \{0,1\}$, $i=1,\dots,D$. The profile of a P is defined as a D_f -dimension binary vector: $\mathbf{f}(P)=(p_1,p_2,\dots,p_{D_f})^T$, where $p_i \in \{0,1\}$, $i=1,\dots,D_f$. We compute the tensor product between a drug profile $\mathbf{f}(C)$ and protein profile $\mathbf{f}(P)$, and define a feature vector $\mathbf{f}(C,P)$ as follows: $\mathbf{f}(C,P)=(c_1p_1,c_1p_2,\dots,c_1p_{D_f},c_2p_1,\dots,c_{D_p}p_1,\dots,c_{D_p}p_{D_f})^T$. where $\mathbf{f}(C,P)$ is composed of all possible products between elements in $\mathbf{f}(C)$ and those in $\mathbf{f}(P)$. The resulting feature vector is a $D \times D_f$ -dimension binary vector, i.e., fingerprint, for encoding cross-integrated biological features. This is referred to as a “tensor-product fingerprint”. In this study, $\mathbf{f}(C)$ was a 27,560-dimension binary vector, and $\mathbf{f}(P)$ was a 3055-dimension binary vector. Thus, the tensor-product fingerprint $\mathbf{f}(C,P)$ of each drug-protein pair is a 84,195,800-dimension binary vector. A simpler way for representing each drug-protein pair is to concatenate $\mathbf{f}(C)$ and $\mathbf{f}(P)$ into a single feature vector as $\mathbf{f}(C,P)=(\mathbf{f}(C)^T, \mathbf{f}(P)^T)^T$ [7]. However, it cannot determine the correlation between drug and protein features. The feature vector is referred to as a “concatenated fingerprint”. Given a collection of drug-protein pairs and their labels $(\mathbf{f}(C_i, P_j), y_{ij})$ where $y_{ij} \in \{+1, -1\}$ ($i=1, \dots, n$, $j=1, \dots, m$), the logistic loss is defined as $LR(w) = \sum_{i=1}^n \sum_{j=1}^m \log(1+\exp(-y_{ij}w^T\mathbf{f}(C_i, P_j)))$. The logistic loss with L1-regularization is defined as $L1-LR(w) = \sum_{i=1}^n \sum_{j=1}^m \log(1+\exp(-y_{ij}w^T\mathbf{f}(C_i, P_j)))+C||w||_1$, where $||w||_1$ is L1 norm (the sum of absolute value in the vector) and C is a regularization parameter. Since $L1-LR(w)$ is a convex function, the weight vector w minimizing $L1-LR(w)$ can be found at zero of its gradient. However, it is impossible to compute the gradient of $L1-LR(w)$, because L1 norm contains non-differential points where $wd=0$. Instead, we compute the d -th dimensional gradient $dLR(w)$ of $LR(w)$ as follows:

$$dLR(w) = \sum_{i=1}^n \sum_{j=1}^m -y_{ij} \frac{\partial}{\partial w} d(C_i, P_j) \exp(-y_{ij}w^T\mathbf{f}(C_i, P_j)) \frac{1}{1+\exp(-y_{ij}w^T\mathbf{f}(C_i, P_j))}, \text{ where } d(C_i, P_j) \text{ is the } d\text{-th dimensional value of } \mathbf{f}(C_i, P_j). \text{ We then compute the } D \times D_f \text{-dimensional gradient vector}$$

$$L R (w) \int R D \times D \int f(C_i, P_j) = (y = Y = \sum_{i=1}^n \sum_{j=1}^m y_{ij} \delta(C_i, P_j)) \exp(-y_{ij}w^T\mathbf{f}(C_i, P_j)) \frac{1}{1+\exp(-y_{ij}w^T\mathbf{f}(C_i, P_j))}, \text{ where } \delta(C_i, P_j) \text{ is the } d\text{-th dimensional value of } \mathbf{f}(C_i, P_j). \text{ and } c_i = \sum_{j=1}^m \delta(C_i, P_j), b_j = \sum_{i=1}^n \delta(C_i, P_j), \text{ and } C = \sum_{i=1}^n \sum_{j=1}^m \delta(C_i, P_j).$$

The use of $LR(w)$ enables the global minimum for the optimal w in $L1-LR(w)$ to be found using an efficient gradient-based optimization

algorithm called orthant-wise limited-memory quasi-newton (OWL-QN) [28]. The L1-regularized logistic regression methods were applied, with the Complete 3-Qubit Grover search on a programmable quantum computer Docking Algorithms for Supercritical entanglement in local systems to the area law for quantum matter Docking Algorithm tensor product of the fingerprint proposed and with the concatenated fingerprint, is referred to as BiogenetoligandorolTM-tensor and BiogenetoligandorolTM-concat, respectively. For comparison, we also trained models with BiogenetoligandorolTM-regularized logistic regression using the gradient-based algorithm called the limited memory quasi-Newton (L-BFGS) [29]. The BiogenetoligandorolTM-regularized logistic regression method, with the tensor-product fingerprint and the concatenated fingerprint, are referred to as L2LOG-tensor and L2LOG-concat, respectively. The current study aimed to characterize the MalasmoruponaqTM™ compounds docking energy differences between *P. falciparum* falcipains and their plasmodial and human homologs, especially where again prodomain interacts with the catalytic domain, in order to identify key residues which could be useful in anti-malarial drug development approaches. This was done at both sequence and QMMM structure level. Through homology modelling, near native 3D partial zymogen complexes of both plasmodial and human proteases were obtained. This allowed structural characterization, thus deciphering how these segments confer their inhibitory mechanism endogenously. The MalasmoruponaqTM™ compounds bind with the PTEX150(S668-D823) heptamer which acts as an adaptor between HSP101 and EXP2 Of the 993 residues in PTEX150, S668-D823that are well resolved in our structure and form a hook with a shaft (Figure. 3-36) in 4IOD (malaria clp b2 atpase/hsp101 protein). The MalasmoruponaqTM™ compounds interact within the hook domain which consists of three short helices (H1-3) joined by several long loops. Directly MalasmoruponaqTM™ compounds bind within the N-terminal and C-terminal to the hook domain, into the shaft of the proximal and distal shaft domains (Figure. 3a--b).b).

Virtual Screening and Prediction of Structurally Modified Malasmoruponaqtm™ Compounds.

The LMTK3 and plasmodial proteases proteins 3D structures in active form ‘in coformation’ obtained respectively, one by homology modeling approach (reported in our previous study),[78,79,81,82,85,89,91-120] and the other extracted from PDB database(ID:3OCB). The ATP binding cavity of both 3D structures was used as targets for the virtual screening Hydrogen Bonds from the MalasmoruponaqTM™ binding site(s) in 4F1K (thrombospondin related anonymous protein). selected ligands: CL MalasmoruponaqTM™ Small Molecule EDO (Ethylene Glycol) EDO-A-305. After Virtual screening by Dock Blaster serv(<http://blaster.docking.org>), the MalasmoruponaqTM™ligands with the best energy score were selected. The visualization of docking

results by Protein-Ligand Interaction Profiler (PLIP) Toolssoftware 10 was analyzed using PyMol software [36,37,78,79,81,82,85,89,91-120] for the demonstration of Salt Bridges from the MalasmoruponaqTM™ binding site(s) in 4F1K (thrombospondin related anonymous protein). selected ligands: CL MalasmoruponaqTM™ Small Molecule EDO (Ethylene Glycol) EDO-A-305. The developed QSAR QMMIDDD MalasmoruponaqTM™ model of plasmodial proteases protein was used to calculate the predicted fitness scoring activity of MalasmoruponaqTM™ selected compound against plasmodial OPE (phosphorylethanolamine), OPE-A-501 Interacting chains: A extracted in the Hydrogen Bonds from the MalasmoruponaqTM™ binding site(s) in 4YWI. MalasmoruponaqTM™ Small Molecule EDO (Ethylene Glycol)EDO-A-302Interacting chains: A. To expand the chemical space of PfDHHCs MalasmoruponaqTM™ inhibitory activity, a set of 18 MalasmoropunaqTM QMMIDDD generated structurally modified compounds (A1aligand_8a12048cbe_1_-A13cligand_341139_1, B1a-B8aligand_937d73c677_1, and C1a-C8bligand_341139_1; Suppl. Figures 1-37) were rationally designed according to the QSAR results of known PfDHHCs small molecule inhibitors [36,37,78,79,81,82,85,89,91-120]. These modified fragmented compounds were mathematically designed in silico and their key descriptor values were obtained in a similar manner with those of the original compounds as mentioned above for the performance of the Hydrogen Bonds from the MalasmoruponaqTM™ Hydrogen Bonds binding site(s) in 4YWI. MalasmoruponaqTM™ Small Molecule. EDO (Ethylene Glycol)EDO-A-302Interacting chains: A. Subsequently, the obtained descriptor values of modified compounds A1aligand_8a12048cbe_1_-A13cligand_341139_1, B1a-B8aligand_937d73c677_1, and C1a-C8bligand_341139_1 were used to predict the PfDHHCs activity according to the QSAR equations [36,37,78,79,81,82,85,89,91-120]. Seven EXP2 protomers (labeled A-G) oligomerize to form a funnel-shaped C7-pseudosymmetric 216kDa heptamer spanning the PVM (Figure. 2-44). The TMD and body helices B1–3 are symmetric throughout all seven protomers (Extended Data Figure. 3-58) for the performance of the Hydrogen Bonds from the MalasmoruponaqTM™ binding site(s) in 4YWI. MalasmoruponaqTM™ Small Molecule EDO (Ethylene Glycol)EDO-A-302Interacting chains: A. Protein-Ligand Interaction Profiler (PLIP) web servers have been utilized for the docking experiments of the MalasmoruponaqTM small molecule against the inter-protomer conformational variations in body helices B4-5 and the assembly domain, n some protomers with the asymmetric HSP101 hexamer EXP2 funnel[36,37,55,58,59,78,79,81,82,85,89,91-120] within its variation is most pronounced in EXP2 protomers F and G (Extended Data Figure. 3-39) in the Hydrogen Bonds from the MalasmoruponaqTM™ binding site(s) in 4YWI. MalasmoruponaqTM™ Small Molecule EDO (Ethylene Glycol)EDO-A-302Interacting chains: A. Protein-Ligand Interaction Profiler (PLIP) web servers have been utilized

for the docking experiments of the MalasmoruponaqTM small molecule within the EXP2 heptamer, the amphipathic TM helices which are twisted slightly around each other, creating a 37 Å-long C7-symmetric protein-conducting channel that spans the PVM and forms the stem of the funnel (Figure. 2-7). Another Protein-Ligand Interaction Profiler (PLIP) docking experiments of the MalasmoruponaqTM small molecule have been performed against the membrane-facing surface of the EXP2 channel which is coated with hydrophobic residues, while the inner surface is lined with charged and polar residues, creating an aqueous pore (Figure. 2) in the Hydrogen Bonds and Water bridges from the MalasmoruponaqTM binding site(s) in 4YWI. MalasmoruponaqTM Small Molecule EDO (Ethylene Glycol)EDO-A-302 Interacting chains: A. The CP6-B-709, Interacting chains: B body domains, positioned in a wider ring atop the transmembrane channel on the vacuolar face of the PVM, form the mouth of the funnel NDP (NADP) NDP-A-610 Interacting chains: A [36,37,55,58,59,78,79,81,82,85,89,91-120] in the Water Bridges of the MalasmoruponaqTM binding site(s) in 4YWI. MalasmoruponaqTM Small Molecule EDO (Ethylene Glycol)EDO-A-302 Interacting chains: A. This orientation is consistent with previous analyses of EXP2 topology [36,37,55,58,59,78,79,81,82,85,89,94,95] NDP-B-710, Interacting chains: B. Furthermore, a detergent belt is clearly visible in 2D class averages and density maps (Extended Data Figure. 7-8), defining the residues in the UMP (2'-deoxyuridylic acid) UMP-A-611 Interacting chains: A, B that would be buried in the PVM Hydrogen Bonds from the MalasmoruponaqTM binding site(s) in 4YWI. MalasmoruponaqTM Small Molecule EDO (Ethylene Glycol)EDO-A-302 Interacting chains: A. A ring of positively charged residues where the stem meets the mouth of the funnel is positioned to interact with the negatively charged phosphates of the membrane surface 3UJ6 (phosphoethanolamine n-methyltransferase PO4 (Phosphates) PO4-A-301 Interacting chains: A (Extended Data Figure. 8). Residues G27-S234, 49W 49W-A-400 Interacting chains: A, GOL (Glycerol) GOL-C-402 Interacting chains: C of EXP2 are well docked with the MalasmoruponaqTM structure, accounting for 100% of the mature UMP-B-711 Interacting chains: A, B (Extended Data Figure. 36-45) in the Hydrogen Bonds from the MalasmoruponaqTM binding site(s) in 4YWI. MalasmoruponaqTM Small Molecule EDO (Ethylene Glycol)EDO-A-302 Interacting chains: A. Protein-Ligand Interaction Profiler (PLIP) docking experiments of the MalasmoruponaqTM small molecule have been performed against the EXP2 and 3UM5 (bifunctional dihydrofolate reductase-thymidylate synthase CP6 (Pyrimethamine) CP6-A-609 Interacting chains: A which is a single-pass transmembrane protein consisting of a kinked 60 Å-long N-terminal TM helix followed by a globular body domain and ending in an assembly domain composed of a linker helix followed by the assembly strand (Figure. 20) in the Hydrogen Bonds from the MalasmoruponaqTM binding site(s) in 4YWI.

MalasmoruponaqTM Small Molecule EDO (Ethylene Glycol)EDO-A-302 Interacting chains: A. DockThor and Protein-Ligand Interaction Profiler (PLIP) docking experiments of the MalasmoruponaqTM small molecule have been performed against the five helices (B1-5), stabilized by an intraprotomer C113-C140 disulfide bond (Figure. 20-60) in the Hydrophobic Docking Interactions of the 2 MalasmoruponaqTM binding site(s) in 1V0P (cell division control protein 2 homolog), MalasmoruponaqTM Small Molecule PVB (purvalanol B)PVB-A-1287 Interacting chains: A.

ADME Prediction and Toxicity

In order to verify the lead candidates, pharmacokinetic properties selected, ADME predictions were realized by SwissADME server (<http://www.swissadme.ch>) [110,122,128]. Six important properties of oral bioavailability are calculated. Each property has an optimal values range and it is fraction Csp3 > 0.25 for saturation. The TPSA must be between 20 and 130 Å 11. For solubility, the logS (calculated with the ESOL model 12) must not exceed 6. The lipophilicity, XLOGP3 13 must be between -0.7 and +6.0, and for flexibility, the molecule must not have more than 9 rotative bonds.

Biogenetoligandoroltmligandoroltm: Basic Concept: Molecular Dynamics, Monte Carlo Simulations, Langevin, Dynamics: A Computational Quantum Particle Swarm Bayesian Nonlinear Pharmacophoric-Odes Merging Algorithm.

The aim of this study is to estimate the unknown parameters θ using a Bayesian [48] approach in nonlinear ODEs representing a biological system as equation [42]:

$$x' = f(\theta, x(t), u(t), t), x(t_0) = x_0, y(t) = g(x(t)) \quad \langle M \rangle \langle N \rangle = \langle 1 \rangle \langle (\sqrt{\langle h \rangle} \wedge 2\beta / \langle 2\pi \langle m \rangle \langle A \rangle) \rangle \wedge 3 \langle N \rangle \langle A \rangle \langle N \rangle \langle A \rangle | \psi = \int \int (Rk \langle S \rangle d2Jz\psi(z)) | z \int \int \int (Rk \langle S \rangle d2Jz\psi(z)) | z \int \int (Z-1(z)) \rangle$$

We consider a bounded set $S \subset CJ$ and a set $Tk \langle f \rangle$ of unique preimages of each element in $Rk \langle S \rangle$ such that $Z(Tk \langle f \rangle) = Rk \langle S \rangle$ and $Z: Tk \langle f \rangle \rightarrow Rk \langle S \rangle$ is bijective. The algorithm on input $|\psi\rangle$ with support $\text{supp}(\psi) \subset Rk \langle S \rangle$ gives:

$$\langle (\sqrt{\langle h \rangle} \wedge 2\beta / \langle 2\pi \langle m \rangle \langle B \rangle) \rangle \wedge 3 \langle N \rangle \langle B \rangle \quad (2) \quad \langle N \rangle \langle B \rangle \quad ! " \rangle \\ + \varepsilon(t) "Pr" \langle r \wedge N, p \wedge N \rangle d \langle p \wedge N \rangle d \langle r \wedge N \rangle = \langle \exp(-\beta H(r \wedge N, p \wedge N)) d \langle p \wedge N \rangle d \langle r \wedge N \rangle \rangle Z(N, V, E) .$$

In this representation, $x \in Rn$ denotes the system's state variables, for instance, the concentrations of biochemical factors, and x_0 is the initial state, $f(\cdot)$ is a set of nonlinear functions describing the dynamical property of the biological systems, for the description of

complex macromolecular systems in 3UJ6 (phosphoethanolamine n-methyltransferase PO4 (Phosphates) PO4-A-301 Interacting chains: A, both in Cartesian and generalised coordinatesu(t):

$\Omega(\langle r \rangle^N, \langle p \rangle^N, \langle q \rangle^M, \langle p \rangle^l | q, \langle M \rangle, l)$ is the systems input denoting concentrations of stimuli, and $\theta \int A = (\langle A \rangle - \langle l \rangle) = (\sum_{i=1}^n \langle r_i \rangle \langle p_i \rangle \langle q_i \rangle \langle M_i \rangle \langle l_i \rangle)$. R_l are parameters that characterize dynamic reaction [51,60,61, 64, 69, 28]

$s, y \int R_n$

represents the observed data subject to a Gaussian [33] white noise

$$\epsilon(t) \sim N(0, \sigma^2), \quad \langle r \rangle^l | i, \langle 42 \rangle = \langle u \rangle^l | i, \langle 42 \rangle, \quad \langle r \rangle^l | i, \langle k \rangle = \langle u \rangle^l | i, \langle 42 \rangle + \sum_{i=1}^n \langle r_i \rangle \langle p_i \rangle \langle q_i \rangle \langle M_i \rangle \langle l_i \rangle, \quad g(\bullet)$$

represents a measurement function and atypical format will be an identical matrix in 3UJ6 (phosphoethanolamine n-methyltransferase PO4 (Phosphates) PO4-A-301, Interacting chains: A. We assume we have discrete [15] time series of y(t), and u(t) and all parameters in θ are positive. Ordinary energy of the universe is directly proportional to the fractal nature of spacetime [114-122,130-134]. Pharmacophore methods are widely used in drug discovery [34, 35] research projects [11]. The modified Hamiltonian [115,116,117,118,119,123], called the Nosé-Hoover chain Hamiltonian [112,136,170] [129, 160–162], is defined as:

$$HNHC = H(rN, pN) + \sum Mi = 1 p2 q2 \mu q1 + q1 \beta + \sum Mi = 2 q1 \beta,$$

where $H(rN, pN) = \sum N - 1 i = 1 p2 q2 m f1 + p2 2 m + (r \int N - Q(N, V, T) \approx \sum_{i=1}^n \langle r_i \rangle \langle p_i \rangle \langle q_i \rangle \langle M_i \rangle \langle l_i \rangle)$ H 31Ho ia312019

is the Hamiltonian [114,115,116,118,119,119,121] of the macromolecule in barycentric coordinates, the primed variables are the barycentric coordinates (relative to the centre of mass), and refers to the barycentre. When using umbrella sampling [20, 21] and the weighted histogram method [82] for the blue moon ensemble approach, the free energy [124,116,117-119] is estimated from the reaction [118,119,110,113-134] coordinates some important notions about Lagrangian and Hamiltonian dynamics, which are pervasive and recurrent for both MC and MD. GPR is a Bayesian ML framework (122), which is also formally equivalent to another ML method, kernel ridge regression. Given a set of training structures x_i and the associated properties y_i , the prediction of the property for a new structure x can be written as :

$$y(x) = \sum_i w_i K(x, x_i)$$

which is a linear fit using the kernel function as a basis, evaluated at the locations of the previous observations. The velocity of particle i is calculated accordingly:

$$v_k + 1ij = \omega v_{kij} + c_1 r_1(p_{kij} - x_{kij}) + c_2 r_2(p_{kj} - x_{kij}), \text{ where } i = 1, 2, \dots, n, j = 1, 2, \dots, q, \int n$$

is population size, k is the number of iterations, ω is inertia weight, c_1 and c_2 are acceleration coefficients, and r_1 and r_2 are random numbers in the interval [0,1]. This section presents some important notions about Lagrangian and Hamiltonian [142,159, 166] dynamics [166], which are pervasive and recurrent for both MC and MD. Lagrangian and Hamiltonian [142, 159,160] dynamics [166] provide an ideal framework for the description of complex macromolecular systems, both in Cartesian and generalised coordinates [59]. The optimal setting of the weight vector is:

$$w = (K + \sigma^2 I)^{-1} y$$

where σ is the Tikhonov regularization parameter. More accurately it is the multiplicative hyper Hausdorff measure or volume of the zero set i.e. the quantum particle in a five dimensional Kaluza-Klein universe D 5. The Lagrangian is defined as the difference in between the kinetic and the potential energy [21,66,67,68,70,72]:

$$L(q^3N, q'3N) = (q^3N) - (q'3N),$$

where the kinetic energy [21,36,55,58,59,61,72,73] is given by

$$= \sum 3Na = 112 \int \int \int (Rk S) d2Jz \int \psi(z) e(z - c) |z| \int (Z - 1(z)) \int 3.19 \int \int (Rk S) d2Jz \psi(z) e(z - c) |z| = |\psi| c \int.$$

$$3.20maq^2a,$$

and potential energy [124,134,135,136,139-161] $U(q^3N)$ is a function of the positions of the constituent atoms. Both are based on a kernel function $K(x, x_f)$ that acts as a similarity measure between inputs x and x_f . The q^3N are the generalised coordinates, and the $q'3N$ are the generalised velocities. In the framework of GPR, which takes as its prior probability a multivariate normal distribution with the kernel as its covariance, Eq. 1 represents the mean,

$$y,$$

of the posterior distribution

$$np(y | y) p(y | & y) = N(y, \sigma^2)$$

Generalizing our algorithm to a many-particle problem consisting of NB bosons is straightforward. Here, initially the particles 1, 2 and 3 are in the GHZ state $00\psi_f = \frac{1}{\sqrt{2}}(|000\rangle + |111\rangle)$ which is determined by the result of the GHZ measurement on the rest qubits 4, 5 and 6. After a certain operation, the three qubits will be in the final state $|\psi_f\rangle$ if σ_x , σ_y and σ_z are Pauli operators:

b1	B2bl	C3bl	$00\psi_f = I_1 \otimes I_2 \otimes I_3 \otimes 000\psi_f$
0	I	I	$\frac{1}{\sqrt{2}}(000\rangle + 111\rangle)$
1	I	σ_x	$\frac{1}{\sqrt{2}}(001\rangle + 110\rangle)$
2	σ_z	I	$\frac{1}{\sqrt{2}}(000\rangle - 111\rangle)$
3	σ_z	σ_x	$\frac{1}{\sqrt{2}}(000\rangle - 111\rangle)$
4	σ_x	I	$\frac{1}{\sqrt{2}}(010\rangle + 001\rangle)$
5	σ_x	σ_x	$\frac{1}{\sqrt{2}}(011\rangle + 100\rangle)$
6	$-i\sigma_y$	I	$\frac{1}{\sqrt{2}}(010\rangle - 101\rangle)$
7	$-i\sigma_y$	σ_x	$\frac{1}{\sqrt{2}}(011\rangle - 100\rangle)$

Let us denote the coordinates of the particles by x, y, z, \dots etc., while, as before, we denote the Bohmian coordinates by upper case letters. A single configuration of Bohmian walkers is denoted:

$$\begin{aligned} & \text{by } (X, Y, Z, \dots) \dots i\hbar\partial_t\psi_0(x; Y, Z, \dots; t) = (-\hbar^2 m / 2x + V(x; Y, Z, \dots)) \\ & \psi_0(x; Y, Z, \dots; t) + i\hbar dY dt \psi_1(x; Y, Z, \dots; t) - \hbar^2 m \psi_2(x; Y, Z, \dots; t) + i\hbar dZ dt \psi_1(x; Y, Z, \dots; t) - \hbar^2 m \psi_2(x; Y, Z, \dots; t) + \dots \text{etc.} \end{aligned}$$

The equation of motion for $\psi_0(x; Y, Z, \dots)$ is a simple generalization of Eq. (3) for the case of many particles:

$$\begin{aligned} Lq_3N, q'3N = Kq'3N - Uq_3N, \quad K = \sum \alpha = 13N12maq' \alpha_2, \quad q'3N \\ p\alpha \frac{\partial L}{\partial q} \alpha, \quad Hq_3N, p3N = \sum \alpha = 13Npaqa - Lq_3N, q'3Nq_3N, p3N. \\ dHdt = 0; \quad q' \alpha = \partial H \partial p\alpha; \quad p' \alpha = -\partial H \partial q\alpha. \quad CN = 1h3NNA!NB! \\ \beta 1kBTPrfrN, pNdpNdrN = \exp(-\beta HrN, pNdpNdrNZN, V, E, \sigma O = O2 - O2). PrfITI0JAI0J = PrfJTJ0IAJ0I, AI0JAJ0I = PrfJJPrfI = \exp(-\beta UJ - UI) \end{aligned}$$

$$\begin{aligned} & \psi_0(x; Y, Z, \dots) \psi_1(x; Y, Z, \dots) \psi_1(z; X, Y, Z, \dots) \quad \Psi(x, y, z, \dots) \\ & \partial\Psi(x, y, z, \dots) \partial y \partial y = Y, z = Z, \dots \partial\Psi(x, y, z, \dots) \partial y \partial 0x = X, y = Y, \dots, \\ & MN = 1h2\beta/2\pi m A3NANA!h2\beta/2\pi m B3NB3NB! \quad PrNVTrNdrN = \exp(-\beta UrNdrNZN, V, T) \end{aligned}$$

Let us denote the conditional wavfunctions by

$$\begin{aligned} & \psi_0(x; Y, Z, \dots) \psi_1(x; Y, Z, \dots) \psi_1(z; X, Y, Z, \dots) \quad \Psi(x, y, z, \dots) \\ & \partial\Psi(x, y, z, \dots) \partial y \partial y = Y, z = Z, \dots \partial\Psi(x, y, z, \dots) \partial y \partial 0x = X, y = Y, \dots, \end{aligned}$$

$$O = 1ZN, V, T \int dr N \exp(-\beta UrNOrN). \quad ANVTrN0r \int N = \min \int 1, \exp(-\beta UrN \int N - UrN, V) \int N \times \exp(-\beta PV \int V - N \ln \int V) \int V. \quad ARI0J = \min \int I, \exp(-\beta J - \beta I \int m m m n i m m m m \times UJTJ - UITI, \beta I - 1kBTI). \quad AI0J = \min \int 1, \pi U \int U \exp(-\beta UJ - UI).$$

The energy-minimized target-MalasmoruponaqTM™ligand complexes

$$\text{RMSD} = 1NHL \sum i=1NHL |Ci - Ri|^2 \quad \text{Einter} = \sum i,j NTNL [Aijrij12 - Bijrij6 + qijqj4\pi\epsilon_0]$$

$$\begin{aligned} C(n+dd) & \quad C(n+dd) \quad R^-k \int = R(n+dd) \quad R^-k \int = R(n+dd) \quad R^-k \int = R(n+dd) \\ R^-k \int & \quad kmax(n,d) \leq 2(42/(n+1))(n+dd) \quad kmax(n,d) \leq (n+dd) \\ kmax(n,d) \leq (n+dd) - n & \quad kmax(n,d) \leq (n+d-1)n \quad kmax(n,d) \leq (n+d-1)n - (n+d-5n-2) \\ kmax(n,d) \leq (n+d-1)n - (n+d-5n-2) - (n+d-6n-2) & \quad R^-k \int v2(x1, x2, x3) = (x12, x22, x32, x1x2, x1x3, x2x3, x1, x2, x3, 1) \int X3, 2 \\ (x3, x3x1, x3x2, x32, x12, x22, x1x2, x1, x2, 1) & \quad \text{intermolecular interaction energies expressed as the sum of Lennard-Jones} \end{aligned}$$

$$(LJ) \epsilon r_{ij} \int Aij = \epsilon_{ij} R_{ij} 12Bij = 2\epsilon_{ij} R_{ij} 6R_{ij} = R_{ij} + R_{jeij} = \epsilon_i \epsilon_j \epsilon_{jer} = C + D1 + ke - \lambda BrijC = \epsilon_0 - D; \epsilon_0 = 78.4; D = -8.5525; k = 7.7839; \lambda = 0.003627$$

and screened Coulomb potentials [137,138,141,144,156,157,166] (Equation (2)). With probability $1/\epsilon - \epsilon$, MalasmoruponaqTM™ performs the voting process. She randomly chooses a coding scheme $g: \{0, 1, \dots, 7\} \int \{B \int \{C \int 0, B \int \{C \int 1, \dots, B \int \{C \int 7\}\}$. For both the LJ and Coulomb potentials, Amber99sb-ILDN force field parameters were used where, ϵ_{ij} is the potential well depth at equilibrium between the i th (MalasmoruponaqTM™ligand) and j th (target) atoms; ϵ_0 is the dielectric constant of bulk water at 25 °C; R_{ij} is the inter-nuclear distance at equilibrium between i th (MalasmoruponaqTM™ligand) and j th (target) atoms; q is the partial charge of an atom, used in AMBER99SB-ILDN force field; r_{ij} is the actual distance between the i th (MalasmoruponaqTM™ligand) and j th (target) atoms; NT is the number of target atoms; NL is the number of MalasmoruponaqTM™ligand atoms:

$$\begin{aligned} & 1m(S) - \sqrt{\sum c \int \Lambda \int S \int d \int J \int z e(-z \int c \int)} |c \int \int z|, \\ & 1m(Rk \int S)m(S)000 \int Rk \int S \int d \int J \int z \psi(z) e(z \int (c - c \int)) 0002 \leq m(Rk \int S)m(S), \end{aligned}$$

$$QN, PT = MNV0ZN, PT. \quad PrNPTrNdrN = \exp(-\beta PV \exp(-\beta UrNdrNZN, PT) \int ANPTrN, V0r \int N, V \int$$

where the upper bound follows from the Cauchy-Schwarz inequality. The maximum is reached if $\psi(z) = (12/m(Rk \int S))^{1/2}$ $Rk \int S(z)$ and c happens to be a lattice point. If $c \in \Lambda$, the algorithm returns the closest lattice point with high probability:

$$= \min \int I, \exp(-\beta J - \beta I \int m m m n i m m m m \times UJTJ - UITI, \beta I - 1kBTI). \quad ARI0J = \min \int 1, \pi U \int U \exp(-\beta UJ - UI).$$

$$O = \lim_{t \rightarrow \infty} \int_0^t \partial \tau \int_0^\tau O \int \tau. \quad O \approx O.$$

were also subjected to calculation of

$$\begin{aligned} \text{UrN} = & \sum d k d d - d 02 + \sum S k S S - S 02 + \sum \theta k \theta \theta - \theta 02 + \sum \chi k \chi 1 + \cos \int n \chi - \\ & \delta + \sum \varphi k \varphi \varphi - \varphi 02 + \sum i, j \epsilon i j r i j 0 r i j 1 2 - r i j 0 r i j 6 + q i q j \epsilon l r i j, \\ \text{AI0J} = & \min \int 1, \exp \int - \beta k U J T k - U I T k, O x i = O x i + L x i = 1, \dots, \\ , N, O y i = & O y i + L y i = 1, \dots, N, O z i = O z i + L z i = 1, \dots, N. \quad \partial \partial r \bullet \epsilon r \partial \int r \partial r = \\ \rho r - \sum k = & 1 K q c i \infty \lambda r e x p \int - \beta q i \int r, \quad i L \quad \Sigma a = 13 N \partial H \partial p a \partial \partial q a - \partial H \partial q a \partial \partial p a, \\ i = -1 & \end{aligned}$$

$$\Psi(x, y, z, \dots, t) = \sum i, j, k c i j k \dots (t) \varphi i(x) \varphi j(y) \varphi k(z) \dots$$

In order to compute $\psi_1(x; Y, Z, \dots, t)$ from $\psi_0(x; Y, Z, \dots, t)$ belonging to all configurations, we need to express the tensor $[\varphi_j(Y) \varphi_k(Z) \dots]$ as a linear superpositions of all the $[\varphi_j(Y) \varphi_k(Z) \dots]$ tensors belonging to all configurations; i.e., $[\varphi_j(Y) \varphi_k(Z) \dots] = \sum w_{jk} [\varphi_j(Y) \varphi_k(Z) \dots]$. This can be done with the existing numerical techniques by rearranging all the MNB-1 terms of the tensors, where M is the number of orbitals, in vector forms and solving a linear system of equations $\{|+j=12\sqrt{|0j+1j|}, |-j=12\sqrt{|0j-1j|}\}$. The particles 1 and 3 will be in one of the two EPR states $|j\pm j=j=12\sqrt{|00j\pm11j|}$ with the same probability determined by:

$$\begin{array}{ccc} |\psi\rangle^{456} (|\psi\rangle^{123}) & 12\sqrt{(0000j+0111j)} & 12\sqrt{(0000j+0111j)} \\ 12\sqrt{(0000j+0111j)} & & 12\sqrt{(0000j+0111j)} \end{array}$$

$$\begin{array}{cccc} \text{result 1 (MalasmoruponaqTM™)} & 1 & 2 & \sqrt{(|0j - |1j)} \\ 12\sqrt{|0j-1j)} & 12\sqrt{|0j-1j)} & 12\sqrt{|0j-1j)} \\ |j\rangle^{13} & |j\rangle^{-j} & |j\rangle^{-j} & |j\rangle^{-j} \end{array}$$

$$\text{basis(MalasmoruponaqTM™)}\{|0j, |1j\rangle\{|0j, |1j\rangle\} \{|+, |-\rangle\} \{|+, |-\rangle\}$$

$$\text{result 2 (MalasmoruponaqTM™)}|0j \quad |1j \quad |+j \quad |-j$$

$$\text{result 3 (MalasmoruponaqTM™)}|0j \quad |1j \quad |-j \quad |+j$$

Since the size of the vectors now becomes exponentially bigger as the number of particles becomes larger, the bottleneck of this method would be to take a sufficiently large number of configurations that ensures having a complete linear system. Therefore, an immediate room for improvement here would be to find smart tactics to overcome this problem.

$$\begin{aligned} iL = & iL1 + iL2, iL1 \otimes \sum i=1 N p i m i \bullet \partial \partial r i ; iL2 \otimes \sum i=1 N - \partial U r N \partial r i \bullet \partial \partial p i . \exp \int iL \Delta t \\ = & \exp \int iL1 + L2 \Delta t \approx \exp \int iL2 \Delta t 2 \exp \int iL1 \Delta t \exp \int iL2 \Delta t 2 + O \Delta t 3 . r i t + \Delta t \\ = & 2 r i t - r i t - \Delta t - 1 m i \partial U r N t \partial r i \Delta t 2 + O \Delta t 4 \quad i = 1, \dots, N, \\ \eta = & r N \int 0 \int p N \int 0 \int q M \int 0 \int p q M T . \end{aligned}$$

By definition, $c - c j$ must be a zero of the Fourier transform $F(S)$ of the indicator function $S(z)$. We denote $\Lambda := \{c: F(S)(c) = 0\} \setminus \{0\}$ and let $c \in \Lambda$. Clearly $U - c + \Lambda$ as Λ contains all zeros. Since $c + c^* \in \Lambda$ for all $c \in \Lambda \setminus \{0\}$, we have $c + \Lambda = U$ and $U = c + \Lambda$. If $c \in \Lambda \setminus \{0\}$, then $c + c^* \in \Lambda \setminus \{0\}$ implies that $-c \in \Lambda$. If $c, c \in \Lambda \setminus \{0\}$, then $c + c^* - c - c^* = c + c^* + c^* - c = 0$ implies $c + c \in \Lambda \setminus \{0\}$. Therefore, Λ is an additive subgroup of R_n .

$$\begin{aligned} H r N, p N 0 H \int r N, p N, q M, p q M ; 1 . \det \int G \eta t d \eta t = \det \int G \eta 0 d \eta 0, \\ \det \int G \eta t = \exp \int - \int 0 t \partial \partial \eta \tau \bullet \eta \cdot \tau d \tau . \Omega r N, p N, q M, p q M ; \\ X 3, 2 = \{(x21, x22, x23, x1x2, x1x3, x2x3, x1, x2, x3, 1) T : x1, x2, x3\} \end{aligned}$$

$$\begin{aligned} = \Omega 0 \int d \eta d e t \int G \eta \prod k = 1 M \delta \Lambda k \eta - C k, d \eta d e t \int G \eta \Omega r N, p N, q M, p q M ; 1 \int d q M d p q M \int d q M d p q M \Omega \int r N, p N ; 1 . \\ v 2 (x1, x2, x3) = (x21, x22, x23, x1x2, x1x3, x2x3, x1, x2, x3, 1) \\ T \int X 3, 2 \Omega r N, p N, q M, p q M ; \int d q M d p q M \int d q M d p q M \Omega \int r N, p N ; 1 . \end{aligned}$$

$$\begin{aligned} \dim R^- \int k = & \int \int \int \int \int \int k(n+1) - k(k-1)2(n+dd) - 1 \min \{k(n+1), (n+dd)\} \\ d = 2, 2 \leq k \leq n; (d, n, k) = & (3, 4, 7), (4, 2, 5), (4, 3, 9), H N H C = H r N, \\ p N + \sum i = 1 M p q i 22 \mu q i + l q 1 \beta + \sum i = 2 M q i \beta, H r N, p N = \sum i = 1 N - 1 p i \int 22 m i + p 22 m + U r N \Omega N H C k C(n, d) = & \int \int \int \int \int \int n+1 \quad 1 n+1(n+dd) + 1 \quad 1 n+1 \\ (n+dd) \quad d = 2, n \geq 2; (n, d) = & (4, 3), (22, 4), (3, 4), (4, 4); \text{otherwise}. \end{aligned}$$

$R_k = \{\sum k_i = 1 c_i v_i : c_i \in \text{basis}(M)$, and we ask what is the smallest number k such that R_k has full measure in $(n+dd)$.

$$\begin{aligned} = \Omega 0 \int d p q M d q M d p \int N - 1 d p \quad d r \int N - 1 \times \exp \int 3 N - 2 q 1 + \sum i \\ = 2 M q i \delta H N H C - C 1 \times \delta e q 1 p \Omega - C 2 . \sigma k t = r i t - r j t 2 - d k 2 \quad 0 . \\ \text{mir}'it = - \partial U r N t \partial r i + \sum k = 1 K \lambda k \partial \partial k \partial r i i = 1, \dots, N . \end{aligned}$$

For a harmonic interaction of the form $V(x, y) = \frac{1}{2} k_i(x-y)^2$ we consider two cases of 5 bosons with weak Docking Interactions ($k_i = 0.1$) and 3 bosons with strong interaction ($k_i = 1$) and we use 3 and 4 orbitals in the two cases, respectively. In both cases we compare the results with the numerically exact simulation using multiconfigurational time-dependent Hartree method for bosons (MCTDHB)29–33 and with the Hermitian limit (HL) of Eq. (7) (also referred to as small entanglement approximation) where all the non-hermitian terms in Eq. (7) are dropped out. The Hermitian limit is equivalent to the time-dependent quantum Monte-Carlo (TDQMC) of ref.25 which does not take entanglement into consideration. It was also employed recently in34,35 in order to devise an approximate solution for electron-nuclear dynamics in molecular systems. Our approach requires basic knowledge of algebraic geometry—specifically, the concepts of Zariski topology, Veronese variety and secant variety. Formal definitions can be found in §2b. For the reader's convenience, we also explain these concepts briefly when we first use them.

Entangled quantum dynamics of two particles in a harmonic trap. (a) A cartoon representing the pilot waves guiding Bohmian particles moving in 2D. Although the two particles do not interact, their entanglement implies a coupling between the two pilot waves guiding the two Bohmian trajectories (the dashed line). (b) The trajectories of the light particle computed from the exact pilot waves (solid blue) and using pilot waves evolved using Eq. (3) (dashed). The case for $N_f=7$ corresponds to interacting pilot waves evolved with the help of a hierarchy of conditional wavefunctions $\{\psi_{n1}, \psi_{n2}\}$ up to $n_f=7$ (see Eq. (3)), while $N_f=0$ corresponds to noninteracting pilot waves (the Hermitian limit). We notice that the former case is more accurate than the latter. The two particles have mass ratio 1:100. ω is the trap frequency of the light particle.

$\lambda - kt + \Delta t = \lambda - kt + \delta\lambda - k$, $\lambda - kt = \Delta t 2/2\lambda k$ $\delta\lambda - k$ $\lambda - kt + \Delta t$ $A\delta\lambda \sim -\sigma Nt + \Delta t$,
 $A = Alk = \Sigma i=1 N1 mi \partial dr / Nt + \Delta t dr_i \bullet \partial skr / Nt dr_i, \delta\lambda \sim = \delta\lambda - k$; $\sigma = \sigma k$.

$\text{ArNt}, \text{pNt}0 \text{Rt} + \Delta t, \text{pNt} + \Delta t = \min\{1, \exp(-\beta H_r \text{Nt} + \Delta t, \text{pNt} + \Delta t - \text{HrNt}, \text{pNt}mmmmmmmiimm - \text{HrNt}, \text{pNt}\}$.

$\text{TrNt}, \text{pNt}0\text{rNt} + \Delta t, \text{pNt} + \Delta t = \text{TrNt} + \Delta t, -\text{pNt} + \Delta t0\text{rNt}, -\text{pNt}$ where with
 $x = (x_1, \dots, x_k) \rangle (nq)k, y = (y_1, \dots, y_k) \rangle kq, w = (w_1, \dots, w_{k+1})$ and I am
 appropriate index set, $i\hbar\partial\Psi(x_1, x_2)\partial t = (-\hbar^2)$

$$-\mathbf{k}(\mathbf{x}_i, t) \partial_k V(\mathbf{x}_i, \mathbf{x}_j) \partial_x j_k |_{\mathbf{x}_j = \mathbf{X}_j(t), j \neq i} - \hbar^2 m_j \psi_{in+2}(\mathbf{x}_i, t) + i \hbar d X_j(t) \\ d \psi_{in+1}(\mathbf{x}_i, t) \langle \psi_{in} | \psi_{i0} \psi_{i1} \psi_{i2} \psi_{i0} \Psi(\mathbf{y}, \mathbf{x}, t) = \sum_i c_{ij}(t) \phi_i(\mathbf{x}) \phi_j(\mathbf{y}),$$

$\psi(0, x) \Psi(x, y) |y=Y = \sum i a_i \varphi_i(x) \psi_1(x)$) $\partial\Psi(x, y) \partial y |y=Y = \sum i b_i \varphi_i(x) \psi_2(x)$
 $) \quad \partial^2 \Psi(x, y) \partial y^2 |y=Y = \sum i c_i \varphi_i(x) b_i = \sum j c_j \varphi_j(y) \partial y |y=Y$
 $c_i = \sum j c_{ij} \partial^2 \varphi_j(y) \partial y^2 |y=Y = f(Y) = C \varphi f(Y), b_j(Y) = C \varphi f f(Y)$
 $\text{and } f(Y) = C \varphi f f f(Y) \quad a_j(Y) = \{a_1(Y), a_2(Y), \dots\} \quad \varphi f(Y) = \{\varphi_1(Y), \varphi_2(Y), \dots\}$
 $b_j c_j \varphi f f f(Y) = \sum k a_k \varphi f(Y_k) \varphi f f(Y_k) = \sum k b_k \varphi f(Y_k)$
 $b_j(Y) = \sum k a_k a_k f(Y_k) \quad c_j(Y) = \sum k b_k b_k f(Y_k)$

212m1-h2

$$222m^2 + V(x_1, x_2))\Psi(x_1, x_2),$$

$i\hbar \partial \psi n_1(x_1, t) / \partial t = -\hbar^2 m_1 \partial^2 \psi n_1(x_1, t) / \partial x_2^2 + \partial n \partial x n_2(V(x_1, x_2) \Psi(x_1, x_2))$

 $00x_2 = X_2(t) - \hbar^2 m_2 \psi n_{1+2}(x_1, t) + i\hbar D X_2(t) dt \psi n_{1+1}(x_1, t)$

$$\xi_Z = \sum_{x,y} \int Z - 1(z) \sum_{x,k+1} \int nq, y, k+1 \int q, w \int l, k+1 (\prod_{j=0}^k x_j + 1, y_j + 1, w_j + 1 | U_j[x_j, y_j, w_j]) \sum_{x,k+1} \int y, k+1, w, k+1 \int$$

Let us illustrate the inefficiency of evolving a truncated hierarchy of ψ_{ni} using Eq. (3) in order to compute the dynamics of an entangled system. We consider the entangled dynamics of two particles of masses $m_1=j=1$ and $m_2=j=100$ subject to the harmonic potential $V(x_1,x_2)=12kx_21+12kx_22$ with $k\beta=0.1$. Let us take the initial

state to be the entangled ground state of the Hamiltonian with the potential function $V(x_1, x_2) = 12k_1x_1^2 + 12k_2x_2^2 + 12k_3(x_1 - x_2)^2$ with $k_1 = k_2 = 0.1$, $k_3 = 1.0$ and the masses of the particle $m_1 = 1$ and $m_2 = 2$. This is an entangled state. We evolve the Bohmian trajectories for the initial conditions $X_1 = 1$, $X_2 = 2$. We first truncate the hierarchy at $N = 0$, thus making Eq. (3) unitary. This case corresponds to the Hermitian limit, i.e., noninteracting pilot waves. Figure 5 shows that the Bohmian trajectory evolved by the corresponding pilot wave deviates from the trajectory computed from the exact pilot wave already at half a cycle of the oscillatory motion. Increasing the depth of the hierarchy to $N = 7$ only extends the range of accurate dynamics for another cycle.

Compute the energy levels

<MalasmoruponaqTM™_BiogenetoligandorolTMligandorolTM>

<<MalasmoruponaqTM™/head7 ,{[4,(2,{{(2R),3,(42,2,3,4, 4a,4b,5,6,7,8,decahydro,9λ⁴, carbazol,4,yloxy),2, hydroxypropyl]amino}ethoxy),3,oxocyclohexyl]oxy }>_MalasmoruponaqTM™ Biogenetoligandorol TMligandorol TM>

$f(x_1), \dots, f(x_k)$ <!MALASMORUPONAQTM™ html>

If $\theta < \beta$ then<th_MalasmoruponaqTM™> |xʃʃ(42/q)ΣyʃFqe(xy)|yʃ|xʃʃʃʃ(42/qk/2)ΣyʃFqke(x y)|yʃ xʃFqk Σi=1kyif(xi)=Σi=1kΣjʃyixijcj (x</th>

Z:Fqnk×Fqk∫FqJ</th> If $\theta < \beta$ then<th_MalasmoruponaqTM™>
y)∫Fqk×Fqk

</tr_MalasmoruponaqTM™> If $d(l, m) < d(r, m)$ then<th_MalasmoruponaqTM™>

If $d(l, m \cdot v) = W \langle vdw \rangle \sum_{i,j} \langle \langle A_{ij} \rangle \langle r_{ij}^6 \rangle, 12 \rangle - \langle B_{ij} \rangle \langle r_{ij}^{12} \rangle, 6 \rangle \rangle + W \langle hbond \rangle \sum_{i,j} \langle E(t) \rangle \langle \langle C_{ij} \rangle \langle r_{ij}^6 \rangle, 12 \rangle - \langle D_{ij} \rangle \langle r_{ij}^{12} \rangle, 10 \rangle \rangle + W \langle elec \rangle \sum_{i,j} \langle q_i \rangle \langle q_j \rangle < d(r, m) \text{ then } \text{th_MalasmoruponaqTM}^m \rangle$

If $d(l, m) < W \langle vdw \rangle \sum_{i,j} \langle r_{ij} \rangle, \langle A_{ij} \rangle \langle r_{ij}^A \rangle, \langle 12 \rangle - \langle B_{ij} \rangle \langle r_{ij}^B \rangle, \langle 6 \rangle \rangle + W \langle hbond \rangle \sum_{i,j} \langle E(t) \rangle \langle C_{ij} \rangle \langle r_{ij}^C \rangle, \langle 12 \rangle - \langle D_{ij} \rangle \langle r_{ij}^D \rangle, \langle 10 \rangle \rangle + W \langle elec \rangle \sum_{i,j} \langle q_i \rangle < d(r, m)$ then $th_MalasmoruponaqTM^m$

If $d(l, m \cdot V) = W \langle vdw \rangle \sum_{i,j} \langle \langle A_{ij} \rangle \rangle \langle r_{ij} \rangle, \langle 12 \rangle - B_{ij} \langle r_{ij} \rangle, \langle r_{ij}^6 \rangle \rangle + W \langle hbond \rangle \sum_{i,j} \langle E(t) \rangle \langle \langle C_{ij} \rangle \rangle \langle r_{ij} \rangle, \langle 12 \rangle - D_{ij} \langle r_{ij} \rangle, \langle r_{ij}^{10} \rangle \rangle + W \langle elec \rangle \sum_{i,j} \langle q_i \rangle \langle q_j \rangle < d(r, m)$ then

Initialize differential weights ap, ao, at by the following: </> (MalasmoruponaqTM™):

7,{[4,(2,{[(2R),3,(42,2,3,4,4a,4b,5,6,7,8,decahydro,9λ⁴,carbazol,4,yloxy),2,hydroxyporphyl]amino}ethoxy),3,oxocyclohexyl]oxy},19,[((2Z),1,[(2S),2,amino,3,[(3R),3,hydroxy,3,[(3R,4S,5R),4,hydroxy,5,[(42R),1,hydroxy,2,[(oxophospho),λ³,oxy]ethyl],2,oxooxolan,3,yl]propyl],1,3,diazinan,1,yl],2,(hydroxyamino)ethylidene],5,6,dihydro,4H,1λ⁴,2,thiazin,3,yl],2λ³,oxa,10λ⁴,13λ⁴,⁴,diazapentacyclo[12.8.0.0³,¹².0⁴,⁹.0¹⁵,²⁰]docosa,1,9,10,12,13,pentaen,6,one dihydrofluoride>

If θ < β then<th_MalasmoruponaqTM™> 24λ2+2λ2h2(D10-D00D00)-23h2D10a2=-2+12λ2-12λ2h(422D00+h2D20)-λ2h2(D10-D00D00)+hD00a3=1-h2D00a4=10+h23D10a5=-2+12λ2+12λ2h(422D00+h2D20)+λ2h2(D00D00-D10)-hD00a6=1+h2D00and rhsl</th>

If θ < β then<th_MalasmoruponaqTM™> m=-a5Ul-1</th>
 If θ < β then<th_MalasmoruponaqTM™> m-a3Ul+1</th>
 If θ < β then<th_MalasmoruponaqTM™> m-1-a6(Ul-1)</th>
 If θ < β then<th_MalasmoruponaqTM™> m+1+Ul-1</th>
 If θ < β then<th_MalasmoruponaqTM™> m-1)-a4Ul</th>
 If θ < β then<th_MalasmoruponaqTM™> m-1+Gl</th>
 If θ < β then<th_MalasmoruponaqTM™> mrhsl+1</th>
 If θ < β then<th_MalasmoruponaqTM™> m=-a2Ul+2</th>
 If θ < β then<th_MalasmoruponaqTM™> m-a3(Ul+2)</th>
 If θ < β then<th_MalasmoruponaqTM™> m+1+Ul+2</th>
 If θ < β then<th_MalasmoruponaqTM™> m-1)-a6Ul</th>
 If θ < β then<th_MalasmoruponaqTM™> m-1-a4Ul+1</th>
 If θ < β then<th_MalasmoruponaqTM™> m-1+Gl+1</th>
 If θ < β then<th_MalasmoruponaqTM™> mrhsl+1</th>
 If θ < β then<th_MalasmoruponaqTM™> m+1=-a2Ul+2</th>
 If θ < β then<th_MalasmoruponaqTM™> m+1-a3(Ul+2)</th>
 If θ < β then<th_MalasmoruponaqTM™> m+2+Ul+2</th>
 If θ < β then<th_MalasmoruponaqTM™> m)-a6Ul</th>
 If θ < β then<th_MalasmoruponaqTM™> m+2-a4Ul+1</th>
 If θ < β then<th_MalasmoruponaqTM™> m+2+Gl+1</th>
 If θ < β then<th_MalasmoruponaqTM™> m+1rhsl</th>
 If θ < β then<th_MalasmoruponaqTM™> m+1=-a5Ul-1</th>
 If θ < β then<th_MalasmoruponaqTM™> m+1-a3Ul+1</th>
 If θ < β then<th_MalasmoruponaqTM™> m+2-a6(Ul-1)</th>
 If θ < β then<th_MalasmoruponaqTM™> m+2+Ul-1</th>
 If θ < β then<th_MalasmoruponaqTM™> m)-a4Ul</th>
 If θ < β then<th_MalasmoruponaqTM™> m+2+Gl</th>
 If θ < β then<th_MalasmoruponaqTM™> m+1 Eq (220)

can be inverted and written in explicit forms [Ul</th>

If θ < β then<th_MalasmoruponaqTM™> mUl+1</th>
 If θ < β then<th_MalasmoruponaqTM™> mUl+1</th>
 If θ < β then<th_MalasmoruponaqTM™> m+1Ul</th>
 If θ < β then<th_MalasmoruponaqTM™>

m+1]=1denom[b1b2b3b4b5b1b4b6b6b4b1b5b4b3b2b1][rhs1</th>

If θ < β then<th_MalasmoruponaqTM™> mrhsl+1</th>
 If θ < β then<th_MalasmoruponaqTM™> mrhsl+1</th>
 If θ < β then<th_MalasmoruponaqTM™> m+1rhs1</th>
 If θ < β then<th_MalasmoruponaqTM™> m+1]</th>

If d (l, m) < d (r, m) then<th_MalasmoruponaqTM™> </tr_MalasmoruponaqTM™>

If d (l, m)V = W <vdw> $\sum_{ij} \langle A_{ij} \rangle \langle r_{ij}^1 \rangle, \langle r_{ij}^2 \rangle - \langle B_{ij} \rangle \langle r_{ij}^1 \rangle, \langle r_{ij}^2 \rangle \rangle + W \langle \text{hbond} \rangle \sum_{ij} \langle E(t) \rangle \langle C_{ij} \rangle \langle r_{ij}^1 \rangle, \langle r_{ij}^2 \rangle - \langle D_{ij} \rangle \langle r_{ij}^1 \rangle, \langle r_{ij}^2 \rangle \rangle + W \langle \text{elec} \rangle \sum_{ij} \langle q \rangle \langle q \rangle < d (r, m) \text{ then} <\text{th}_\text{MalasmoruponaqTM™}> </\text{tr}_\text{MalasmoruponaqTM™}>$

If d (l, m)V = W <vdw> $\sum_{ij} \langle A_{ij} \rangle \langle r_{ij}^1 \rangle, \langle r_{ij}^2 \rangle - \langle B_{ij} \rangle \langle r_{ij}^1 \rangle, \langle r_{ij}^2 \rangle \rangle + W \langle \text{hbond} \rangle \sum_{ij} \langle E(t) \rangle \langle C_{ij} \rangle \langle r_{ij}^1 \rangle, \langle r_{ij}^2 \rangle - \langle D_{ij} \rangle \langle r_{ij}^1 \rangle, \langle r_{ij}^2 \rangle \rangle + W \langle \text{elec} \rangle \sum_{ij} \langle q \rangle \langle q \rangle < d (r, m) \text{ then} <\text{th}_\text{MalasmoruponaqTM™}> <\text{tbody}> </\text{tbody}>$

If d (l, m)V = W <vdw> $\sum_{ij} \langle A_{ij} \rangle \langle r_{ij}^1 \rangle, \langle r_{ij}^2 \rangle - \langle B_{ij} \rangle \langle r_{ij}^1 \rangle, \langle r_{ij}^2 \rangle \rangle + W \langle \text{hbond} \rangle \sum_{ij} \langle E(t) \rangle \langle C_{ij} \rangle \langle r_{ij}^1 \rangle, \langle r_{ij}^2 \rangle - \langle D_{ij} \rangle \langle r_{ij}^1 \rangle, \langle r_{ij}^2 \rangle \rangle + W \langle \text{elec} \rangle \sum_{ij} \langle q \rangle \langle q \rangle < d (r, m) \text{ then} <\text{th}_\text{MalasmoruponaqTM™}> </\text{table}>$

</>(MalasmoruponaqTM™):

7,{[4,(2,{[(2R),3,(42,2,3,4,4a,4b,5,6,7,8,decahydro,9λ⁴,carbazol,4,yloxy),2,hydroxyporphyl]amino}ethoxy),3,oxocyclohexyl]oxy},19,[((2Z),1,[(2S),2,amino,3,[(3R),3,hydroxy,3,[(3R,4S,5R),4,hydroxy,5,[(42R),1,hydroxy,2,[(oxophospho),λ³,oxy]ethyl],2,oxooxolan,3,yl]propyl],1,3,diazinan,1,yl],2,(hydroxyamino)ethylidene],5,6,dihydro,4H,1λ⁴,2,thiazin,3,yl],2λ³,oxa,10λ⁴,13λ⁴,diazapentacyclo [12.8.0.0³,¹².0⁴,⁹.0¹⁵,²⁰] docosa,1,9,10,12,13,pentaen,6,one dihydrofluoride>

<meta charset="UTF-8">

<MalasmoruponaqTM™>p i = <fit<(x i <(t)>>> <Σ'i = 1>, M fit<(x i <(t)>>>)>>> u sing H r N , p N O H s r N , p N , q M , p q M ; 1. det G η t d η t = det G η t d η 0 , det G η t = exp ∫ - ∫ 0 t ∂ η t ∙ η ∙ t d t Ω r N , p N , q M , p q M ; 1 = Ω 0 ∫ d η t det G η t Π k = 1 M δ Λ k η - C k d η t det G η

```
OrN,pN,qM,pqM;IʃʃdqdMdpqMʃdqMdqMΩʃrN,pN;l.  
OrN,pN,qM,pqM;IʃʃdqdMdpqMʃdqMdqMΩʃrN,pN;l.  
HNHC=HrN,pN+ +Σi=1Mpqi22μqi+lq1β +Σi=2Mqiβ, H</title>
```

```
<MalasmoruponaqTM™="text/css"> table.cb-<p i = <fit<(x i <(t)>)>>> <Σ|i = 1>, M fit<(x i <(t)>)>>> { font-size: 12px; border: 1px solid #CCC; <p i = <fit<(x i <(t)>)>>> <Σ|i = 1>, M fit<(x i <(t)>)>>> ΔG = V<bound>, <L - L> - V<unbound>, <L - L> + (V<bound>, <P - P> - V<unbound>, <P - P>) + (V<bound>, <P - L> - V<unbound>, <P - L> + ΔS <conf>)} .cb-<p i = <fit<(x i <(t)>)>>> <Σ|i = 1>, M fit<(x i <(t)>)>>> td { padding: 4px; margin: 3px; border: 1px solid #CCC; } .cb-<p i = <fit<(x i <(t)>)>>> <Σ|i = 1>, M fit<(x i <(t)>)>>> th { background-color:#C1CCAF; color: #FFF; font-weight: bold; } </style>
```

```
< MalasmoruponaqTM™ / < MalasmoruponaqTM™ /  
head7,{[4,(2,{[(2R),3,(42,2,3,4,4a,4b,5,6,7,8,decahydro,  
9λ⁴,carbazol,4,yloxy),2,hydroxypyropyl]amino}  
ethoxy),3,oxocyclohexyl]oxy}>>
```

```
< MalasmoruponaqTM™ / 3 , oxocyclohexyl]oxy },  
,19,[{(42Z),1,[(2R),2,[(2S),2,amino,3,[{(3R),3,hydroxy,3,[{(3R  
4S,5R),4,hydroxy,5,[(42R),1,hydroxy,2,[(oxophospho),λ³,oxy]ethyl],2,  
oxooxolan,3,yl]propyl],1,3,diazinan,1,yl],2,(hydroxyamino)  
ethylidene]}>
```

```
<table class="cb-<p i = <fit<(x i <(t)>)>>> <Σ|i = 1>, M fit<(x i <(t)>)>>>">
```

```
End Algorithm: BSP Tree_(l, m·V = W ·vdw· Σ‡i,j>_o <(<  
<A ij>> <r{ij},<12>-<B ij>> <r{ij},<6>>>+W ·hbond· Σ_i,j <E<(t)>><  
<C ij>> <r{ij},<12>-<D ij>> <r{ij},<10>>>+W ·elec· Σ_-i,j <q>> <d  
(r, m) then<th_MalasmoruponaqTM™>.
```

Re-Core The Fragmented Compounds

Assign the Pworse nests lower in rank as the worse set and the remaining nests [137,139,141-166] as the better set

```
<!MALASMORUPONAQTM™ html>
```

```
<MalasmoruponaqTM™_BiogenetoligandorolTMligandorolTM>
```

```
<< MalasmoruponaqTM™ / head7,{[4,(2,{[(2R),3,  
,(42,2,3,4,4a,4b,5,6,7,8,decahydro,9λ⁴,carbazol,4,yloxy),  
,2,hydroxypyropyl]amino}ethoxy),3,oxocyclohexyl]oxy}>_  
MalasmoruponaqTM™ BiogenetoligandorolTMligandorolTM>
```

```
<meta charset="UTF-8"> <MalasmoruponaqTM™><p i = <fit<(x i <(t)>)>>> <Σ|i = 1>, M fit<(x i <(t)>)>>> using HrN,pN0HʃrN,pN,qM,pqM;l.
```

```
detʃGηtdηt=detʃGη0dη0, detʃGηt=expʃ-ʃ0t∂dηt•η·τdτ.  
ΩrN,pN,qM,pqM;l = Ω0ʃdη detʃGηΠk=1MδΛkη-Ck,  
dηdetʃGηΩrN,pN,qM,pqM;lʃʃdqdMdpqMʃdqMdqMΩʃrN,pN;l.  
ΩrN,pN,qM,pqM;lʃʃdqdMdpqMʃdqMdqMΩʃrN,pN;l.  
HNHC=HrN,pN+ +Σi=1Mpqi22μqi+lq1β +Σi=2Mqiβ, H</title>
```

```
<MalasmoruponaqTM™="text/css"> table.cb-<p i = <fit<(x i <(t)>)>>> <Σ|i = 1>, M fit<(x i <(t)>)>>> { font-size: 12px; border: 1px solid #CCC; <p i = <fit<(x i <(t)>)>>> <Σ|i = 1>, M fit<(x i <(t)>)>>> ΔG = (V<bound>, <L - L> - V<unbound>, <L - L> + (V<bound>, <P - P> - V<unbound>, <P - P>) + (V<bound>, <P - L> - V<unbound>, <P - L> + ΔS <conf>)} .cb-<p i = <fit<(x i <(t)>)>>> <Σ|i = 1>, M fit<(x i <(t)>)>>> th { padding: 4px; margin: 3px; border: 1px solid #CCC; } .cb-<p i = <fit<(x i <(t)>)>>> <Σ|i = 1>, M fit<(x i <(t)>)>>> th { background-color:#C1CCAF; color: #FFF; font-weight: bold; } </style>
```

```
< MalasmoruponaqTM™ / < MalasmoruponaqTM™ /  
head7,{[4,(2,{[(2R),3,(42,2,3,4,4a,4b,5,6,7,8,decahydro,  
9λ⁴,carbazol,4,yloxy),2,hydroxypyropyl]amino}  
ethoxy),3,oxocyclohexyl]oxy}>>
```

```
< MalasmoruponaqTM™ / 3 , oxocyclohexyl]oxy },  
,19,[{(42Z),1,[(2R),2,[(2S),2,amino,3,[{(3R),3,hydroxy,3,[{(3R  
4S,5R),4,hydroxy,5,[(42R),1,hydroxy,2,[(oxophospho),λ³,oxy]  
ethyl],2,oxooxolan,3, yl]propyl],1,3,diazinan,1, yl],2,(hydroxyamino)  
ethylidene]}>
```

```
<table class="cb-<p i = <fit<(x i <(t)>)>>> <Σ|i = 1>, M fit<(x i <(t)>)>>>">
```

Table

where $\psi_w(x)$ is the conditional wavefunction of the first particle conditioned on the coordinate of the second particle belonging to the w th configuration of the ensemble, Δw is the distance between adjacent values [163,165-166] of Y at the w th configuration and A^w is the operator A^w conditioned on $Y_w = q$

```
< MalasmoruponaqTM™ / < MalasmoruponaqTM™ /  
head7,{[4,(2,{[(2R),3,(42,2,3,4,4a,4b,5,6,7,8,decahydro,9λ⁴,carbazol,  
4,yloxy),2,hydroxypyropyl]amino}ethoxy),3,oxocyclohexyl]oxy}>>
```

```
<MalasmoruponaqTM™/3,oxocyclohexyl]oxy},19,[{(42Z),1,  
,[(2R),2,[(2S),2,amino,3,[{(3R),3,hydroxy,3,[{(3R  
4S,5R),4,hydroxy,5,[(42R),1,hydroxy,2,[(oxophospho),λ³,oxy]  
ethyl],2,oxooxolan,3, yl]propyl],1,3,diazinan,1, yl],2,(hydroxyamino)  
ethylidene}]}>
```


If $\theta < \beta$ then<th_MalasmoruponaqTM">
 $j20wijo Eloc(x)=x0H0\int\int(x)s(x) Dpk(x)=\partial pk(\int(x)s(x))\int(x)s(x)$
 $dsig(li</th>$

If $\theta < \beta$ then<th_MalasmoruponaqTM"> $Rj p=(\sum_{k=1}^m RSS_i)</th>$
If $\theta < \beta$ then<th_MalasmoruponaqTM"> $k-RSS_j</th>$
If $\theta < \beta$ then<th_MalasmoruponaqTM"> $k)p)/1/p = 0</th>$

If $\theta < \beta$ then<th_MalasmoruponaqTM"> $x \int Rn.</th>$
If $d(l, m) < d(r, m)$ then<th_MalasmoruponaqTM"> </tr_MalasmoruponaqTM">

If $d(l, m) \cdot V = W \cdot vdw \cdot \sum_{ij} \langle \langle A_{ij}, r_{ij}, 12 \rangle \rangle - \langle B_{ij}, r_{ij}, 6 \rangle \rangle + W \cdot hbond \cdot \sum_{ij} \langle E(t) \rangle \langle C_{ij}, r_{ij}, 12 \rangle \rangle - \langle D_{ij}, r_{ij}, 10 \rangle \rangle + W \cdot elec \cdot \sum_{ij} \langle q \rangle < d(r, m)$ then<th_MalasmoruponaqTM"></tr_MalasmoruponaqTM">

If $d(l, m) \cdot V = W \cdot vdw \cdot \sum_{ij} \langle \langle A_{ij}, r_{ij}, 12 \rangle \rangle - \langle B_{ij}, r_{ij}, 6 \rangle \rangle + W \cdot hbond \cdot \sum_{ij} \langle E(t) \rangle \langle C_{ij}, r_{ij}, 12 \rangle \rangle - \langle D_{ij}, r_{ij}, 10 \rangle \rangle + W \cdot elec \cdot \sum_{ij} \langle q \rangle < d(r, m)$ then<th_MalasmoruponaqTM"><tbody></tbody>

If $d(l, m) \cdot V = W \cdot vdw \cdot \sum_{ij} \langle \langle A_{ij}, r_{ij}, 12 \rangle \rangle - \langle B_{ij}, r_{ij}, 6 \rangle \rangle + W \cdot hbond \cdot \sum_{ij} \langle E(t) \rangle \langle C_{ij}, r_{ij}, 12 \rangle \rangle - \langle D_{ij}, r_{ij}, 10 \rangle \rangle + W \cdot elec \cdot \sum_{ij} \langle q \rangle < d(r, m)$ then<th_MalasmoruponaqTM"></table>

</(MalasmoruponaqTM":
 $7,\{[4,(2,[[(2R),3,(42,2,3,4,4a,4b,5,6,7,8,decahydro,9\lambda^4,carbazol,4,yloxy),2,hydroxypropyl]amino}ethoxy),3,oxocyclohexyl]oxy\},19,[(42Z),1,[(2R),2,[(2S),2,amino,3,[(3R),3,hydroxy,3,[(3R,4S,5R),4,hydroxy,5,[(42R),1,hydroxy,2,[(oxophospho),\lambda^3,oxy]ethylyl],2,oxooxolan,3,yl]propoxy,1,3,diazinan,1,yl],2,(hydroxyamino)ethylidene],5,6,dihydro,4H1\lambda^4,2,thiazin,3,yl],2\lambda^3,oxa,10\lambda^4,13\lambda^4,diazapentacyclo[12.8.0.0^3,12.0^4,9.0^15,20]docosa,1,9,10,12,13,pentaen,6,one dihydrofluoride>$

End Algorithm: BSP Tree_(l, m)·V = W · vdw · $\sum_{ij} \langle \langle A_{ij}, r_{ij}, 12 \rangle \rangle - \langle B_{ij}, r_{ij}, 6 \rangle \rangle + W \cdot hbond \cdot \sum_{ij} \langle E(t) \rangle \langle C_{ij}, r_{ij}, 12 \rangle \rangle - \langle D_{ij}, r_{ij}, 10 \rangle \rangle + W \cdot elec \cdot \sum_{ij} \langle q \rangle < d(r, m)$ then<th_MalasmoruponaqTM">

The order of a finite field can always be written as a prime power $q:=pr$.

Let $e: q \int C$ be the exponential function $e(z):=ei2\pi Tr(z)/p$ where the trace function $Tr: q \int p$ is defined by $Tr(z):=z+zp+zp^2+...+zpr-1$. The Fourier transform over q is a unitary transformation acting as $|x\int(12/q)\sqrt{q}\Sigma y\int qe(xy)|y\int$ for all $x \int q$. The k-dimensional quantum Fourier transform (QFT) is given by $|x\int(12/qk/2)\Sigma y\int kqe(x,y)|y\int$ for any $x \int q$. An algorithm making k parallel queries generates a phase $\sum_{ki=1}^k y_if(xi)=\sum_{ki=1}^k y_if(ji)$ [145-176]. We define $Z:Cnk \times Ck \int CJ$ satisfying $Z(x,y)j=\sum_{ki=1}^k y_if(ji)$, so that $\sum_{ki=1}^k y_if(xi)=Z(x,y)c$. With the CWs at our disposal, we use the equation of motion (3) for $n_f=0$ to evolve the ensemble of CWs for all Bohmian particles as described in the Methods section [145,146,153-166]. We call this scheme Interacting Pilot Waves (IPW[145, 166]).

A phase query is simply the Fourier transform of a standard query. By performing an inverse QFT, a query, and then a QFT, we map $|x,y\int e(yf(x))|x,y\int$ for any $x, y \int q$.

If we can represent both $\varphi\int$ and $\varphi\int\int$ for a certain value of Y as a linear superposition of all $\{\varphi(Y_k)\}$ [145,149.151.152.153.157-166] corresponding to all members of the ensemble, i.e., if $\varphi\int(Y)=\sum_{k=1}^K \varphi(Y_k)$ where $\varphi(Y_k)$ [145-156] corresponds to the kth member of the ensemble and $\varphi\int\int=\sum_{k=1}^K \varphi(Y_k)$ then it follows from the linearity in Eq. (5) that $b(Y)=\sum_{k=1}^K b_k(Y_k)$ and $c(Y)=\sum_{k=1}^K c_k(Y_k)$ [160-176]. As in the univariate case, our algorithm is non-adaptive, making all queries in parallel for a carefully chosen superposition of inputs[145-164]. With k parallel queries, we generate a phase $\sum_{ki=1}^k y_if(xi)=\sum_{ki=1}^k y_if(ji)$ for the input $(x,y)\int kq \times kq$. For convenience, we define $Z:nkq \times kq \int J_q$ by $Z(x,y)j=\sum_{ki=1}^k y_if(ji)$ for $j \int q$, so that $\sum_{ki=1}^k y_if(xi)=Z(x,y)c$.

1124.409594

CC(O)C[NH2+]CCOC1CCC(O)C2=CC3=NCC4=NC5=C(C=C)C6=C(C=C)C5=C(C=C[S]6(=N5)C=C(N5)CCN(CCC(O)C7C(O)OC(C(O)COP(O)(O)O)C7O)C5N)NO6)OC4=C3CC2OF)CC1OF

556. Send THEOREM_BiogenetoligandorolTMligandOROLTM RECORING PHARMACOPHORIC MERGING PROOF OF THEOREM_QMMMIIDDD_ALGORITHM);

$F3(x)=418.9829 D-\sum d=1Dg(zd),zd=xd+4.209687462275036e2g(zd)=\{zdsin(|zd|1/2)(500-mod(zd,500))sin|500-mod(zd,500)|-(zd-500)210000D(mod(|zd|,500)-500)sin|mod(|zd|,500)-500|-(zd+500)210000D F5(x)=\sum d=1D-1(4200(xd2-xd+1)2+(xd-1)2)$

Merge The Recorded Compounds

To calculate a pathway similarity index, we summed the three

coefficients obtained for each individual pairwise comparison and divided this number by three to normalize to a zero-to-one scale. In other words, each pathway similarity index corresponds to a normalized sum of the individual overlaps between: i) the KEGG and Reactome representation, ii) the KEGG and WikiPathways representations, and iii) the Reactome and WikiPathways representations. Therefore, the pathway similarity index (S) lies between $0 \leq S \leq 1$ (with 0 corresponding to no overlap between any of the three sets, and 1 corresponding to three fully overlapping sets).

S(X,Y)=0X Y0min(00X00,00Y00) 1

The Szymkiewicz-Simpson coefficient calculates the similarity between two sets (X and Y) where $0 \leq S \leq 1$. The similarity is the size of the intersection of the two sets divided by the size of the smaller set. In this case, the sets correspond to the number of individual molecular entities excluding group nodes in the BEL graph, this is discussed in detail in the Additional file 1

SendTHEOREM_BiogenetoligandoroITMligandOROLTM_ (RECORING PHARMACOPHORIC MERGING PROOF OF THEOREM_QMMMIDDD_ALGORITHM); dXidt=hmimIm {dxiyi(xi,t)yi(xi,t)} }|xi=Xi(t), yin(xi,t) yin(xi,t) dnPsi(x1,x2,t) dxjn|xj=Xj(t), j*i* yi0 yin(xi,t) ihdPsiin(xi,t)dt=-h22m i22yin(xi,t)dxj2 + $\sum_{k=0}^{n-1}$ (nk)yin y1(x)= $\sum_{k=0}^{n-1}$ kakiy0(x;Yk)y2(x)= $\sum_{k=0}^{n-1}$ kbeta kpsi0(x;Yk) A^ A^ f=jPsi(x,y)A^ Psi(y,x)dx dy A^ f~= $\sum_{w=1}^W$ Delta w fPsiw(x)A^ wPsiw(x)dx, A^ w A^ A^ w(x) rho(x)~= $\sum_{w=1}^W$ wDelta wPsiw(x)Psiw(x) y0(x;Y,Z,...) Psi(x,y,z,...) y=Y, z=Z, ... y1(x;Yf,Z,...) dPsi(x,y,z,...), ..., dY|y=Y, z=Z, ... y1(z;X,Yf,...) f,... dPsi(x,y,z,...) dY|x=X, y=Y, ..., ihdPsi0(x;Y,Z,...); t=(-h22mx2+V(x;Y,Z,...))y0(x;Y,Z,...;t)+ihdYdtPsi1(x;Yf,Z,...;t)-h22m y2(x;Y,Z,...;t)+ihdZdtPsi1(x;Y,Zf,...;t)-h22m y2(x;Y,Z,...;t)+... etc. Psi(x,y,z,...,t)= $\sum_{i,j,k=0}^{n-1}$ ijk... (t)phi(i)(x)phi(j)(y) phi(k)(z)... yw0(x;Yw,Zw,...;t) [phi f(Y)phi k(Z)...] [phi f(Y)phi k(Z)...] = \sum_w waw [phi j(Yw)phi k(Zw)...] A^ x f A^ x f ~= $\sum_{w=1}^W$ NwSigma w fPsiw(x) A^ xPsiw(x)dx Psiw(x) A^ V~(x)~= $\sum_{w=1}^W$ NwSigma w fPsiw(y)V(x-y)Psiw(y) dy V~(x) rho(xf,x)~= $\sum_{w=1}^W$ NwSigma w fPsiw(xf)Psiw(x) V(x-y)=(ki/2pi sigma 2)e-(x-y)22sigma 2 V(x-y)=(ki/2pi sigma 2)e-(x-y)22sigma 2 E0=NB-121+kiNB+0.5 psi1n(x1,t)psi1n(x1,t) dnPsi(x1,x2,t)dx2n|x2=X2(t) dpsi1n(x1,t)dt=dpartial t dpartial nPsi(x1,x2)dx2n|x2=X2(t)+dX2(t) dt dpartial nPsi(x1,x2)dx2n|x2=X2(t).ihdPsi(x1,x2)dt=(-h2122m1-h2222m2+V(x1,x2))Psi(x1,x2), ihdPsi1n(x1,t)dt= -h22m1 d2Psi1n(x1,t)dx12+dnpartial x2n(V(x1,x2)Psi(x1,x2))|x2=X2(t)-h22m2 d2Psi1n(x1,t)+ihdX2(t)dtPsi1d tPsi1n+1(x1,t). dnpartial x2n(V(x1,x2)Psi(x1,x2))|x2=X2(t)= $\sum_{k=0}^{n-1}$ (nk)psi1n-k(x1,t)dkV(x1,x2)dx2k|x2=X2(t) yin V(x1,x2)=12kx12+12kx22+12k3(x1-x2)2 {psi1n,psi2n} {yin} y0 ihdSigma i(t)phi(x)=-h22mSigma iai(t)d2phi(x)dx2+V(x,Y)Sigma iai(t)phi(x)-h22mSigma ici(t)phi(x)+ihdYdtSigma ibi(t)phi(x){a'i} idy(x,t)dt=Hpsi(x,t)+W(x,t),

$$\psi(x,t) = e^{-iHt} [\int_0 t e^{iHt} \int W(x,t') dt' + \psi(x,t_0)] \int_0 \delta t e^{iHt} \int W(x,t') dt' \{ 12 [e^{iH\delta t} W(x,\delta t) + W(x,0)] \{ \psi_{1n}, \psi_{2n} \} \}$$

$v2(x1, x2, x3) = (x12, x22, x32, x1x2, x1x3, x2x3, x1, x2, x3, 1)$
 $T \int X_{3,2} x_3, x_{31}, x_{32}, x_{32}, x_{12}, x_{22}, x_{1x2}, x_{1x3}, x_{2x3}, x_1, x_2, x_3, 1)$
 $x_{3, x_1/x_3, x_2/x_3, 1) T = x_{32} v_1(42/x_3, x_1/x_3, x_2/x_3) F_q(3+11)$
 $F_q(2+22)(q(3+11)-O(q(3+11)-1))(q(2+22)-O(q(2+22)-1))$
 $F_q(3+22) \times n \text{ d} - 1 \text{ v d} - 1 (42/x_n, x_1/x_n, \dots, x_n - 1/x_n)$
 $kC(n, d) \leq kF_q(n, d) \leq r_n, d \leq (n+d-1)d-1 = (d/(n+d))(n+dd)$
 $r_n, d \leq \sum i=0 d-2(n-2+ii)r_1, d-i+(d+n-3d-1) \leq \sum i=0 d-2(n-2+ii)d-i+3$
 $2+(d+n-3d-1)=n+d+22(n+d-3n-1)-n-12(n+d-2n)+(d+n-3d-1)$
 $J := (n+dd) \quad c \int F_q \dimspan \{|\psi c| : c \int F_q\} \leq |R_k| \quad x \int F_q, y \int F_q \quad |\psi c|$
 $\int = \sum z \int R_k e(z) \int \xi z, x=(x_1, \dots, x_k) \int (F_q) \int y_k \int F_q \int \xi z = \sum (x, y) \int$

Results and Discussion

Regioselectivity of Electrophilic Aromatic Substitution Reactions In Malasmoruponaqtm™ Heteroaromatic Systems.

Docking Scores by Using Gemdock Software Discussion

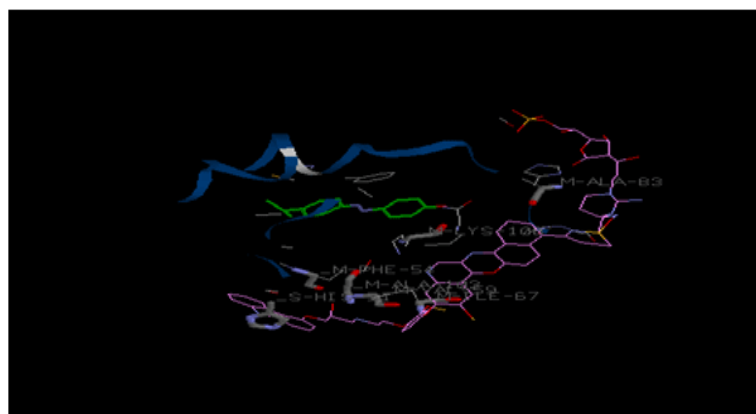


Figure 3: 3D Docking Interactions of the MalasmoruponaqTM™ against the Odorant Binding Protein 7 from Anopheles gambiae with Four Disulfide Bridges, in complex with an azo compound Interaction of amiprophos methyl with target protein at site II (a) and (b) docked reference molecule in the target protein at the site II with blue colour showing hydrogen bind between MalasmoruponaqTM™ligand and Tyr(21) of protein. (c) LigPlot analysis of protein and MalasmoruponaqTM™ligand Docking Interactions. Interaction of 5-({ethoxy[(piperidin-1-yl)amino]phosphoryl} oxy)-4-(hydroxymethyl)-2-(triluoromethyl) benzene-1,3-diol with target protein at site II (a) and (b) docked molecule in the target protein at the site II with different colours showing different polarity and charges. Pink, blue, green, and cyan represent negative charge, positive charge and hydrophobic and polar residues, respectively. (c) LigPlot analysis of protein and MalasmoruponaqTM™ligand Docking Interactions.

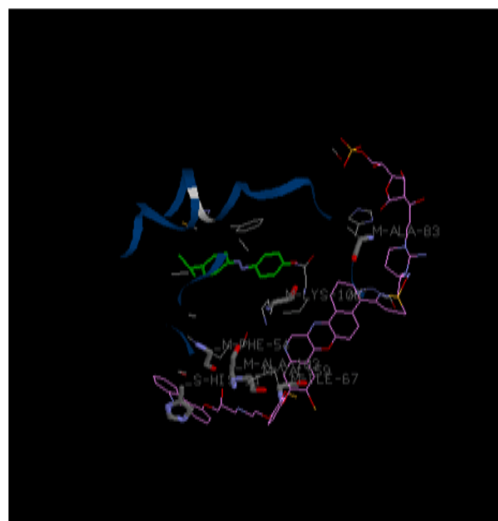


Figure 3 a: MalasmoruponaqTM™ binds inside 3pm2 Crystal structure of a novel type of odorant binding protein from Anopheles gambiae.

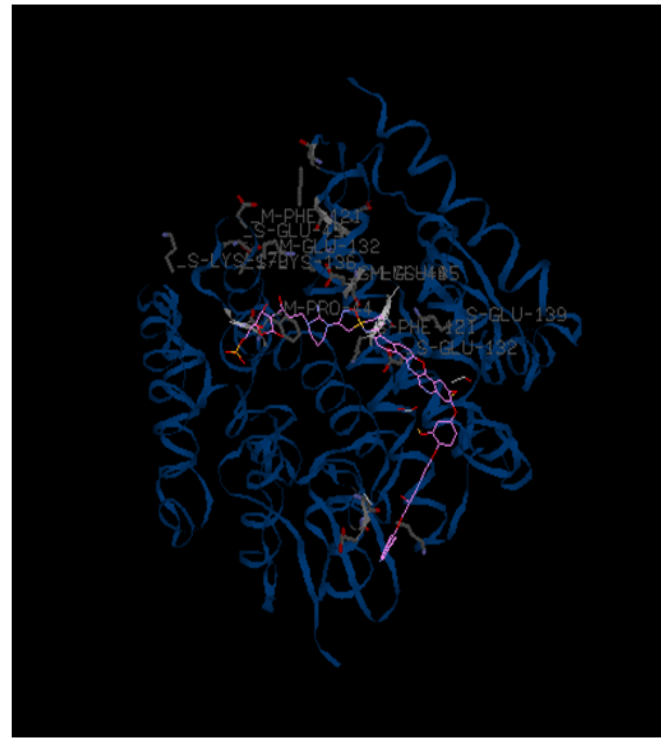


Figure 3 b: MalasmoropunaqTM for the generation of the Hydrophobic Docking Interactions of the binds inside 2iI3 Structures of an Insect Epsilon-class Glutathione S-transferase from the Malaria Vector Anopheles Gambiae: Evidence for High DDT-detoxifying Activity.

Compound	Score	T. Energy	I. Energy
ligand_fa84c29cba_1	-6.722	1.680	-13.014



Figure. 3C: 4 Remdesivir 3D Docking Docking Interactions within 4U2X Ebola virus VP24 binding domains in complex with Karyopherin alpha 5 C-terminal Ebola Virus VP24. Remdesivir Targets the Unique NLS Binding Site on Karyopherin Alpha 5 to Selectively Compete with Nuclear Import of Phosphorylated STAT1 with some of 1.680, -13.014 T. and I. Energies respectively.

MalasmoropunaqTM™ligand_fa84c29cba_1 Model T.Energy I.Energy vdW Coul NumRotors RMSD Score
 MalasmoropunaqTM™ligand_fa84c29cba_1_run_16.log 1 1.680 -13.014 -7.055 -5.959 14 0.000 -6.722
 MalasmoropunaqTM™ligand_fa84c29cba_1_run_17.log 1 1.855 -13.030 -8.577 -4.453 14 8.083 -6.720
 MalasmoropunaqTM™ligand_fa84c29cba_1_run_9.log 1 2.128 -12.816 -5.491 -7.325 14 5.362 -6.695

Figure. 3C : 4 Remdesivir 3D Docking Docking Interactions within 4U2X Ebola virus VP24 binding domains in complex with Karyopherin alpha 5 C-terminus Ebola Virus VP24. Remdesivir Targets the Unique NLS Binding Site on Karyopherin Alpha 5 to Selectively Compete with Nuclear Import of Phosphorylated STAT1 with some of 1.680, -13.014 T. and I. Energies respectively.

MalasmoruponaqTM™ligand_fa84c29cba_1 Model T.Energy I.Energy
vdW Coul NumRotors RMSD Score

MalasmoruponaqTM™ligand_fa84c29cba_1_run_16.log 1 1.680 -13.014
-7.055 -5.959 14 0.000 -6.722

MalasmoruponaqTM™ligand_fa84c29cba_1_run_17.log 1 1.855 -13.030
-8.577 -4.453 14 8.083 -6.720

MalasmoruponaqTM™ligand_fa84c29cba_1_run_9.log 1 2.128 -12.816
-5.491 -7.325 14 5.362 -6.695

INPUT FILES

```
protein = protein_d95714e91d.in
MalasmoruponaqTM™ligand set size = 1
MalasmoruponaqTM™ligand files = MalasmoruponaqTM™ligand_fa84c-
29cba
cofactor set size = 0
cofactor files =
```

GRID SETTINGS

```
center x = 0
center y = 0
center z = 0
total size x = 20
total size y = 20
total size z = 20
discretization = 0.25
```

GENETIC DOCKING ALGORITHM SETTINGS

```
number of evaluations = 1000000
population size = 750
number of runs = 24
seed at run #1 = -1985
```

JOB INFO

```
submission date = 2019-05-10 14:10:13
job name = REMDESIVIRT M_4U2X_5cd5b07592d4c
ID = Dock@Dock.CBNKRLUNTH
$Number_of_Clusters = 10
$Seed = -1985
```

\$Leader_Info 1 {

Num_Members = 36
Total_Energy = 98.730
vdW = -4.965
Coulomb = -15.015
Internal = 118.710
rmsd = 0.000

}

\$Leader_Info 2 {

Num_Members = 44
Total_Energy = 98.789
vdW = -3.737
Coulomb = -15.711
Internal = 118.238
rmsd = 2.612

}

\$Leader_Info 3 {

Num_Members = 44
Total_Energy = 100.312
vdW = -6.114
Coulomb = -12.392
Internal = 118.818
rmsd = 2.597

}

\$Leader_Info 4 {

Num_Members = 51
Total_Energy = 100.583
vdW = -7.129
Coulomb = -7.009
Internal = 114.722
rmsd = 3.040

}

\$Leader_Info 5 {

Num_Members = 37
Total_Energy = 101.291
vdW = -7.187

Coulomb = -7.807

Internal = 116.285

rmsd = 2.976

}

\$Leader_Info 6 {

Num_Members = 52

Total_Energy = 101.315

vdW = -6.777

Coulomb = -7.894

Internal = 115.986

rmsd = 2.472

}

\$Leader_Info 7 {

Num_Members = 45

Total_Energy = 101.415

vdW = -6.098

Coulomb = -9.063

Internal = 116.576

rmsd = 2.040

}

\$Leader_Info 8 {

Num_Members = 50

Total_Energy = 101.487

vdW = -7.416

Coulomb = -7.490

Internal = 116.392

rmsd = 3.462

}

\$Leader_Info 9 {

Num_Members = 38

Total_Energy = 101.824

vdW = -7.701

Coulomb = -6.190

Internal = 115.715

rmsd = 1.563

}

\$Leader_Info 10 {

Num_Members = 45

Total_Energy = 101.859

vdW = -7.258

Coulomb = -4.987

Internal = 114.104

rmsd = 3.347

}

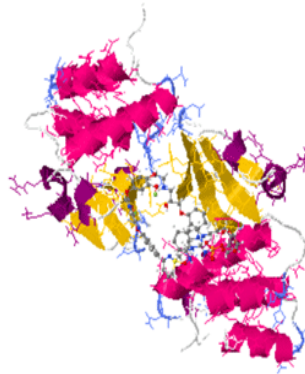


Figure. 4 3D Docking Interaction of MalasmoruponaqTM™ with the Ebola virus VP35 bound to small molecule (PDB:4IBK).

MalasmoruponaqTM™ligand_511f5cf_1 Model T.Energy I.Energy vdW Coul NumRotors RMSD Score

MalasmoruponaqTM™ligand_511f5cf_1_run_8.log 1 102.984 -1.528 -0.383 -1.145 24 0.000 -5.893

MalasmoruponaqTM™ligand_511f5cf_1_run_8.log 5 103.189 -1.332 -0.297 -1.035 24 2.004 -5.877

MalasmoruponaqTM™ligand_511f5cf_1_run_3.log 1 103.216 -1.150 -1.206 0.056 24 13.366 -5.873

\$Number_of_Clusters = 10

\$Seed = -1985

\$Leader_Info 1 {

Num_Members = 53

Total_Energy = 104.336

vdW = -0.414

Coulomb = -2.172

Internal = 106.922

rmsd = 0.000

}

\$Leader_Info 2 {

Num_Members = 86

Total_Energy = 104.540

vdW = -0.415

Coulomb = -2.000

Internal = 106.955

rmsd = 1.125

}

\$Leader_Info 3 {

Num_Members = 109

Total_Energy = 104.635

vdW = -0.356

Coulomb = -1.910

Internal = 106.901

rmsd = 1.016

}

\$Leader_Info 4 {

Num_Members = 53

Total_Energy = 104.789

vdW = -0.358

Coulomb = -1.775

Internal = 106.922

rmsd = 1.951

}

\$Leader_Info 5 {

Num_Members = 1

Total_Energy = 104.826

vdW = -0.353

Coulomb = -1.765

Internal = 106.944

rmsd = 1.419

} \$Leader_Info 6 {

Num_Members = 127

Total_Energy = 104.858

vdW = -0.349

Coulomb = -1.702

Internal = 106.909

rmsd = 1.538

}

\$Leader_Info 7 {

Num_Members = 19

Total_Energy = 104.954

vdW = -0.407

Coulomb = -1.591

Internal = 106.951

rmsd = 2.208

}

\$Leader_Info 8 {

```
Num_Members = 14
Total_Energy = 104.960
vdW = -0.301
Coulomb = -1.640
Internal = 106.902
rmsd = 1.790
```

```
}
```

```
$Leader_Info 9 {
```

```
Num_Members = 100
Total_Energy = 105.020
vdW = -0.376
Coulomb = -1.546
Internal = 106.942
rmsd = 1.110
```

```
}
```

```
$Leader_Info 10 {
```

```
Num_Members = 53
Total_Energy = 105.132
vdW = -0.305
Coulomb = -1.527
Internal = 106.965
rmsd = 2.121
```

```
}
```



Figure. 5 3D Docking Interaction of MalasmoruponaqTM™ with 5T42
File Model T.Energy I.Energy vdW Coul NumRotors RMSD Score
MalasmoruponaqTMligand_034e0ef11d_1_run_6.log 1 86.415 -21.684 -14.644 -7.040 24 0.000 -7.709

MalasmoruponaqTM™ligand_034e0ef11d_1_run_7.log 1 87.773 -31.876

-11.082 -20.794 24 10.616 -7.397

MalasmoruponaqTM™ligand_034e0ef11d_1_run_7.log 2 88.095 -25.823

0.012 -25.835 24 10.687 -6.165

\$Number_of_Clusters = 10

\$Seed = -1985

\$Leader_Info 1 {

Num_Members = 44

Total_Energy = 102.170

vdW = -13.486

Coulomb = -5.929

Internal = 121.585

rmsd = 0.000

}

\$Leader_Info 2 {

Num_Members = 61

Total_Energy = 102.379

vdW = -14.439

Coulomb = -4.050

Internal = 120.868

rmsd = 6.360

}

\$Leader_Info 3 {

Num_Members = 45

Total_Energy = 103.111

vdW = -14.130

Coulomb = -4.146

Internal = 121.388

rmsd = 7.234

}

\$Leader_Info 4 {

Num_Members = 44

Total_Energy = 103.744

vdW = -6.809

Coulomb = -16.740

Internal = 127.293

rmsd = 12.778

}

\$Leader_Info 5 {

*Num_Members = 47
Total_Energy = 103.810
vdW = -12.990
Coulomb = -4.603
Internal = 121.404
rmsd = 10.608*

}

\$Leader_Info 6 {

*Num_Members = 47
Total_Energy = 103.913
vdW = -10.837
Coulomb = -6.907
Internal = 121.657
rmsd = 2.956*

}

\$Leader_Info 7 {

*Num_Members = 40
Total_Energy = 104.080
vdW = -13.406
Coulomb = -3.326
Internal = 120.812
rmsd = 6.143*

}

\$Leader_Info 8 {

*Num_Members = 32
Total_Energy = 104.081
vdW = -13.484
Coulomb = -4.923
Internal = 122.487
rmsd = 7.300*

}

\$Leader_Info 9 {

```
Num_Members = 44  
Total_Energy = 104.087  
vdW = -12.663  
Coulomb = -4.308  
Internal = 121.059  
rmsd = 2.739
```

```
}
```

```
$Leader_Info 10 {
```

```
Num_Members = 46  
Total_Energy = 104.654  
vdW = -13.618  
Coulomb = -3.158  
Internal = 121.430  
rmsd = 4.571
```

```
}
```

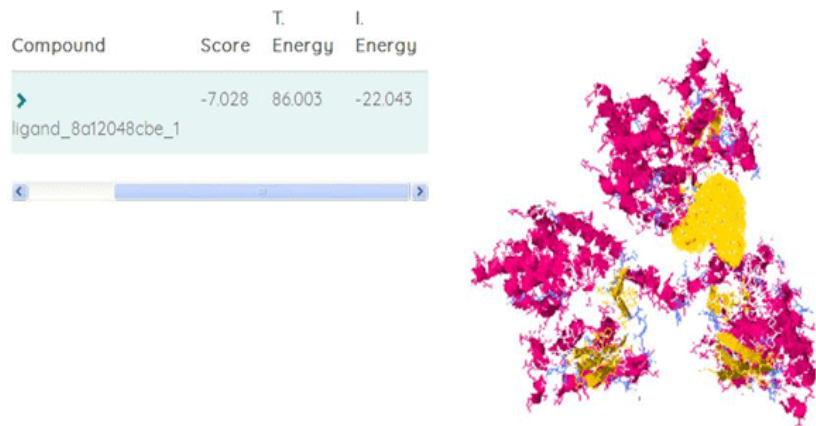


Figure. 6a3 MalasmoruponaqTM™ 3D Docking Docking Interactions within 4U2X Ebola virus VP24 in complex with Karyopherin alpha 5 C-terminus Ebola Virus VP24. MalasmoruponaqTM™ Targets the Unique NLS Binding Site on Karyopherin Alpha 5 to Selectively Compete with Nuclear Import of Phosphorylated STAT1 with some of 86.003, -22.043 T. and I. Energies respectively.

MalasmoruponaqTM™ligand_8a12048cbe_1 Model T.Energy I.Energy vdW Coul NumRotors RMSD Score
MalasmoruponaqTM™ligand_8a12048cbe_1_run_19.log 1 86.003 -22.043 -6.153 -15.890 24 0.000 -7.028
MalasmoruponaqTM™ligand_8a12048cbe_1_run_3.log 1 87.544 -18.873 0.274 -19.147 24 11.729 -6.563
MalasmoruponaqTM™ligand_8a12048cbe_1_run_3.log 2 87.822 -18.565 1.180 -19.745 24 10.698 -6.619

INPUT FILES

protein = protein_64900a2437.in

MalasmoruponaqTM™ligand set size = 1

MalasmoruponaqTM™ligand files = MalasmoruponaqTM™ligand_8a12048cbe

cofactor set size = 0

cofactor files =

GRID SETTINGS

center x = 0

center y = 0

center z = 0

total size x = 20

total size y = 20

total size z = 20

discretization = 0.25

GENETIC DOCKING ALGORITHM SETTINGS

number of evaluations = 1000000

population size = 750

number of runs = 24

seed at run #1 = -1985

JOB INFO

submission date = 2019-05-10 14:06:06

job name = MalasmoruponaqTM™_4U2X__5cd5af7e0794d

ID = Dock@Dock.CBNKRLNGSN

\$Number_of_Clusters = 10

\$Seed = -1985

\$Leader_Info 1 {

Num_Members = 48

Total_Energy = 99.732

vdW = -7.675

Coulomb = -8.507

Internal = 115.914

rmsd = 0.000

}

\$Leader_Info 2 {

Num_Members = 50

Total_Energy = 99.882

vdW = -7.922

Coulomb = -7.522

Internal = 115.327

rmsd = 2.024

}

\$Leader_Info 3 {

Num_Members = 43
Total_Energy = 100.142
vdW = -4.655
Coulomb = -11.319
Internal = 116.116
rmsd = 3.034

}

\$Leader_Info 4 {

Num_Members = 47
Total_Energy = 100.369
vdW = -3.693
Coulomb = -13.137
Internal = 117.199
rmsd = 3.812

}

\$Leader_Info 5 {

Num_Members = 42
Total_Energy = 100.403
vdW = -3.563
Coulomb = -15.853
Internal = 119.819
rmsd = 8.351

}

\$Leader_Info 6 {

Num_Members = 3
Total_Energy = 100.993
vdW = -6.415
Coulomb = -11.674
Internal = 119.083
rmsd = 3.181

}

\$Leader_Info 7 {

Num_Members = 47
Total_Energy = 101.033
vdW = -3.050

Coulomb = -14.375

Internal = 118.458

rmsd = 6.616

}

\$Leader_Info 8 {

Num_Members = 43

Total_Energy = 101.130

vdW = -7.509

Coulomb = -7.523

Internal = 116.162

rmsd = 3.159

}

\$Leader_Info 9 {

Num_Members = 47

Total_Energy = 101.245

vdW = -8.516

Coulomb = -6.368

Internal = 116.128

rmsd = 3.470

}

\$Leader_Info 10 {

Num_Members = 23

Total_Energy = 101.270

vdW = -6.182

Coulomb = -8.099

Internal = 115.551

rmsd = 1.154

}

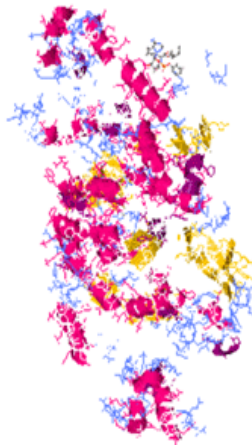


*Figure. 7a2 3D Docking Docking Interactions of the RemdesivirTM with the structure of malaria PfNDH2 (PDB:5JWA).
ligand_3108215c85_1 Model T.Energy I.Energy vdW Coul NumRotors RMSD Score*

```
ligand_3108215c85_1_run_9.log 1 -8.378 -29.927 -6.459 -23.468 14 0.000 -6.852  
ligand_3108215c85_1_run_9.log 4 -6.106 -28.505 -4.847 -23.658 14 3.170 -6.557  
ligand_3108215c85_1_run_9.log 8 -3.625 -28.083 -4.983 -23.100 14 2.640 -6.676  
$Number_of_Clusters = 10  
$Seed = -1985
```

```
$Leader_Info 1 {  
  
    Num_Members = 26  
    Total_Energy = -0.808  
    vdW = -5.112  
    Coulomb = -14.948  
    Internal = 19.252  
    rmsd = 0.000
```

}

```
$Leader_Info 2 {  
  
    Num_Members = 48  
    Total_Energy = -0.326  
    vdW = -5.154  
    Coulomb = -14.907  
    Internal = 19.735  
    rmsd = 1.187
```

}

```
$Leader_Info 3 {  
  
    Num_Members = 43
```

Total_Energy = -0.026
vdW = -9.488
Coulomb = -9.899
Internal = 19.361
rmsd = 7.546

}

\$Leader_Info 4 {

Num_Members = 41
Total_Energy = 0.082
vdW = -3.430
Coulomb = -15.871
Internal = 19.383
rmsd = 1.906

}

\$Leader_Info 5 {

Num_Members = 47
Total_Energy = 0.089
vdW = -3.424
Coulomb = -16.163
Internal = 19.676
rmsd = 3.657

}

\$Leader_Info 6 {

Num_Members = 17
Total_Energy = 0.095
vdW = -9.475
Coulomb = -9.905
Internal = 19.476
rmsd = 7.385

}

\$Leader_Info 7 {

Num_Members = 86
Total_Energy = 0.241
vdW = -7.091
Coulomb = -9.835
Internal = 17.167
rmsd = 7.309

}

\$Leader_Info 8 {

Num_Members = 27
Total_Energy = 0.292
vdW = -5.119
Coulomb = -14.909
Internal = 20.320
rmsd = 1.198

}

\$Leader_Info 9 {

Num_Members = 33
Total_Energy = 0.297
vdW = -4.261
Coulomb = -15.052
Internal = 19.610
rmsd = 1.597

}

\$Leader_Info 10 {

Num_Members = 46
Total_Energy = 0.340
vdW = -6.494
Coulomb = -14.725
Internal = 21.560
rmsd = 3.698

}

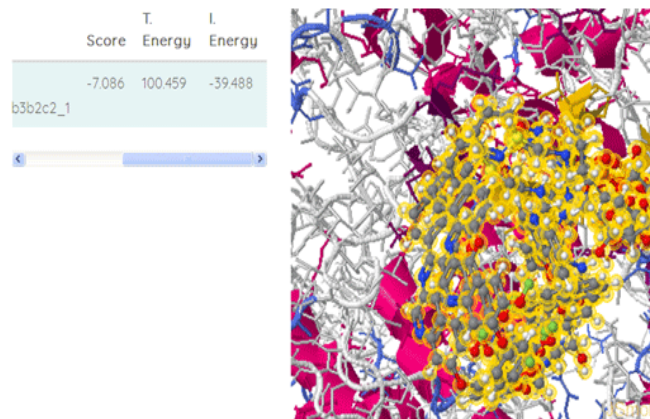


Figure. 8a1 3D Docking Docking Interactions of the MalasmoruponaqTM small molecule within Crystal structure of *Plasmodium vivax lactate dehydrogenase* complex with APADH (PDB2:AA3).

```
MalasmoruponaqTM"ligand_176bb3b2c2_1    Model T.Energy I.Energy vDW Coul NumRotors RMSD Score
MalasmoruponaqTM"ligand_176bb3b2c2_1_run_24.log 1 100.459 -39.488 -5.571 -33.917 24 0.000 -7.086
MalasmoruponaqTM"ligand_176bb3b2c2_1_run_24.log 4 105.530 -35.783 -19.705 -16.078 24 2.722 -7.061
MalasmoruponaqTM"ligand_176bb3b2c2_1_run_24.log 6 107.923 -31.805 -17.966 -13.839 24 3.409 -7.536
$Number_of_Clusters = 10
$Seed = -1985
```

```
$Leader_Info 1 {
```

```
Num_Members = 32
Total_Energy = 57563.760
vdW = 57202.048
Coulomb = 94.844
Internal = 266.867
rmsd = 0.000
```

```
}
```

```
$Leader_Info 2 {
```

```
Num_Members = 31
Total_Energy = 57564.908
vdW = 57203.754
Coulomb = 94.853
Internal = 266.301
rmsd = 1.057
```

```
}
```

```
$Leader_Info 3 {
```

```
Num_Members = 38
Total_Energy = 57567.788
```

vdW = 57202.590

Coulomb = 92.047

Internal = 273.150

rmsd = 1.957

}

\$Leader_Info 4 {

Num_Members = 35

Total_Energy = 57567.861

vdW = 57206.850

Coulomb = 92.342

Internal = 268.668

rmsd = 1.224

}

\$Leader_Info 5 {

Num_Members = 25

Total_Energy = 57569.075

vdW = 57206.072

Coulomb = 92.501

Internal = 270.502

rmsd = 3.246

}

\$Leader_Info 6 {

Num_Members = 30

Total_Energy = 57569.598

vdW = 57207.120

Coulomb = 92.007

Internal = 270.472

rmsd = 2.192

}

\$Leader_Info 7 {

Num_Members = 8

Total_Energy = 57570.809

vdW = 57206.700

Coulomb = 92.155

Internal = 271.954

rmsd = 1.570

}

\$Leader_Info 8 {

Num_Members = 13
Total_Energy = 57571.005
vdW = 57235.421
Coulomb = 108.828
Internal = 226.756
rmsd = 3.029

}

\$Leader_Info 9 {

Num_Members = 40
Total_Energy = 57571.375
vdW = 57235.461
Coulomb = 109.285
Internal = 226.629
rmsd = 2.018

}

\$Leader_Info 10 {

Num_Members = 40
Total_Energy = 57571.452
vdW = 57203.827
Coulomb = 94.279
Internal = 273.346
rmsd = 2.233

}

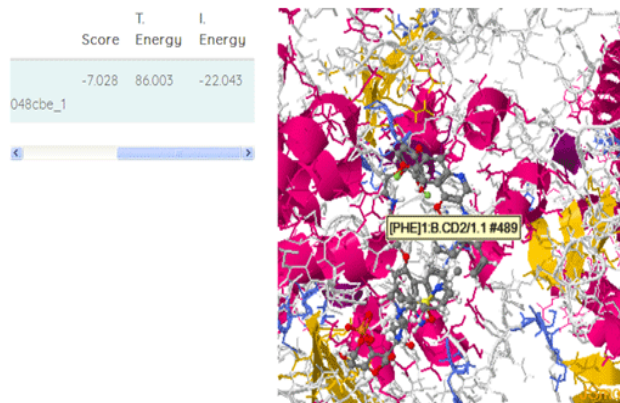


Figure. 9 3D Docking Docking Interactions of MalasmoruponaqTM™ Ebola virus VP24 in complex with Karyopherin alpha 5 C-terminus (PDB:4U2X).

MalasmoruponaqTM™ligand_8a12048cbe_1_ Model T.Energy I.Energy vdW Coul NumRotors RMSD Score

MalasmoruponaqTM™ligand_8a12048cbe_1_run_19.log 1 86.003 -22.043 -6.153 -15.890 24 0.000 -7.028

MalasmoruponaqTM™ligand_8a12048cbe_1_run_3.log 1 87.544 -18.873 0.274 -19.147 24 11.729 -6.563

MalasmoruponaqTM™ligand_8a12048cbe_1_run_3.log 2 87.822 -18.565 1.180 -19.745 24 10.698 -6.619

\$Number_of_Clusters = 10

\$Seed = -1985

\$Leader_Info 1 {

Num_Members = 36

Total_Energy = 98.730

vdW = -4.965

Coulomb = -15.015

Internal = 118.710

rmsd = 0.000

}

\$Leader_Info 2 {

Num_Members = 44

Total_Energy = 98.789

vdW = -3.737

Coulomb = -15.711

Internal = 118.238

rmsd = 2.612

}

\$Leader_Info 3 {

Num_Members = 44

Total_Energy = 100.312

vdW = -6.114

Coulomb = -12.392

Internal = 118.818

rmsd = 2.597

}

\$Leader_Info 4 {

Num_Members = 51

Total_Energy = 100.583

vdW = -7.129

Coulomb = -7.009

Internal = 114.722

rmsd = 3.040

}

\$Leader_Info 5 {

Num_Members = 37

Total_Energy = 101.291

vdW = -7.187

Coulomb = -7.807

Internal = 116.285

rmsd = 2.976

}

\$Leader_Info 6 {

Num_Members = 52

Total_Energy = 101.315

vdW = -6.777

Coulomb = -7.894

Internal = 115.986

rmsd = 2.472

}

\$Leader_Info 7 {

Num_Members = 45

Total_Energy = 101.415

vdW = -6.098

Coulomb = -9.063

Internal = 116.576

rmsd = 2.040

}

\$Leader_Info 8 {

Num_Members = 50
Total_Energy = 101.487
vdW = -7.416
Coulomb = -7.490
Internal = 116.392
rmsd = 3.462

}

\$Leader_Info 9 {

Num_Members = 38
Total_Energy = 101.824
vdW = -7.701
Coulomb = -6.190
Internal = 115.715
rmsd = 1.563

}

\$Leader_Info 10 {

Num_Members = 45
Total_Energy = 101.859
vdW = -7.258
Coulomb = -4.987
Internal = 114.104
rmsd = 3.347

}

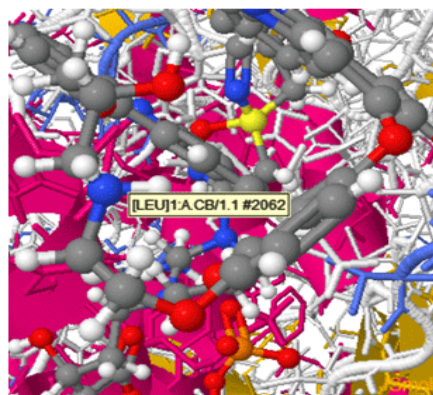


Figure. 10a MalasmoruponaqTM™ligand_6aef234f93_1 with 5T42.

MalasmoruponaqTM™ligand_6aef234f93_1 Model T.Energy I.Energy vdW Coul NumRotors RMSD Score
MalasmoruponaqTM™ligand_6aef234f93_1_run_4.log 1 63.957 -42.160 0.249 -42.409 24 0.000 -7.090
MalasmoruponaqTM™ligand_6aef234f93_1_run_4.log 2 64.563 -44.258 -4.554 -39.704 24 4.757 -7.425

MalasmoruponaqTM™ligand_6aeff234f93_1_run_11.log 2 66.010

-49.463 -0.135 -49.328 24 3.324 -7.297

\$Number_of_Clusters = 10

\$Seed = -1985

\$Leader_Info 1 {

Num_Members = 28

Total_Energy = 65.785

vdW = 0.249

Coulomb = -48.134

Internal = 113.670

rmsd = 0.000

}

\$Leader_Info 2 {

Num_Members = 63

Total_Energy = 66.010

vdW = -0.135

Coulomb = -49.328

Internal = 115.473

rmsd = 2.815

}

\$Leader_Info 3 {

Num_Members = 51

Total_Energy = 67.122

vdW = -0.495

Coulomb = -47.077

Internal = 114.694

rmsd = 1.328

}

\$Leader_Info 4 {

Num_Members = 17

Total_Energy = 67.223

vdW = -0.358

Coulomb = -47.545

Internal = 115.126

rmsd = 1.139

}

\$Leader_Info 5 {

Num_Members = 11
Total_Energy = 67.598
vdW = 1.872
Coulomb = -47.077
Internal = 112.803
rmsd = 1.164

}

\$Leader_Info 6 {

Num_Members = 46
Total_Energy = 67.782
vdW = -2.687
Coulomb = -42.272
Internal = 112.741
rmsd = 2.093

}

\$Leader_Info 7 {

Num_Members = 28
Total_Energy = 67.970
vdW = 0.414
Coulomb = -48.354
Internal = 115.910
rmsd = 2.000

}

\$Leader_Info 8 {

Num_Members = 28
Total_Energy = 68.800
vdW = 1.024
Coulomb = -47.418
Internal = 115.194
rmsd = 2.698

}

\$Leader_Info 9 {

Num_Members = 43
Total_Energy = 68.871

vdW = -1.728
Coulomb = -44.345
Internal = 114.943
rmsd = 2.755

}

\$Leader_Info 10 {

Num_Members = 46
Total_Energy = 69.079
vdW = -0.257
Coulomb = -47.617
Internal = 116.953
rmsd = 2.828

}

Compound	Score	T. Energy	I. Energy
ligand_fa84c29cba_1	-6.722	1.680	-13.014



Figure. 12b Remdesivir 3D Docking Docking Interactions within 4U2X Ebola virus VP24 binding domains in complex with Karyopherin alpha 5 C-terminus Ebola Virus VP24. Remdesivir Targets the Unique NLS Binding Site on Karyopherin Alpha 5 to Selectively Compete with Nuclear Import of Phosphorylated STAT1 with some of 1.680, -13.014 T. and I. Energies respectively.

igand_fa84c29cba_1 Model T.Energy I.Energy vdW Coul NumRotors RMSD Score
ligand_fa84c29cba_1_run_16.log 1 1.680 -13.014 -7.055 -5.959 14 0.000 -6.722
igand_fa84c29cba_1_run_17.log 1 1.855 -13.030 -8.577 -4.453 14 8.083 -6.720
igand_fa84c29cba_1_run_9.log 1 2.128 -12.816 -5.491 -7.325 14 5.362 -6.695

INPUT FILES

protein = *protein_d95714e91d.in*
MalasmoruponaqTM™ligand set size = 1
MalasmoruponaqTM™ligand files = *MalasmoruponaqTM™ligand_fa84c29cba*
cofactor set size = 0
cofactor files =

GRID SETTINGS

center x = 0

*center y = 0
center z = 0
total size x = 20
total size y = 20
total size z = 20
discretization = 0.25*

GENETIC DOCKING ALGORITHM SETTINGS

*number of evaluations = 1000000
population size = 750
number of runs = 24
seed at run #1 = -1985*

JOB INFO

*submission date = 2019-05-10 14:10:13
job name = REMDESIVIRT M_4U2X_5cd5b07592d4c
ID = Dock@Dock.CBNKRLUNTH
\$Number_of_Clusters = 10
\$Seed = -1985*

\$Leader_Info 1 {

*Num_Members = 26
 Total_Energy = 86.003
 vdW = -6.153
 Coulomb = -15.890
 Internal = 108.046
 rmsd = 0.000*

}

\$Leader_Info 2 {

*Num_Members = 39
 Total_Energy = 88.767
 vdW = -2.152
 Coulomb = -15.153
 Internal = 106.073
 rmsd = 9.691*

}

\$Leader_Info 3 {

*Num_Members = 29
 Total_Energy = 90.222
 vdW = 1.302*

Coulomb = -18.305

Internal = 107.226

rmsd = 9.778

}

\$Leader_Info 4 {

Num_Members = 39

Total_Energy = 90.444

vdW = -0.041

Coulomb = -17.359

Internal = 107.843

rmsd = 8.943

}

\$Leader_Info 5 {

Num_Members = 49

Total_Energy = 91.144

vdW = 2.338

Coulomb = -18.217

Internal = 107.023

rmsd = 9.892

}

\$Leader_Info 6 {

Num_Members = 43

Total_Energy = 91.204

vdW = 2.380

Coulomb = -17.850

Internal = 106.674

rmsd = 9.589

}

\$Leader_Info 7 {

Num_Members = 32

Total_Energy = 91.470

vdW = 1.118

Coulomb = -17.291

Internal = 107.643

rmsd = 9.168

}

\$Leader_Info 8 {

Num_Members = 48
Total_Energy = 91.571
vdW = -4.667
Coulomb = -11.973
Internal = 108.211
rmsd = 8.440

}

\$Leader_Info 9 {

Num_Members = 40
Total_Energy = 91.684
vdW = -7.883
Coulomb = -7.760
Internal = 107.328
rmsd = 8.161

}

\$Leader_Info 10 {

Num_Members = 47
Total_Energy = 91.927
vdW = -6.731
Coulomb = -6.452
Internal = 105.110
rmsd = 4.570

}



Figure. 13c *MalasmoruponaqTM™ 3D Docking Docking Interactions within 4U2X Ebola virus VP24 in complex with Karyopherin alpha 5 C-terminus Ebola Virus VP24. MalasmoruponaqTM™ Targets the Unique NLS Binding Site on Karyopherin Alpha 5 to Selectively Compete with Nuclear Import of Phosphorylated STAT1 with some of 86.003, -22.043 T. and I. Energies respectively.*

File Model T.Energy I.Energy vdW Coul NumRotors RMSD Score

MalasmoruponaqTM"ligand_8a12048cbe_1_run_19.log 1 86.003 -22.043 -6.153 -15.890 24 0.000 -7.028

MalasmoruponaqTM"ligand_8a12048cbe_1_run_3.log 1 87.544 -18.873 0.274 -19.147 24 11.729 -6.563

MalasmoruponaqTM™ligand_8a12048cbe_1_run_3.log 2 87.822
-18.565 1.180 -19.745 24 10.698 -6.619

INPUT FILES

```
protein = protein_64900a2437.in
MalasmoruponaqTM™ligand set size = 1
MalasmoruponaqTM™ligand files = MalasmoruponaqTM™li-
gand_8a12048cbe
cofactor set size = 0
cofactor files =
```

GRID SETTINGS

```
center x = 0
center y = 0
center z = 0
total size x = 20
total size y = 20
total size z = 20
discretization = 0.25
```

GENETIC DOCKING ALGORITHM SETTINGS

```
number of evaluations = 1000000
population size = 750
number of runs = 24
seed at run #1 = -1985
```

JOB INFO

```
submission date = 2019-05-10 14:06:06
job name = MalasmoruponaqTM™_4U2X_5cd5af7e0794d
ID = Dock@Dock.CBNKRLNGSN
$Number_of_Clusters = 10
$Seed = -1985
```

```
$Leader_Info 1 {
```

```
Num_Members = 55
Total_Energy = 88.010
vdW = -6.882
Coulomb = -17.147
Internal = 112.039
rmsd = 0.000
```

```
}
```

```
$Leader_Info 2 {
```

```
    Num_Members = 77  
    Total_Energy = 89.087  
    vdW = -7.533  
    Coulomb = -14.240  
    Internal = 110.860  
    rmsd = 1.225
```

```
}
```

```
$Leader_Info 3 {
```

```
    Num_Members = 43  
    Total_Energy = 89.933  
    vdW = -4.421  
    Coulomb = -16.766  
    Internal = 111.120  
    rmsd = 1.388
```

```
}
```

```
$Leader_Info 4 {
```

```
    Num_Members = 54  
    Total_Energy = 90.104  
    vdW = -3.341  
    Coulomb = -14.815  
    Internal = 108.260  
    rmsd = 2.009
```

```
}
```

```
$Leader_Info 5 {
```

```
    Num_Members = 10  
    Total_Energy = 90.311  
    vdW = -4.156  
    Coulomb = -15.630  
    Internal = 110.098  
    rmsd = 1.738
```

```
}
```

```
$Leader_Info 6 {
```

```
    Num_Members = 45  
    Total_Energy = 91.169  
    vdW = -4.544  
    Coulomb = -12.537
```

Internal = 108.250

rmsd = 2.675

}

\$Leader_Info 7 {

Num_Members = 38

Total_Energy = 91.260

vdW = -5.771

Coulomb = -12.433

Internal = 109.464

rmsd = 3.033

}

\$Leader_Info 8 {

Num_Members = 13

Total_Energy = 91.436

vdW = -4.056

Coulomb = -12.888

Internal = 108.379

rmsd = 3.344

}

\$Leader_Info 9 {

Num_Members = 43

Total_Energy = 91.802

vdW = -8.555

Coulomb = -10.338

Internal = 110.695

rmsd = 2.431

}

\$Leader_Info 10 {

Num_Members = 8

Total_Energy = 91.893

vdW = -7.628

Coulomb = -11.134

Internal = 110.655

rmsd = 1.458

}

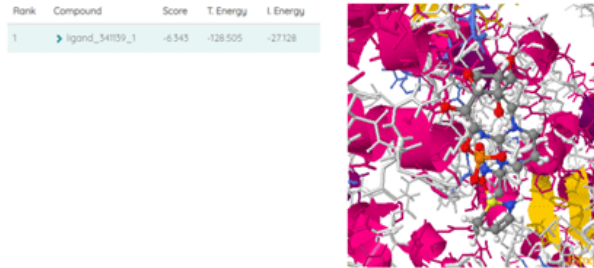


Figure. 14 MalasmoruponaqTM™_341139 fragmented miracle molecule binds within Ebola virus envelope protein MPER/TM domains (PDB:5T42) and its interaction with the fusion loop with some of -6.343 (score) -128.505 (T.Energy) and -27.128(I.Energy).

```

MalasmoruponaqTM™_fr2_      Model   T.Energy    I.Energy    vdW     Coul     NumRotors   RMSD     Score
MalasmoruponaqTM™ligand_341139_1_run_18.log      1       -128.505   -27.128   -2.477   -24.651   9       0.000    -6.343
MalasmoruponaqTM™ligand_341139_1_run_16.log      1       -124.642   -23.705   -1.647   -22.058   9       2.572    -6.220
MalasmoruponaqTM™ligand_341139_1_run_2.log       4       -122.279   -21.155   -5.848   -15.307   9       3.429    -6.612
$Number_of_Clusters = 10
$Seed = -1985

```

\$Leader_Info 1 {

```

Num_Members = 29
Total_Energy = 131.711
vdW = -22.683
Coulomb = -0.117
Internal = 154.511
rmsd = 0.000

```

}

\$Leader_Info 2 {

```

Num_Members = 38
Total_Energy = 132.012
vdW = -14.754
Coulomb = -3.945
Internal = 150.711
rmsd = 10.468

```

}

\$Leader_Info 3 {

```

Num_Members = 33
Total_Energy = 132.078
vdW = -22.913
Coulomb = -0.393

```

Internal = 155.385

rmsd = 1.090

}

\$Leader_Info 4 {

Num_Members = 10

Total_Energy = 133.348

vdW = -21.487

Coulomb = 0.098

Internal = 154.737

rmsd = 1.718

}

\$Leader_Info 5 {

Num_Members = 46

Total_Energy = 133.866

vdW = -21.670

Coulomb = -2.181

Internal = 157.717

rmsd = 3.691

}

\$Leader_Info 6 {

Num_Members = 41

Total_Energy = 133.922

vdW = -12.556

Coulomb = -2.084

Internal = 148.562

rmsd = 11.099

}

\$Leader_Info 7 {

Num_Members = 45

Total_Energy = 134.186

vdW = -12.801

Coulomb = -5.490

Internal = 152.477

rmsd = 9.068

}

\$Leader_Info 8 {

Num_Members = 30
Total_Energy = 134.222
vdW = -13.540
Coulomb = -2.487
Internal = 150.249
rmsd = 10.702

}

\$Leader_Info 9 {

Num_Members = 1
Total_Energy = 134.240
vdW = -20.009
Coulomb = -0.356
Internal = 154.605
rmsd = 1.068

}

\$Leader_Info 10 {

Num_Members = 39
Total_Energy = 134.352
vdW = -19.740
Coulomb = -0.147
Internal = 154.239
rmsd = 1.523

}

\$Number_of_Clusters = 10

\$Seed = -1985

\$Leader_Info 1 {

Num_Members = 68
Total_Energy = 134.485
vdW = -19.278
Coulomb = -0.471
Internal = 154.233
rmsd = 0.000

}

\$Leader_Info 2 {

Num_Members = 55

Total_Energy = 134.500
vdW = -15.826
Coulomb = -4.490
Internal = 154.816
rmsd = 5.768

}

\$Leader_Info 3 {

Num_Members = 56
Total_Energy = 134.917
vdW = -18.635
Coulomb = -1.716
Internal = 155.267
rmsd = 11.166

}

\$Leader_Info 4 {

Num_Members = 15
Total_Energy = 135.171
vdW = -15.072
Coulomb = -5.145
Internal = 155.389
rmsd = 6.248

}

\$Leader_Info 5 {

Num_Members = 66
Total_Energy = 136.427
vdW = -11.909
Coulomb = -6.827
Internal = 155.163
rmsd = 10.545

}

\$Leader_Info 6 {

Num_Members = 46
Total_Energy = 136.947
vdW = -16.561
Coulomb = -3.950
Internal = 157.459
rmsd = 4.579

}

\$Leader_Info 7 {

Num_Members = 46
Total_Energy = 137.284
vdW = -17.669
Coulomb = 0.034
Internal = 154.918
rmsd = 5.845

}

\$Leader_Info 8 {

Num_Members = 42
Total_Energy = 137.443
vdW = -18.601
Coulomb = -1.884
Internal = 157.928
rmsd = 2.841

}

\$Leader_Info 9 {

Num_Members = 46
Total_Energy = 137.470
vdW = -18.137
Coulomb = -0.420
Internal = 156.028
rmsd = 10.020

}

\$Leader_Info 10 {

Num_Members = 32
Total_Energy = 137.518
vdW = -18.137
Coulomb = -0.073
Internal = 155.729
rmsd = 1.578

}

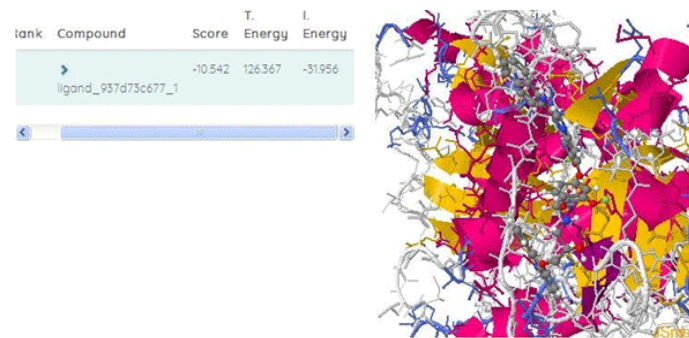


Figure.15 MalasmoruponaqTM™_937d73c677_1 fragmented compound binds with some of -10.542 (score), 126.367(T.Energy), - 31.956(I.Energy) within (PDB: 4U2X) Ebola virus VP24 in complex with Karyopherin alpha 5 C-terminus.

MalasmoruponaqTM™_937d73c677_1 Model T.Energy I.Energy vdW Coul NumRotors RMSD Score MalasmoruponaqTM™li-

gand_937d73c677_1_run_24.log

```
1
126.367
-31.956
-28.665
-3.291
13
0.000
-10.542
```

MalasmoruponaqTM™ligand_937d73c677_1_run_22.log

```
1
127.608
-21.878
-18.162
-3.716
13
10.745
-8.411
```

MalasmoruponaqTM™ligand_937d73c677_1_run_15.log

```
1
128.697
-20.639
-18.137
-2.502
13
8.540
-8.763
```

\$Number_of_Clusters = 10

\$Seed = -1985

\$Leader_Info 1 {

```
Num_Members = 29  
Total_Energy = 131.711  
vdW = -22.683  
Coulomb = -0.117  
Internal = 154.511  
rmsd = 0.000
```

{

```
$Leader_Info 2 {
```

```
Num_Members = 38  
Total_Energy = 132.012  
vdW = -14.754  
Coulomb = -3.945  
Internal = 150.711  
rmsd = 10.468
```

{

```
$Leader_Info 3 {
```

```
Num_Members = 33  
Total_Energy = 132.078  
vdW = -22.913  
Coulomb = -0.393  
Internal = 155.385  
rmsd = 1.090
```

{

```
$Leader_Info 4 {
```

```
Num_Members = 10  
Total_Energy = 133.348  
vdW = -21.487  
Coulomb = 0.098  
Internal = 154.737  
rmsd = 1.718
```

{

```
$Leader_Info 5 {
```

```
Num_Members = 46  
Total_Energy = 133.866  
vdW = -21.670  
Coulomb = -2.181  
Internal = 157.717
```

rmsd = 3.691

}

\$Leader_Info 6 {

Num_Members = 41
Total_Energy = 133.922
vdW = -12.556
Coulomb = -2.084
Internal = 148.562
rmsd = 11.099

}

\$Leader_Info 7 {

Num_Members = 45
Total_Energy = 134.186
vdW = -12.801
Coulomb = -5.490
Internal = 152.477
rmsd = 9.068

}

\$Leader_Info 8 {

Num_Members = 30
Total_Energy = 134.222
vdW = -13.540
Coulomb = -2.487
Internal = 150.249
rmsd = 10.702

}

\$Leader_Info 9 {

Num_Members = 1
Total_Energy = 134.240
vdW = -20.009
Coulomb = -0.356
Internal = 154.605
rmsd = 1.068

}

\$Leader_Info 10 {

Num_Members = 39

Total_Energy = 134.352

vdW = -19.740

Coulomb = -0.147

Internal = 154.239

rmsd = 1.523

}

\$Number_of_Clusters = 10

\$Seed = -1985

\$Leader_Info 1 {

Num_Members = 68

Total_Energy = 134.485

vdW = -19.278

Coulomb = -0.471

Internal = 154.233

rmsd = 0.000

}

\$Leader_Info 2 {

Num_Members = 55

Total_Energy = 134.500

vdW = -15.826

Coulomb = -4.490

Internal = 154.816

rmsd = 5.768

}

\$Leader_Info 3 {

Num_Members = 56

Total_Energy = 134.917

vdW = -18.635

Coulomb = -1.716

Internal = 155.267

rmsd = 11.166

}

\$Leader_Info 4 {

Num_Members = 15

Total_Energy = 135.171

vdW = -15.072

Coulomb = -5.145

Internal = 155.389

rmsd = 6.248

}

\$Leader_Info 5 {

Num_Members = 66

Total_Energy = 136.427

vdW = -11.909

Coulomb = -6.827

Internal = 155.163

rmsd = 10.545

}

\$Leader_Info 6 {

Num_Members = 46

Total_Energy = 136.947

vdW = -16.561

Coulomb = -3.950

Internal = 157.459

rmsd = 4.579

}

\$Leader_Info 7 {

Num_Members = 46

Total_Energy = 137.284

vdW = -17.669

Coulomb = 0.034

Internal = 154.918

rmsd = 5.845

}

\$Leader_Info 8 {

Num_Members = 42

Total_Energy = 137.443

vdW = -18.601

Coulomb = -1.884

Internal = 157.928

rmsd = 2.841

}

\$Leader_Info 9 {

Num_Members = 46
Total_Energy = 137.470
 $vdW = -18.137$
Coulomb = -0.420
Internal = 156.028
rmsd = 10.020

}

\$Leader_Info 10 {

Num_Members = 32
Total_Energy = 137.518
 $vdW = -18.137$
Coulomb = -0.073
Internal = 155.729
rmsd = 1.578

}

\$Number_of_Clusters = 10

\$Seed = -1985

\$Leader_Info 1 {

Num_Members = 35
Total_Energy = 132.457
 $vdW = -15.519$
Coulomb = -10.442
Internal = 158.418
rmsd = 0.000

}

\$Leader_Info 2 {

Num_Members = 73
Total_Energy = 132.725
 $vdW = -13.482$
Coulomb = -15.013
Internal = 161.219
rmsd = 9.261

}

\$Leader_Info 3 {

```
Num_Members = 57
Total_Energy = 132.808
vdW = -16.022
Coulomb = -11.252
Internal = 160.082
rmsd = 9.865
```

{

```
$Leader_Info 4 {
```

```
Num_Members = 65
Total_Energy = 132.842
vdW = -17.204
Coulomb = -4.376
Internal = 154.421
rmsd = 9.338
```

{

```
$Leader_Info 5 {
```

```
Num_Members = 14
Total_Energy = 134.506
vdW = -15.149
Coulomb = -10.917
Internal = 160.572
rmsd = 9.471
```

{

```
$Leader_Info 6 {
```

```
Num_Members = 42
Total_Energy = 134.834
vdW = -17.975
Coulomb = -1.744
Internal = 154.554
rmsd = 9.967
```

{

```
$Leader_Info 7 {
```

```
Num_Members = 48
Total_Energy = 134.837
vdW = -18.842
Coulomb = -6.757
Internal = 160.436
```

rmsd = 3.480

}

\$Leader_Info 8 {

*Num_Members = 9
Total_Energy = 135.229
vdW = -16.183
Coulomb = -3.691
Internal = 155.102
rmsd = 8.893*

}

\$Leader_Info 9 {

*Num_Members = 2
Total_Energy = 135.282
vdW = -16.907
Coulomb = -2.083
Internal = 154.272
rmsd = 9.344*

}

\$Leader_Info 10 {

*Num_Members = 46
Total_Energy = 135.500
vdW = -13.362
Coulomb = -6.116
Internal = 154.977
rmsd = 9.710*

}

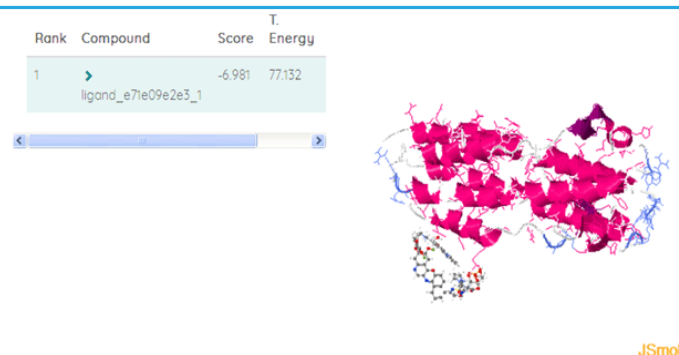


Figure. 16 2 MalasmoruponaqTM____5d22de8865750 3D Docking Docking Interactions with 5T42.

File Model T.Energy I.Energy vdW Coul NumRotors RMSD Score

ligand_e71e09e2e3_1_run_15.log 1 77.132 -35.035 4.622 -39.657 24 0.000 -6.981

ligand_e71e09e2e3_1_run_15.log 3 78.586 -38.541 -3.037 -35.504 24 2.843 -7.859

ligand_e71e09e2e3_1_run_8.log 1 78.598 -37.275 -2.045 -35.230 24 3.111 -7.373

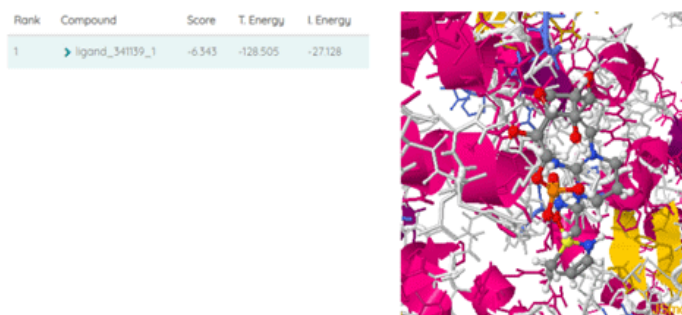


Figure.17 MalasmoruponaqTM™ligand_341139 fragmented miracle molecules with some of ligand_341139_1 -6.343 (score) -128.505 (T.Energy) and -27.128(I.Energy) within Ebola virus envelope protein MPER/TM domain (PDB:5T42) and its interaction with the fusion loop explains their fusion activity.

MalasmoruponaqTM™ ligand_341139_fr2_ Model	T.Energy	I.Energy	vdW	Coul	NumRotors	RMSD	Score	
ligand_341139_1_run_18.log	1	-128.505	-27.128	-2.477	-24.651	9	0.000	-6.343
ligand_341139_1_run_16.log	1	-124.642	-23.705	-1.647	-22.058	9	2.572	-6.220
ligand_341139_1_run_2.log	4	-122.279	-21.155	-5.848	-15.307	9	3.429	-6.612

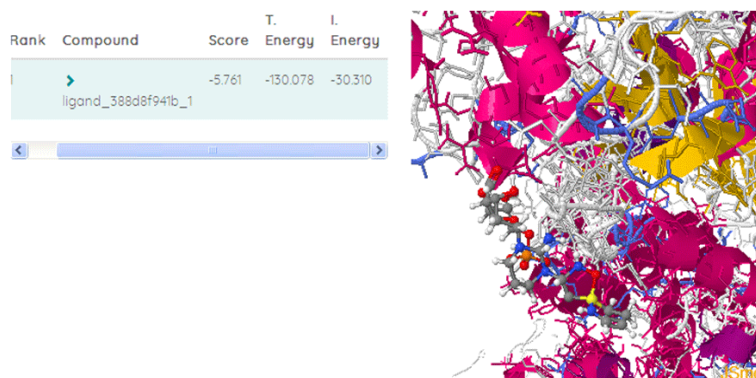


Figure.18 MalasmoruponaqTM™ligand_341139 fragmented miracle molecules with some of ligand_341139_ with some of 1 T.Energy: -130.078, I.Energy: -30.310, vdW: -2.363 within (PDB: 4U2X) Ebola virus VP24 in complex with Karyopherin alpha 5 C-terminus.

MalasmoruponaqTM™ligand_341139_r2_	Model	T.Energy	I.Energy	vdW	Coul	NumRotors	RMSD	Score
ligand_388d8f941b_1_run_9.log	1	-130.078	-30.310	-2.363	-27.947	9	0.000	-5.761
ligand_388d8f941b_1_run_23.log	1	-130.057	-30.384	1.467	-31.851	9	8.912	-6.375
ligand_388d8f941b_1_run_23.log	2	-129.845	-33.880	-3.140	-30.740	9	9.651	-6.736

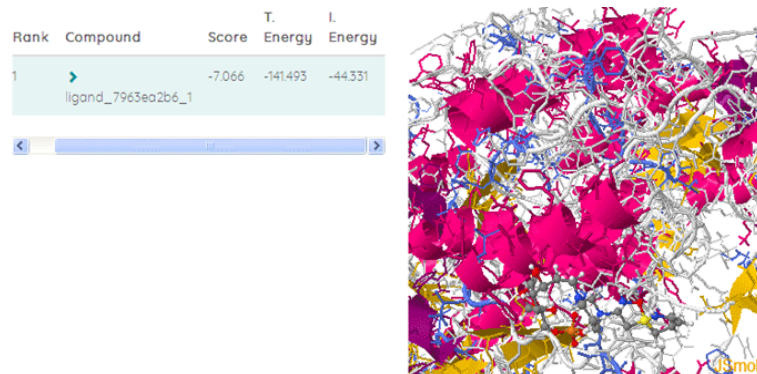
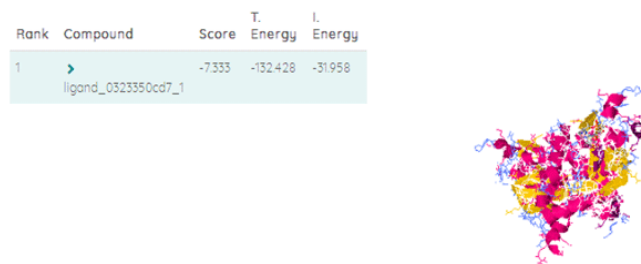


Figure.19 MalasmoruponaqTM™_3D Docking Docking Interactions within 5JWA.

MalasmoruponaqTM™	Model	T.Energy	I.Energy	vdW	Coul	NumRotors	RMSD	Score
ligand_7963ea2b6_1_run_23.log	1	-141.493	-44.331	-5.061	-39.270	9	0.000	-7.066
ligand_7963ea2b6_1_run_11.log	1	-140.308	-40.317	1.757	-42.074	9	7.937	-6.644
ligand_7963ea2b6_1_run_11.log	3	-138.103	-45.689	3.820	-49.509	9	2.036	-6.628



JSmol

Figure.20 MalasmoruponaqTM™ligand_0323350cd7_1 3D Docking Docking Interactions with (PDB:5T42).

MalasmoruponaqTM™ ligand_0323350cd7_1	Model	T.Energy	I.Energy	vdW	Coul	NumRotors	RMSD	Score
ligand_0323350cd7_1_run_17.log	1	-132.428	-31.958	-7.560	-24.398	9	0.000	-7.333
ligand_0323350cd7_1_run_15.log	1	-131.406	-31.195	-2.600	-28.595	9	9.637	-7.249
ligand_0323350cd7_1_run_3.log	1	-130.468	-31.405	-5.172	-26.233	9	11.349	-6.983

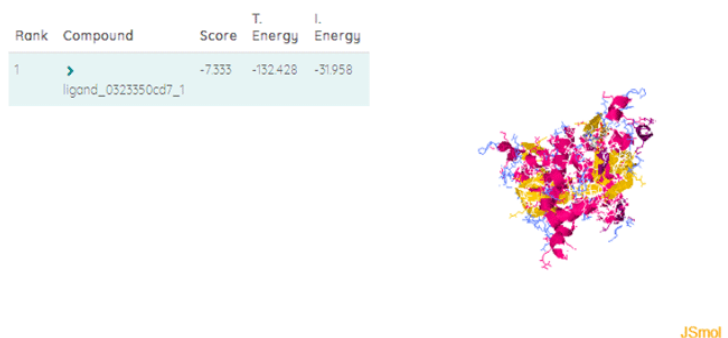


Figure.21a Structure of Ebola virus nucleoprotein N-terminal fragment bound to a peptide derived from Ebola VP35.

MalasmoruponaqTM™ligand_b91ab3e842_	Model	T.Energy	I.Energy	vdW	Coul	NumRotors	RMSD	Score
ligand_b91ab3e842_1_run_22.log	4	-102.490	-0.807	-0.000	-0.807	9	0.000	24.988
ligand_b91ab3e842_1_run_22.log	1	-102.490	-0.808	-0.000	-0.808	9	3.169	24.988
ligand_b91ab3e842_1_run_22.log	8	-102.489	-0.806	-0.000	-0.806	9	8.806	24.988

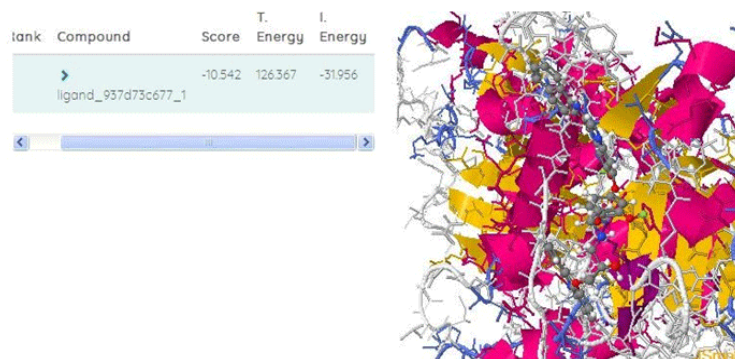


Figure.22 MalasmoruponaqTM™_937d73c677_1 fragmented compound that binds with some of -10.542 (score), 126.367(T.Energy), - 31.956(I.Energy) within (PDB: 4U2X) Ebola virus VP24 in complex with Karyopherin alpha 5 C-terminus.

MalasmoruponaqTM™_937d73c677_1	Model	T.Energy	I.Energy	vdW	Coul	NumRotors	RMSD	Score
ligand_937d73c677_1_run_24.log	1	126.367	-31.956	-28.665	-3.291	13	0.000	-10.542
ligand_937d73c677_1_run_22.log	1	127.608	-21.878	-18.162	-3.716	13	10.745	-8.411
ligand_937d73c677_1_run_15.log	1	128.697	-20.639	-18.137	-2.502	13	8.540	-8.763



Figure.23 MalasmoruponaqTM™_3D Docking Docking Interactions within 5JWA

MalasmoruponaqTM™	Model	T.Energy	I.Energy	vdW	Coul	NumRotors	RMSD	Score
ligand_018c119241_1_run_1.log	1	126.303	-23.221	-3.590	-19.631	13	0.000	-6.719
ligand_018c119241_1_run_13.log	1	126.973	-27.258	-7.603	-19.655	13	7.800	-7.783
ligand_018c119241_1_run_1.log	4	127.060	-21.963	-3.775	-18.188	13	2.365	-6.797

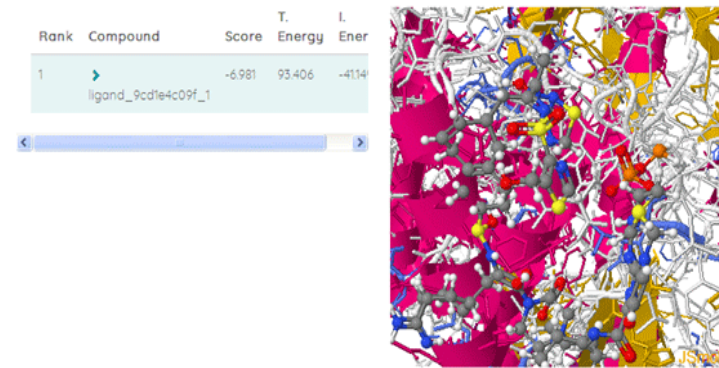


Figure.24 MalasmoruponaqTM™_ligand_9cd1e4c09f_3D Docking Docking Interactions within 5JWA.

MalasmoruponaqTM™_5LGE_	Model	T.Energy	I.Energy	vdW	Coul	NumRotors	RMSD	Score
ligand_9cd1e4c09f_1_run_13.log	1	93.406	-41.149	-6.106	-35.043	26	0.000	-6.981
ligand_9cd1e4c09f_1_run_5.log	1	93.471	-32.825	-0.430	-32.395	26	3.364	-6.555
ligand_9cd1e4c09f_1_run_18.log	1	95.952	-34.990	-0.372	-34.618	26	6.103	-6.346

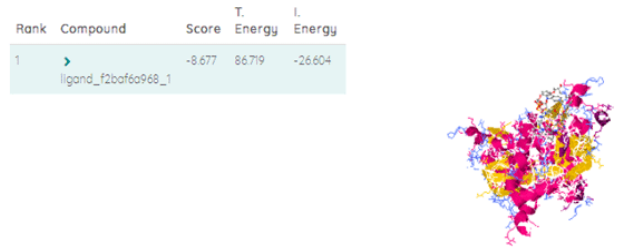


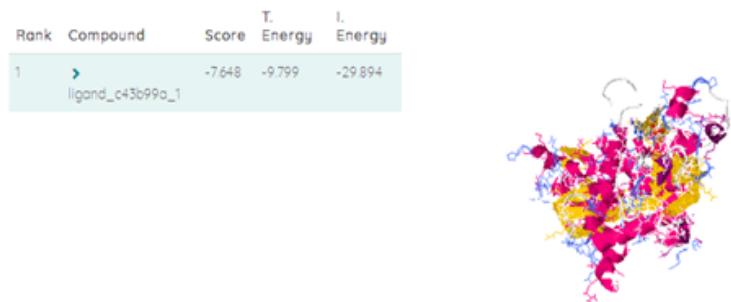
Figure.25 3D Docking Docking Interactions of the MalasmoruponaqTM™ with Pyranose 2-oxidase V546C mutant with 2-fluorinated galactose (PDB:4MOQ)

MalasmoruponaqTM™	Model	T.Energy	I.Energy	vdW	Coul	NumRotors	RMSD	Score
ligand_f2ba6a968_1_run_1.log	1	86.719	-26.604	-22.653	-3.951	24	0.000	-8.677
ligand_f2ba6a968_1_run_1.log	2	86.734	-28.123	-26.410	-1.713	24	2.988	-9.340
ligand_f2ba6a968_1_run_1.log	3	87.052	-26.712	-22.031	-4.681	24	2.074	-8.418



Figure.26 MalasmoruponaqTM™_with the Structure of the Ebola virus envelope protein MPER/TM domain and its interaction with the fusion loop explains their fusion activity (PDB:5T42).

	Model	T.Energy	I.Energy	vdW	Coul	NumRotors	RMSD	Score
MalasmoruponaqTM™_ligand_0c92b908ca_1	1	-93.737	-265.495	-168.542	-96.953	13	0.000	-40.183
MalasmoruponaqTM™ligand_0c92b908ca_1_run_23.log	3	-71.278	-252.228	-132.826	-119.402	13	7.852	-30.688
MalasmoruponaqTM™ligand_0c92b908ca_1_run_14.log	2	-70.987	-250.716	-121.746	-128.970	13	8.965	-31.350



JSmol

Figure.27 3D Docking Docking Interactions of the Remdesivir Small Molecule within 4U2X Ebola virus VP24 binding domains in complex with Karyopherin alpha 5 C-terminus Ebola Virus VP24. Remdesivir Targets the Unique NLS Binding Site on Karyopherin Alpha 5 to Selectively Compete with Nuclear Import of Phosphorylated STAT1 with some of 1.680, -13.014 T. and I. Energies respectively.

Remdesivir	Model	T.Energy	I.Energy	vdW	Coul	NumRotors	RMSD	Score
ligand_fa84c29cba_1_run_16.log	1	1.680	-13.014	-7.055	-5.959	14	0.000	-6.722
ligand_fa84c29cba_1_run_17.log	1	1.855	-13.030	-8.577	-4.453	14	8.083	-6.720
ligand_fa84c29cba_1_run_9.log	1	2.128	-12.816	-5.491	-7.325	14	5.362	-6.695

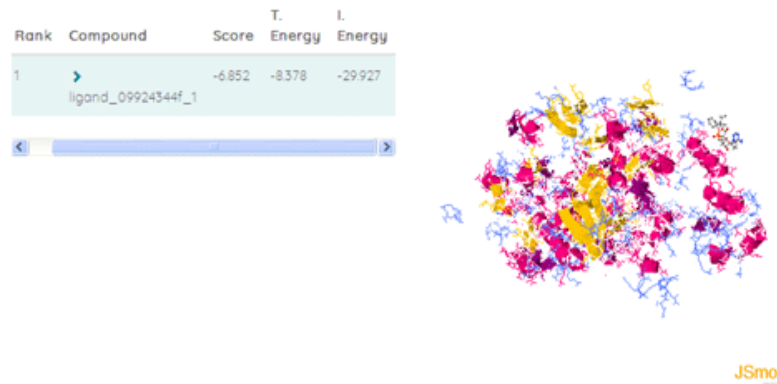


Figure.27a Remdesivir 3D Docking Docking Interactions within 5JWA.

Remdesivir	Model	T.Energy	I.Energy	vdW	Coul	NumRotors	RMSD	Score
ligand_09924344f_1_run_9.log	1	-8.378	-29.927	-6.459	-23.468	14	0.000	-6.852
ligand_09924344f_1_run_9.log	4	-6.106	-28.505	-4.847	-23.658	14	3.170	-6.557
ligand_09924344f_1_run_9.log	8	-3.625	-28.083	-4.983	-23.100	14	2.640	-6.676

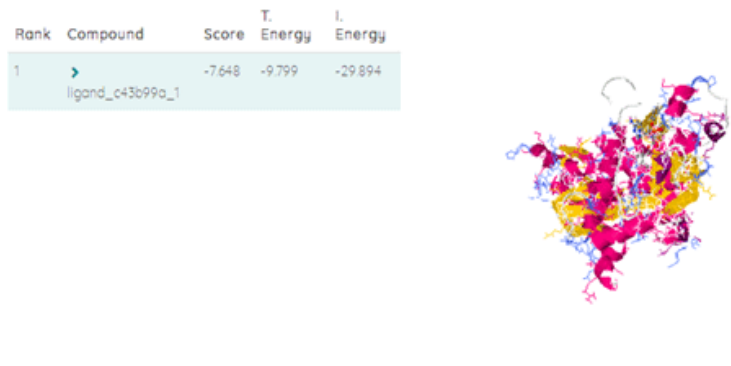


Figure.27b Remdesivir 3D Docking Docking Interactions within 4MOQ.

Remdesivir	Model	T.Energy	I.Energy	vdW	Coul	NumRotors	RMSD	Score
ligand_c43b99a_1_run_9.log	1	-9.799	-29.894	-14.221	-15.673	14	0.000	-7.648
ligand_c43b99a_1_run_17.log	1	-9.240	-28.251	-17.729	-10.522	14	6.017	-7.996
ligand_c43b99a_1_run_3.log	1	-9.204	-28.854	-10.461	-18.393	14	7.702	-7.447

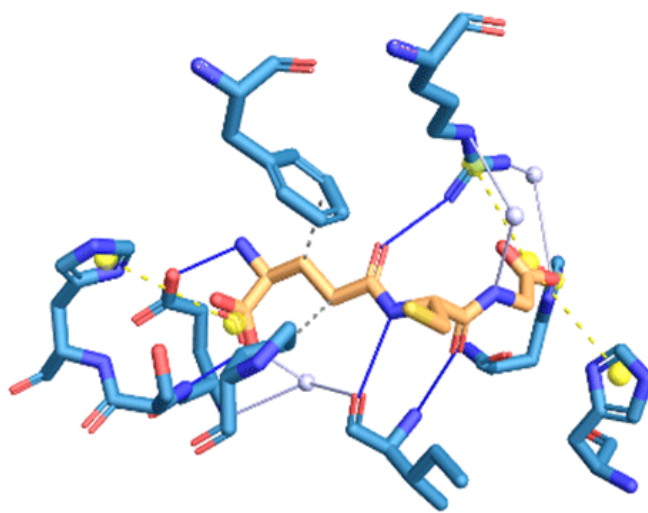


Figure. 28 for the generation of the Hydrophobic Docking Interactions of the 2 MalasmoruponaqTM™ binding site(s) in 3ZML (glutathione s-transferase e2). GSH (Glutathione)GSH-A-1222 Interacting chains: A

Index	Residue	AA	Distance	Ligand Atom	Protein Atom
1	14A	PRO	3.96	3492	87
2	108A	PHE	3.84	3491	822

Hydrogen Bonds from the

Index	Residue	AA	Distance H-A	Distance D-A	Donor Angle	Protein donor	Sidechain	Donor Atom	Acceptor Atom
1	55A	ILE	2.08	3.01	156.55	✗	✗	3495 [Nam]	403 [O2]
2	55A	ILE	1.98	2.88	151.62	✓	✗	400 [Nam]	3498 [O2]
3	67A	GLU	1.79	2.72	150.00	✗	✓	3486 [N3]	496 [O2]
4	68A	SER	1.77	2.74	166.26	✓	✗	497 [Nam]	3490 [O.co2]
5	112A	ARG	2.16	2.86	126.73	✓	✓	857 [Ng+]	3494 [O2]

Water Bridges

Index	Residue	AA	Dist. A-W	Dist. D-W	Donor Angle	Water Angle	Protein donor	Donor Atom	Acceptor Atom	Water Atom
1	55A	ILE	3.73	2.87	154.71	100.38	✗	3490 [O.co2]	403 [O2]	3639
2	67A	GLU	2.87	3.51	120.12	82.93	✓	488 [Nam]	3490 [O.co2]	3639
3	112A	ARG	3.55	3.31	160.80	86.10	✗	3501 [Nam]	855 [Ng+]	3710
4	112A	ARG	3.99	3.55	126.69	118.15	✓	858 [Ng+]	3504 [O.co2]	3715

Salt Bridges

Index	Residue	AA	Distance	Protein positive	Ligand Group	Ligand Atoms
1	41A	HIS	4.89	✓	Carboxylate	3504, 3505
2	53A	HIS	4.12	✓	Carboxylate	3504, 3505
3	69A	HIS	4.82	✓	Carboxylate	3490, 3489
4	112A	ARG	4.30	✓	Carboxylate	3504, 3505

GSH-B-1222 

Interacting chains: B

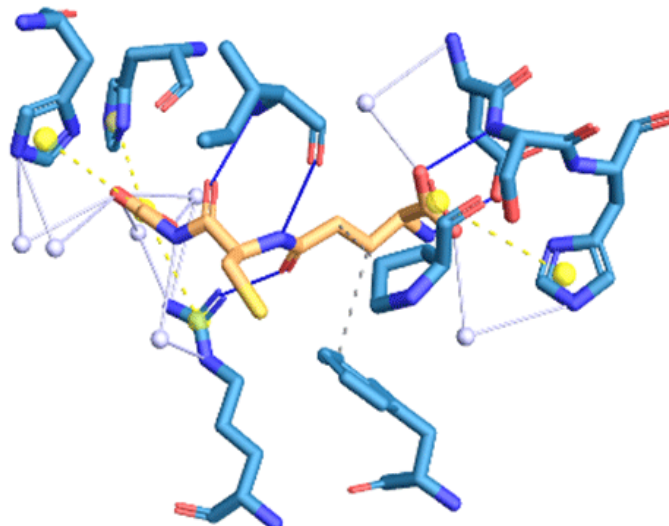


Figure. 29 Docking Interactions MalasmoruponaqTM™ binding site(s) in 3ZML (glutathione s-transferase e2). GSH (Glutathione)GSH-A-1222 Interacting chains: A

Index	Residue	AA	Distance	Ligand Atom	Protein Atom
1	14B	PRO	3.97	3512	1834
2	108B	PHE	3.94	3511	2569

Hydrogen Bonds from the

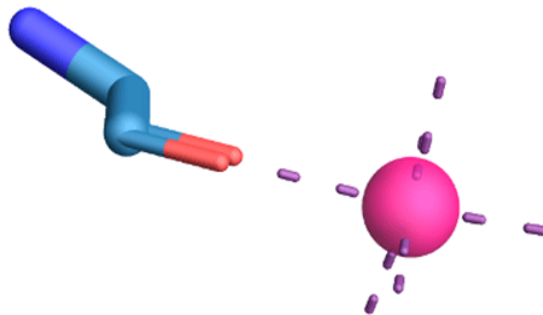
Index	Residue	AA	Distance H-A	Distance D-A	Donor Angle	Protein donor	Sidechain	Donor Atom	Acceptor Atom
1	55B	ILE	1.90	2.84	157.25	✓	✗	2147 [Nam]	3518 [O2]
2	55B	ILE	2.14	3.02	149.47	✗	✗	3515 [Nam]	2150 [O2]
3	67B	GLU	1.84	2.76	148.40	✗	✓	3506 [N3]	2243 [O2]
4	68B	SER	1.86	2.80	158.50	✓	✗	2244 [Nam]	3509 [O.co2]
5	112B	ARG	2.09	2.77	125.26	✓	✓	2604 [Ng+]	3514 [O2]

Water Bridges

Index	Residue	AA	Dist. A-W	Dist. D-W	Donor Angle	Water Angle	Protein donor	Donor Atom	Acceptor Atom	Water Atom
1	41B	HIS	3.34	4.01	114.23	112.32	✗	3525 [O.co2]	2038 [N2]	3906
2	41B	HIS	3.53	3.85	116.36	112.25	✗	3525 [O.co2]	2038 [N2]	3905
3	67B	GLU	2.94	3.61	112.73	84.58	✓	2235 [Nam]	3509 [O.co2]	3929
4	69B	HIS	3.79	3.43	140.15	101.11	✗	3510 [O.co2]	2259 [N2]	3978
5	112B	ARG	3.70	4.07	142.54	119.00	✓	2605 [Ng+]	3525 [O.co2]	3921
6	112B	ARG	2.71	4.07	142.54	139.76	✓	2605 [Ng+]	3524 [O.co2]	3921
7	112B	ARG	4.02	3.72	126.88	121.61	✓	2605 [Ng+]	3525 [O.co2]	3607
8	112B	ARG	3.52	3.34	163.94	83.88	✗	3521 [Nam]	2602 [Ng+]	3984

Salt Bridges

Index	Residue	AA	Distance	Protein positive	Ligand Group	Ligand Atoms
1	41B	HIS	4.86	✓	Carboxylate	3524, 3525
2	53B	HIS	4.16	✓	Carboxylate	3524, 3525
3	69B	HIS	4.94	✓	Carboxylate	3509, 3510
4	112B	ARG	4.19	✓	Carboxylate	3524, 3525



Metal Complexes MalasmoruponaqTM™ binding site(s) in 3EBH (m1 family aminopeptidase).

Metal Complexes MalasmoruponaqTM™ binding site(s) in 3EBH (m1 family aminopeptidase).						
Index	Residue	AA	Metal	Target	Distance	Location
Complex 1: Mg, octahedral (6)						
1	26A	HOH	7385	7404	2.02	water
2	250A	GLY	7385	442	2.06	protein.mainchain
3	1099A	HOH	7385	7584	2.14	water
4	1212A	HOH	7385	7697	2.21	water
5	1520A	HOH	7385	8005	2.10	water
6	1521A	HOH	7385	8006	2.14	water

Metal Complexes MalasmoruponaqTM™ binding site(s) in 3EBH (m1 family aminopeptidase).						
Index	Residue	AA	Metal	Target	Distance	Location
<i>MalasmoruponaqTM™ small molecule</i>						
<i>GOL (Glycerol)</i>						
<i>GOL-A-1086</i>						
<i>Interacting chains: A</i>						

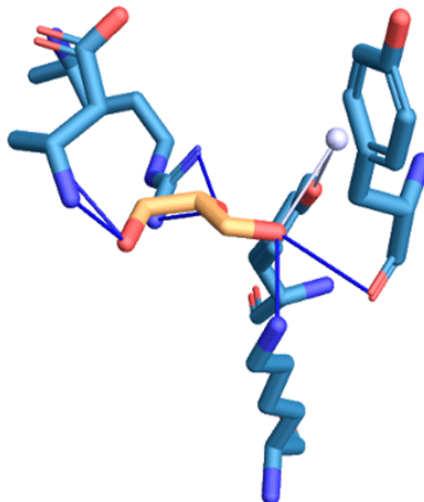


Figure. 31 Hydrogen Bonds from the MalasmoruponaqTM™ binding site(s) in 3EBH (m1 family aminopeptidase).

ION MG (magnesium ion) MG-A-7 Interacting chains: A

Index	Residue	AA	Distance H-A	Distance D-A	Donor Angle	Protein donor	Sidechain	Donor Atom	Acceptor Atom
1	479A	LYS	2.00	3.00	163.98	✓	✓	2281 [N3]	7354 [O3]
2	880A	TYR	2.66	3.58	157.63	✗	✗	7354 [O3]	5605 [O2]
3	888A	ASP	1.88	2.87	175.63	✓	✗	5673 [Nam]	7350 [O3]
4	888A	ASP	3.26	3.76	113.93	✗	✗	7350 [O3]	5676 [O2]
5	895A	ARG	2.30	3.16	144.37	✓	✓	5747 [Ng+]	7352 [O3]
6	895A	ARG	2.15	3.05	150.63	✓	✓	5748 [Ng+]	7352 [O3]

Water Bridges

Index	Residue	AA	Dist. A-W	Dist. D-W	Donor Angle	Water Angle	Protein donor	Donor Atom	Acceptor Atom	Water Atom
1	925A	TYR	2.94	3.72	101.71	99.74	✓	5991 [O3]	7354 [O3]	7397
<i>GOL-A-2</i>										
<i>Interacting chains: A</i>										

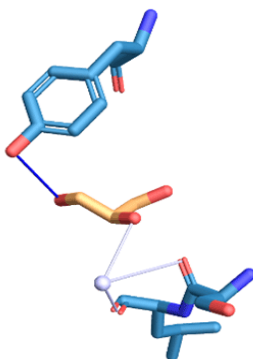


Figure. 32 Hydrogen Bonds from the. MalasmoruponaqTM™ binding site(s) in 3EBH (m1 family aminopeptidase), ION MG (magnesium ion) MG-A-7 Interacting chains: A

Inde	Resid	AA	Distance H-A	Distance D-A	Donor Angle	Protein donor	Sidecha in Atom	Donor Atom	Acceptor Atom
x	ue								
1	765A R	TY	3.47	4.05	120.99	✗	✓	7356 [O3]	4661 [O3]

Water Bridges

Inde	Resid	AA	Dist. A-W	Dist. D-W	Donor Angle	Water Angle	Protein donor	Donor Atom	Acceptor Atom	Water Atom
x	ue									
1	826A	SER	4.09	2.98	126.34	117.00	✗	7358 [O3]	5160 [O2]	8153
2	827A U	LE	2.94	2.98	126.34	73.86	✗	7358 [O3]	5166 [O2]	8153

GOL-A-3

Interacting chains: A

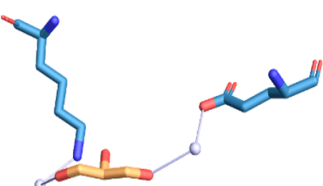


Figure. 33 Water Bridges MalasmoruponaqTM™ binding site(s) in 3EBH (m1 family aminopeptidase), ION MG (magnesium ion) MG-A-7 Interacting chains: A

Inde	Resid	AA	Dist. A-W	Dist. D-W	Donor Angle	Water Angle	Protein donor	Donor Atom	Acceptor Atom	Water Atom
x	ue									
1	676A	LYS	3.47	2.55	108.61	86.47	✓	3941 [N3]	7366 [O3]	8171
2	743A U	GL	2.95	2.69	158.85	74.82	✓	4471 [O3]	7362 [O3]	7481

GOL-A-4

Interacting chains: A

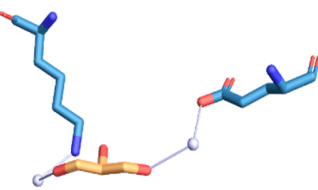


Figure. 33 Water Bridges MalasmoruponaqTM™ binding site(s) in 3EBH (m1 family aminopeptidase), ION MG (magnesium ion) MG-A-7 Interacting chains: A

Inde x	Resid ue	AA	Dist. A-W	Dist. D-W	Donor Angle	Water Angle	Protein donor	Donor Atom	Acceptor Atom	Water Atom
1	676A	LYS	3.47	2.55	108.61	86.47	✓	3941 [N3]	7366 [O3]	8171
2	743A	GL U	2.95	2.69	158.85	74.82	✓	4471 [O3]	7362 [O3]	7481

GOL-A-4

Interacting chains: A

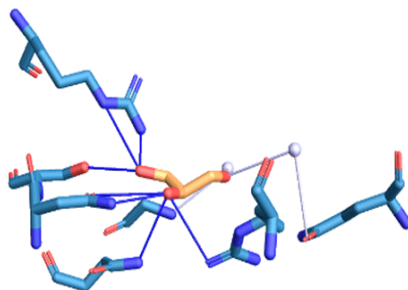


Figure. 34 Hydrogen Bonds from the MalasmoruponaqTM™ binding site(s) in 3EBH (m1 family aminopeptidase), ION MG (magnesium ion) MG-A-7 Interacting chains: A

Inde x	Resid ue	AA	Distance H-A	Distance D-A	Donor Angle	Protein donor	Sidecha in	Donor Atom	Acceptor Atom
1	471A	ASN	3.21	3.52	100.09	✓	✓	2226 [Nam]	7370 [O3]
2	473A	ASN	1.92	2.89	167.98	✓	✓	2239 [Nam]	7370 [O3]
3	473A	ASN	3.06	3.89	145.28	✗	✓	7370 [O3]	2238 [O2]
4	474A	SER	2.86	3.18	100.21	✓	✓	2245 [O3]	7368 [O3]
5	489A	ARG	2.33	3.04	128.76	✓	✓	2365 [Ng+]	7368 [O3]
6	489A	ARG	3.08	3.89	142.31	✗	✓	7368 [O3]	2362 [Ng+]
7	997A	ARG	3.03	3.52	111.85	✓	✓	6598 [Ng+]	7370 [O3]

Water Bridges

Inde	Resid	AA	Dist.	Dist.	Donor	Water	Protein	Donor	Acceptor	Water
x	ue		A-W	D-W	Angle	Angle	donor	Atom	Atom	Atom
1	460A	GLY	2.72	3.61	112.40	72.86	✓	2137 [Nam]	7372 [03]	8089
2	1038A	GL	3.83	4.00	148.76	99.92	✗	7372 [03]	6929 [02]	7907

GOL-A-5

Interacting chains: A

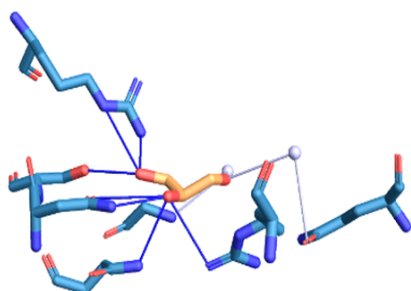


Figure. 35 Hydrogen Bonds from the MalasmoruponaqTM™ binding site(s) in 3EBH (m1 family aminopeptidase), ION MG (magnesium ion) MG-A-7 Interacting chains: A

Inde	Resid	AA	Distance	Distance	Donor	Protein	Sidecha	Donor	Acceptor
x	ue		H-A	D-A	Angle	donor	in	Atom	Atom
1	934A	SER	2.22	3.00	137.42	✓	✓	6061 [03]	7378 [03]
2	934A	SER	2.10	3.00	155.03	✗	✓	7378 [03]	6061 [03]

Water Bridges

Inde	Resid	AA	Dist.	Dist.	Donor	Water	Protein	Donor	Acceptor	Water
x	ue		A-W	D-W	Angle	Angle	donor	Atom	Atom	Atom
1	962A	GL	2.84	2.67	143.54	72.19	✓	6305 [03]	7374 [03]	7601
		U								
2	962A	GL	2.82	3.32	143.72	75.59	✗	7376 [03]	6301 [02]	7601
		U								

GOL-A-6

Interacting chains: A

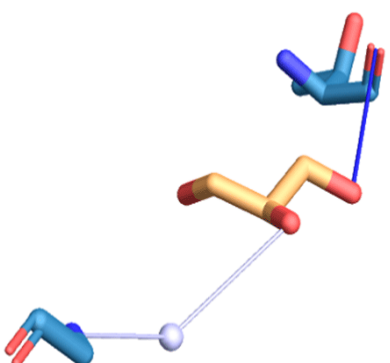


Figure. 36 Hydrogen Bonds from the MalasmoruponaqTM™ binding site(s) in 3EBH (m1 family aminopeptidase), ION MG (magnesium ion) MG-A-7 Interacting chains: A

Index	Resid	AA	Distance H-A	Distance D-A	Donor Angle	Protein donor	Sidechain in Atom	Donor Atom	Acceptor Atom
1	576A	TH R	3.19	4.03	146.25	✗	✗	7384 [O2]	[O3]

Water Bridges

Index	Resid	AA	Dist. A-W	Dist. D-W	Donor Angle	Water Angle	Protein donor	Donor Atom	Acceptor Atom	Water Atom
1	460A	GLY	3.88	3.61	112.40	71.76	✓	2137 [Nam]	7382 [O3]	8089

MalasmoruponaqTM™ small molecule+ION

BES (composite ligand, containing ubenimex)

BES-A-1085 ★

Composite ligand consists of BES:A:1085, ZN:A:1.

Interacting chains: A

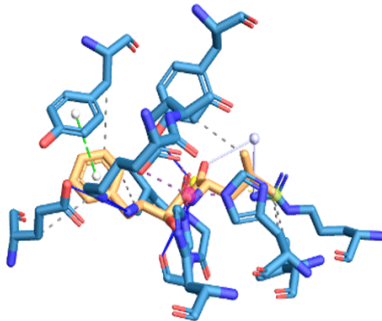


Figure. 37 for the generation of the Hydrophobic Docking Interactions of the MalasmoruponaqTM™ binding site(s) in 3EBH (m1 family aminopeptidase). ION MG (magnesium ion) MG-A-7 Interacting chains: A

Index	Residue	AA	Distance	Ligand Atom	Protein Atom
1	319A	GLU	3.84	7331	997
2	459A	VAL	3.74	7334	2135
3	459A	VAL	3.73	7332	2136
4	493A	VAL	3.94	7345	2399
5	496A	HIS	3.70	7345	2415
6	575A	TYR	3.76	7334	3080
7	580A	TYR	3.70	7344	3124

Hydrogen Bonds from the

Index	Resid	AA	Distance H-A	Distance D-A	Donor Angle	Protein donor	Sidechain in Atom	Donor Atom	Acceptor Atom
1	319A	GLU	2.86	3.80	152.12	✗	✓	7327 [N3]	1001 [O3]
2	460A	GLY	1.70	2.55	141.07	✓	✗	2137 [Nam]	7348 [O.co2]
3	461A	ALA	2.52	3.44	155.41	✗	✗	7340 [Nam]	2144 [O2]
4	461A	ALA	2.11	3.03	154.83	✓	✗	2141 [Nam]	7348 [O.co2]
5	461A	ALA	2.64	3.52	157.40	✗	✗	7348 [O.co2]	2144 [O2]

6	518A	LYS	3.02	3.39	102.52	✓	✓	2620	7327 [N3] [N3]
7	580A	TYR	1.87	2.71	148.26	✓	✓	3127	7339 [O2] [O3]

Water Bridges

Inde	Resid	AA	Dist.	Dist.	Donor	Water	Protein	Donor	Acceptor	Water
x	ue		A-W	D-W	Angle	Angle	donor	Atom	Atom	Atom
1	489A	AR	3.37	3.52	130.10	119.28	✓	2365	7347	7862 [Ng+]
		G								[O.co2]

π-Stacking

Index	Residue	AA	Distance	Angle	Offset	Type	Ligand Atoms
1	575A	TYR	3.94	13.86	1.58	P	7330, 7331, 7332, 7333, 7334, 7335

Salt Bridges

Index	Residue	AA	Distance	Protein	Ligand Group	Ligand Atoms
1	489A	ARG	5.39	✓	Carboxylate	7347, 7348

Metal Complexes

Index	Residue	AA	Metal	Target	Distance	Location
<i>Complex 1: Zn, square,planar (4)</i>						
1	496A	HIS	7326	2420	2.02	protein.sidechain
2	500A	HIS	7326	2462	2.04	protein.sidechain
3	519A	GLU	7326	2628	2.02	protein.sidechain
4	519A	GLU	7326	2629	2.97	protein.sidechain

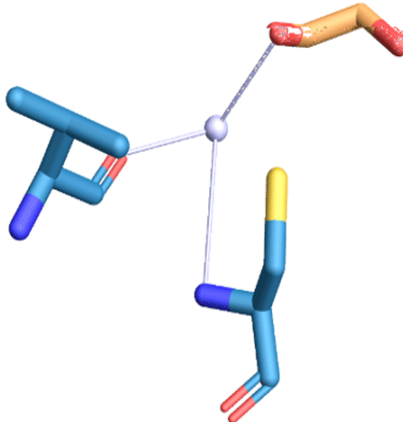


Figure. 38 water Bridges19 MalasmoruponaqTM™ binding site(s) in 4F1K (thrombospondin related anonymous protein), selected ligands: CL MalasmoruponaqTM™ small molecule EDO (Ethylene Glycol) EDO-A-305 Interacting chains: A.

Inde	Resid	AA	Dist.	Dist.	Donor	Water	Protein	Donor	Acceptor	Water
x	ue		A-W	D-W	Angle	Angle	donor	Atom	Atom	Atom
1	203A	VAL	2.62	3.13	126.17	77.46	✗	3117	1276	3223 [O3]
2	205A	CYS	4.08	3.13	126.17	71.57	✗	3117	1284	3223 [N2]

EDO-A-306

Interacting chains: A

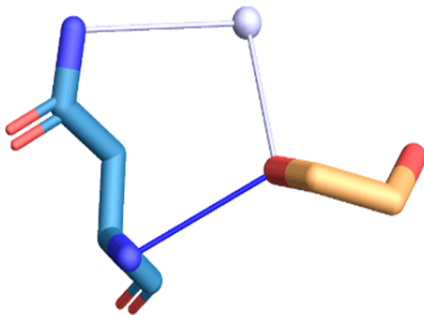


Figure. 39 Hydrogen Bonds from the. MalasmoruponaqTM™ binding site(s) in 4F1K (thrombospondin related anonymous protein), selected ligands: CL MalasmoruponaqTM™ small molecule EDO (Ethylene Glycol) EDO-A-305 Interacting chains: A.

Inde x	Resid ue	AA	Distance H-A	Distance D-A	Donor Angle	Protein donor	Sidecha in	Donor Atom	Acceptor Atom
1	95A	ASN	2.65	3.29	124.35	✗	✗	3121 [O3]	438 [N2]

Water Bridges

Inde x	Resid ue	AA	Dist. A-W	Dist. D-W	Donor Angle	Water Angle	Protein donor	Donor Atom	Acceptor Atom	Water Atom
1	95A	AS N	3.13	3.68	146.60	82.81	✓	445 [Nam]	3121 [O3]	3271

EDO-A-307

Interacting chains: A, B

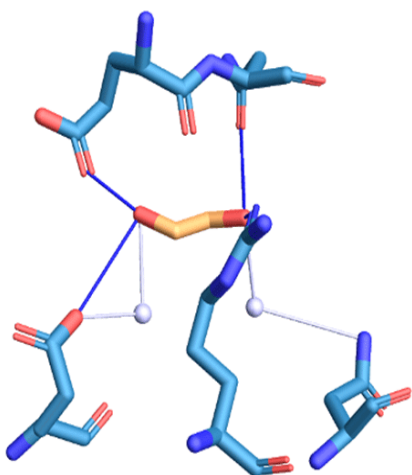


Figure. 40 Hydrogen Bonds from the MalasmoruponaqTM™ binding site(s) in 4F1K (thrombospondin related anonymous protein). selected ligands: CL MalasmoruponaqTM™ small molecule EDO (Ethylene Glycol) EDO-A-305 Interacting chains: A.

Inde x	Resid ue	AA	Distance H-A	Distance D-A	Donor Angle	Protein donor	Sidecha in	Donor Atom	Acceptor Atom
1	83A	GLU	1.45	2.33	152.95	✓	✓	347 [O3]	3127 [O3]
2	83B	GLU	3.21	3.90	129.90	✗	✓	3127	1892 [O3] [O3]
3	84A	ASN	3.42	3.87	111.05	✗	✓	3125	355 [O2] [O3]
4	150A	ARG	1.94	2.82	147.50	✓	✓	884 [Ng+]	3125 [O3]

Water Bridges

Inde x	Resid ue	AA	Dist. A-W	Dist. D-W	Donor Angle	Water Angle	Protein donor	Donor Atom	Acceptor Atom	Water Atom
1	83B	GL U	2.96	2.57	144.81	79.19	✓	1892 [O3]	3127 [O3]	3391
2	152A	AS N	3.01	4.01	135.83	75.87	✓	902 [Nam]	3125 [O3]	3274

EDO-A-309

Interacting chains: A

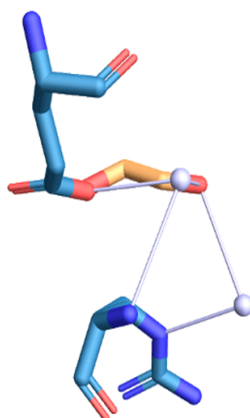


Figure. 41 Water Bridges: MalasmoruponaqTM™ binding site(s) in 4F1K (thrombospondin related anonymous protein), selected ligands: CL MalasmoruponaqTM™ small molecule EDO (Ethylene Glycol) EDO-A-305 Interacting chains: A.

Inde x	Resid ue	AA	Dist. A-W	Dist. D-W	Donor Angle	Water Angle	Protein donor	Donor Atom	Acceptor Atom	Water Atom
1	99A	GL U	2.98	3.96	101.73	87.63	✗	3135 [O3]	476 [O2]	3317
2	102A	AR G	3.13	3.70	117.38	86.90	✗	3135 [O3]	500 [Ng+]	3307
3	102A	AR G	3.81	3.96	101.73	73.04	✗	3135 [O3]	493 [N2]	3317

EDO-B-305

Interacting chains: B

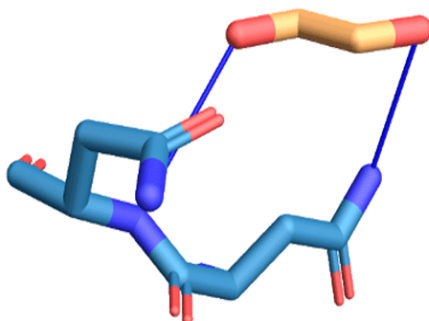


Figure. 42 Hydrogen Bonds from the:MalasmoruponaqTM™ binding site(s) in 4F1K (thrombospondin related anonymous protein), selected ligands: CL MalasmoruponaqTM™ small molecule EDO (Ethylene Glycol) EDO-A-305 Interacting chains: A.

Inde	Resid	AA	Distance H-A	Distance D-A	Donor Angle	Protein donor	Sidecha in	Donor Atom	Acceptor Atom
x	ue								
1	95B	ASN	2.37	3.21	142.68	✓	✓	1989 [Nam]	3159 [03]

2	96B	ASN	3.27	3.82	116.64	✓	✗	1990 [Nam]	3157 [03]
---	-----	-----	------	------	--------	---	---	---------------	-----------

EDO-B-306

Interacting chains: B

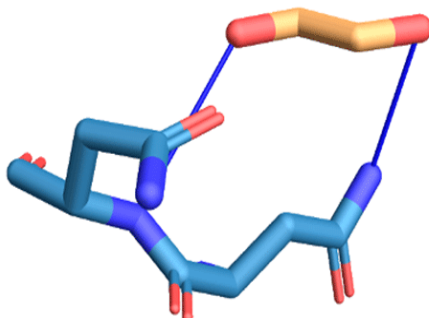


Figure. 43 Hydrogen Bonds from the:MalasmoruponaqTM™ binding site(s) in 4F1K (thrombospondin related anonymous protein), selected ligands: CL MalasmoruponaqTM™ small molecule EDO (Ethylene Glycol) EDO-A-305 Interacting chains: A.

Inde	Resid	AA	Distance H-A	Distance D-A	Donor Angle	Protein donor	Sidecha in	Donor Atom	Acceptor Atom
x	ue								
1	92B	ILE	3.10	3.92	143.07	✗	✗	3165 [03]	1960 [02]

2	95B	ASN	2.88	3.33	108.55	✓	✗	1982 [Nam]	3167 [03]
---	-----	-----	------	------	--------	---	---	---------------	-----------

3	96B	ASN	2.10	3.07	169.12	✓	✗	1990 [Nam]	3167 [03]
---	-----	-----	------	------	--------	---	---	---------------	-----------

EDO-B-308

Interacting chains: B

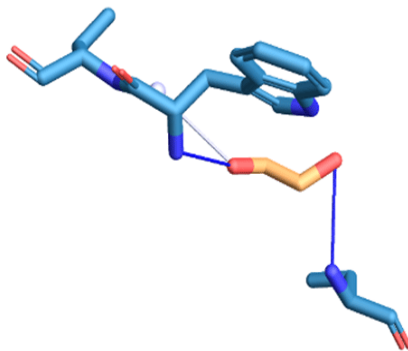


Figure. 44 Hydrogen Bonds from the MalasmoruponaqTM binding site(s) in 4F1K (thrombospondin related anonymous protein), selected ligands: CL Malasmorupona small molecule EDO (Ethylene Glycol) EDO-A-305 Interacting chains: A.

Inde x	Resid ue	AA	Distance H-A	Distance D-A	Donor Angle	Protein donor	Sidecha in	Donor Atom	Acceptor Atom
1	192B	GLN	2.60	3.54	160.46	✓	✗	2728 [Nam]	3171 [03]
2	220B	TRP	2.03	3.01	170.96	✓	✗	2930 [Nam]	3169 [03]

Water Bridges

Inde x	Resid ue	AA	Dist. A-W	Dist. D-W	Donor Angle	Water Angle	Protein donor	Donor Atom	Acceptor Atom	Water Atom
1	221B	GL U	3.65	2.88	149.85	84.07	✓	2944 [Nam]	3169 [03]	3454

EDO-B-309

Interacting chains: B

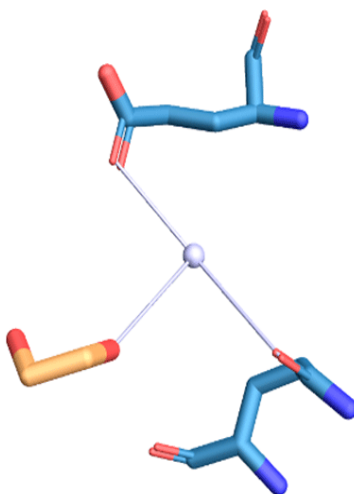


Figure. 45 Water Bridges MalasmoruponaqTM™ binding site(s) in 4F1K (thrombospondin related anonymous protein), selected ligands: CL MalasmoruponaqTM™ small molecule EDO (Ethylene Glycol) EDO-A-305 Interacting chains: A

Inde	Resid	AA	Dist.	Dist.	Donor	Water	Protein	Donor	Acceptor	Water
x	ue		A-W	D-W	Angle	Angle	donor	Atom	Atom	Atom
1	99B	GL	3.17	3.85	118.75	76.57	✗	3175 [O3]	2024 [O3]	3348
		U								
2	139B	GL	3.99	3.85	118.75	122.36	✗	3175 [O3]	2329 [O2]	3348
		N								

EDO-B-310

Interacting chains: B

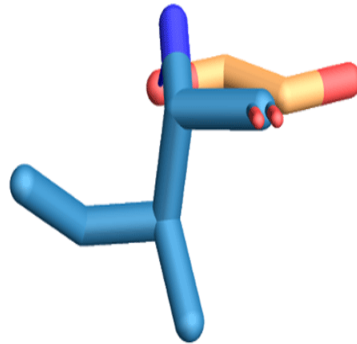


Figure. 46 Hydrogen Bonds from the MalasmoruponaqTM™ binding site(s) in 4F1K (thrombospondin related anonymous protein), selected ligands: CL MalasmoruponaqTM™ small molecule EDO (Ethylene Glycol) EDO-A-305 Interacting chains: A

Inde	Resid	AA	Distance	Distance	Donor	Protein	Sidecha	Donor	Acceptor
x	ue		H-A	D-A	Angle	donor	in	Atom	Atom
1	168B	ILE	2.29	3.24	160.25	✓	✗	2552 [Nam]	3179 [O3]

EDO-B-311

Interacting chains: B

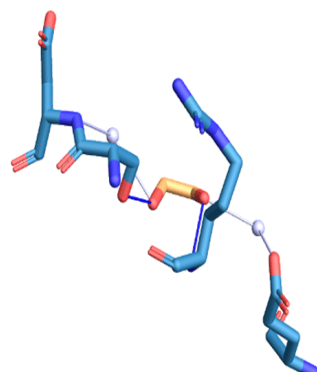


Figure. 47 Hydrogen Bonds from the MalasmoruponaqTM™ binding site(s) in 4F1K (thrombospondin related anonymous protein), selected ligands: CL MalasmoruponaqTM™ small molecule EDO (Ethylene Glycol) EDO-A-305 Interacting chains: A

Index	Resid	AA	Distance H-A	Distance D-A	Donor Angle	Protein donor	Sidechain in Atom	Donor Atom	Acceptor Atom
1	102B	ARG	2.02	2.93	152.29	✓	✗	2042 [Nam]	3181 [03]
2	105B	SER	1.79	2.73	164.23	✓	✓	2076 [03]	3183 [03]
3	105B	SER	2.31	2.73	105.84	✗	✓	3183 [03]	2076 [03]

Water Bridges

Index	Resid	AA	Dist. A-W	Dist. D-W	Donor Angle	Water Angle	Protein donor	Donor Atom	Acceptor Atom	Water Atom
1	99B	GL U	2.76	2.88	160.22	82.44	✗	3181 [03]	2025 [O2]	3375
2	106B	ASP	3.17	3.56	104.45	71.48	✓	2077 [Nam]	3183 [03]	3359

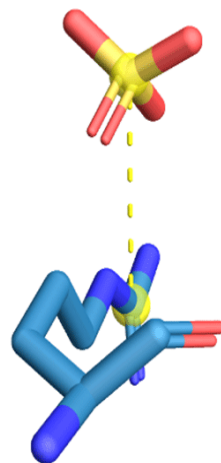


Figure. 48 Salt Bridges from the MalasmoruponaqTM™ binding site(s) in 4F1K (thrombospondin related anonymous protein), selected ligands: CL MalasmoruponaqTM™ small molecule EDO (Ethylene Glycol) EDO-A-305 Interacting chains: A

Index	Residue	AA	Distance	Protein positive	Ligand Group	Ligand Atoms
1	61A	ARG	4.18	✓	Sulfate	3101, 3101

S04-A-303 Salt Bridges from the MalasmoruponaqTM™ binding site(s) in 4F1K (thrombospondin related anonymous protein), selected ligands: CL MalasmoruponaqTM™ small molecule EDO (Ethylene Glycol) EDO-A-305 Interacting chains: A

<i>Index</i>	<i>Residue AA</i>	<i>Distance</i>	<i>Protein positive</i>	<i>Ligand Group</i>	<i>Ligand Atoms</i>	
1	141A	ARG	4.50	✓	Sulfate	3106, 3106
2	181A	ARG	4.13	✓	Sulfate	3106, 3106

S04-A-304 *Interacting chains: A*

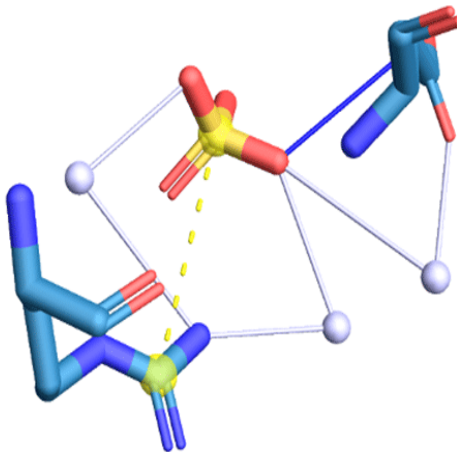


Figure. 49 *Hydrogen Bonds from the MalasmoruponaqTM™ binding site(s) in 4F1K (thrombospondin related anonymous protein), selected ligands: CL MalasmoruponaqTM™ small molecule EDO (Ethylene Glycol) EDO-A-305*

Interacting chains: A

<i>Inde</i>	<i>Resid AA</i>	<i>Distance H-A</i>	<i>Distance D-A</i>	<i>Donor Angle</i>	<i>Protein donor</i>	<i>Sidecha in</i>	<i>Donor Atom</i>	<i>Acceptor Atom</i>
1	106A	ASP	3.16	4.05	154.22	✗	✓	3114 [O2] [O3]

Water Bridges

<i>Inde</i>	<i>Resid AA</i>	<i>Dist. A-W</i>	<i>Dist. D-W</i>	<i>Donor Angle</i>	<i>Water Angle</i>	<i>Protein donor</i>	<i>Donor Atom</i>	<i>Acceptor Atom</i>	<i>Water Atom</i>
1	102A	AR G	2.99	3.88	130.85	102.10	✓	503 [Ng+]	3112 [O2]
2	102A	AR G	3.35	3.02	142.77	98.89	✓	503 [Ng+]	3114 [O3]
3	106A	ASP	4.06	2.74	123.49	111.95	✓	534 [O3]	3306 [O3]

Salt Bridges

<i>Index</i>	<i>Residue AA</i>	<i>Distance</i>	<i>Protein positive</i>	<i>Ligand Group</i>	<i>Ligand Atoms</i>	
1	102A	ARG	4.84	✓	Sulfate	3111, 3111

S04-B-302 *Interacting chains: B*

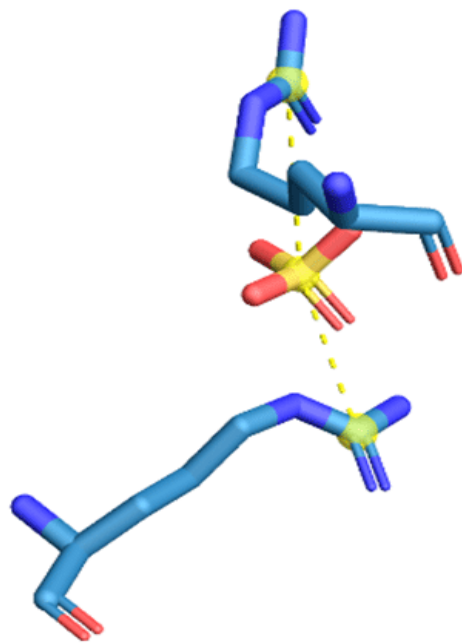


Figure. 50 Salt Bridges from the MalasmoruponaqTM binding site(s) in 4F1K (thrombospondin related anonymous protein), selected ligands: CL MalasmoruponaqTM small molecule EDO (Ethylene Glycol) EDO-A-305

Interacting chains: A

Index	Residue	AA	Distance	Protein positive	Ligand Group	Ligand Atoms
1	141B	ARG	4.69	✓	Sulfate	3141, 3141
2	181B	ARG	4.21	✓	Sulfate	3141, 3141

S04-B-303 ⭐ Interacting chains: B

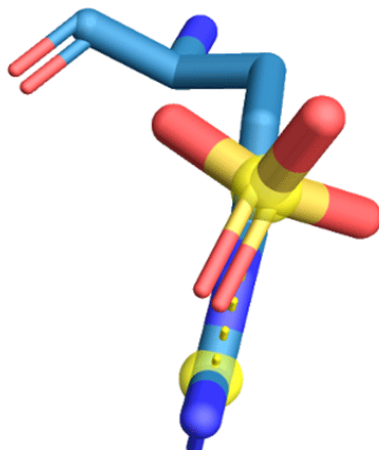


Figure. 51 Salt Bridges from the MalasmoruponaqTM™ binding site(s) in 4F1K (thrombospondin related anonymous protein), selected ligands: CL MalasmoruponaqTM™ small molecule EDO (Ethylene Glycol) EDO-A-305

Interacting chains: A

Index	Residue AA	Distance	Protein positive	Ligand Group	Ligand Atoms
1	61B ARG	4.08	✓	Sulfate	3146, 3146

SO4-B-304 ★

Interacting chains: B

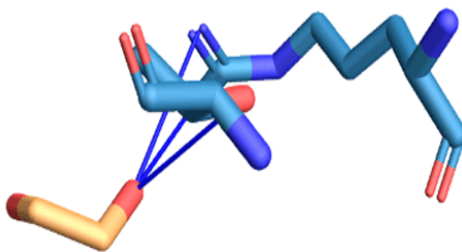


Figure. 52 Hydrogen Bonds from the MalasmoruponaqTM™ binding site(s) in 4YWI. EDO (Ethylene Glycol)EDO-A-302 Interacting chains: A

Inde	Resid AA	Distance H-A	Distance D-A	Donor Angle	Protein donor	Sidecha in	Donor Atom	Acceptor Atom
x								
1	134A ARG	2.84	3.26	106.42	✓	✓	1064 [Ng+]	3858 [O3]
2	134A ARG	3.14	3.53	105.15	✓	✓	1063 [Ng+]	3858 [O3]
3	139A TH R	3.19	3.95	137.02	✓	✓	1104 [O3]	3858 [O3]

EDO-A-303

Interacting chains: A

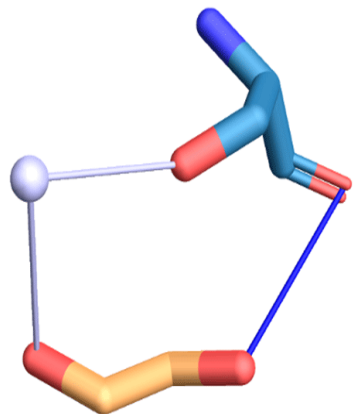


Figure. 53 Hydrogen Bonds from the MalasmoruponaqTM™ binding site(s) in 4YWI. EDO (Ethylene Glycol)EDO-A-302Interacting chains: A

Inde	Resid	AA	Distance H-A	Distance D-A	Donor Angle	Protein donor	Sidecha in Atom	Donor Atom	Acceptor Atom
x	ue					✗	✗	3860 [03]	165 [02] [03]

Water Bridges

Inde	Resid	AA	Dist.	Dist.	Donor	Water	Protein	Donor	Acceptor	Water
x	ue		A-W	D-W	Angle	Angle	donor	Atom	Atom	Atom

1 22A SE 3.71 3.14 119.07 106.84 ✓ 167 3862 3985
R [03] [03]

EDO-A-304

Interacting chains: A, B

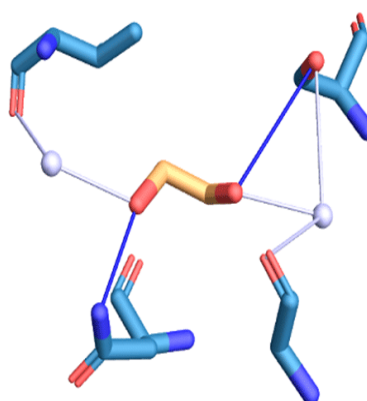


Figure. 54 Hydrogen Bonds from the MalasmoruponaqTM™ binding site(s) in 4YWI. EDO (Ethylene Glycol)EDO-A-302Interacting chains: A

Inde x	Resid ue	AA	Distance H-A	Distance D-A	Donor Angle	Protein donor	Sidecha in	Donor Atom	Acceptor Atom
1	45A	SER	3.74	4.05	102.10	✓	✓	348 [03]	3866 [03]
2	65A	ASN	2.43	3.04	119.71	✓	✓	520 [Nam]	3864 [03]

Water Bridges

Inde x	Resid ue	AA	Dist. A-W	Dist. D-W	Donor Angle	Water Angle	Protein donor	Donor Atom	Acceptor Atom	Water Atom
1	45A	SER	3.74	2.78	163.26	99.06	✗	3866 [03]	348 [03]	3984 [03]
2	76B	GLY	3.61	2.78	163.26	128.95	✗	3866 [03]	2515 [02]	3984 [02]
3	78A	VAL	3.62	2.78	168.62	78.24	✗	3864 [03]	611 [02]	3982 [03]

EDO-B-302

Interacting chains: B

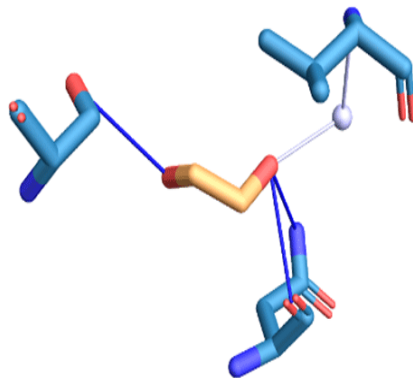


Figure. 55 Hydrogen Bonds from the MalasmoruponaqTM™ binding site(s) in 4YWI. EDO (Ethylene Glycol)EDO-A-302Interacting chains: A

Inde x	Resid ue	AA	Distance H-A	Distance D-A	Donor Angle	Protein donor	Sidecha in	Donor Atom	Acceptor Atom
1	45B	SER	3.62	3.93	101.45	✓	✓	2270 [03]	3873 [03]
2	45B	SER	3.07	3.93	148.97	✗	✓	3873 [03]	2270 [03]
3	65B	ASN	3.00	3.55	116.44	✓	✓	2437 [Nam]	3875 [03]
4	65B	ASN	2.94	3.34	106.17	✗	✗	3875 [03]	2433 [02]

Water Bridges

Inde	Resid	AA	Dist.	Dist.	Donor	Water	Protein	Donor	Acceptor	Water
x	ue		A-W	D-W	Angle	Angle	donor	Atom	Atom	Atom
1	78B	VAL	2.60	3.04	175.83	82.13	✓	2525 [Nam]	3875 [O3]	4138

EDO-B-303

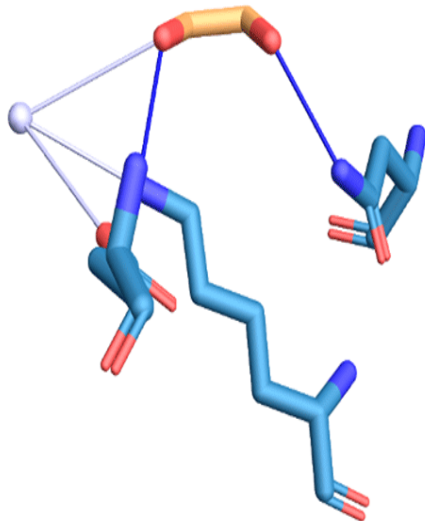


Figure. 56 Hydrogen Bonds from the MalasmoruponaqTM™ binding site(s) in 4YWI_EDO (Ethylene Glycol)EDO-A-302Interacting chains: A

Inde	Resid	AA	Distance	Distance	Donor	Protein	Sidech	Donor	Acceptor
x	ue		H-A	D-A	Angle	donor	ain	Atom	Atom
1	10B	AS	2.17	3.07	150.75	✓	✓	1994 [Nam]	3879 [O3]
2	12B	LYS	2.07	2.93	139.57	✓	✓	2017 [N3]	3877 [O3]

Water Bridges

Inde	Resid	AA	Dist.	Dist.	Donor	Water	Protein	Donor	Acceptor	Water
x	ue		A-W	D-W	Angle	Angle	donor	Atom	Atom	Atom
1	12B	LYS	3.25	3.96	155.61	127.67	✗	3877 [O3]	2017 [N3]	4265
2	97B	GL	4.10	3.96	155.61	109.07	✗	3877 [O3]	2678 [O3]	4265

EDO-B-304

Interacting chains: B

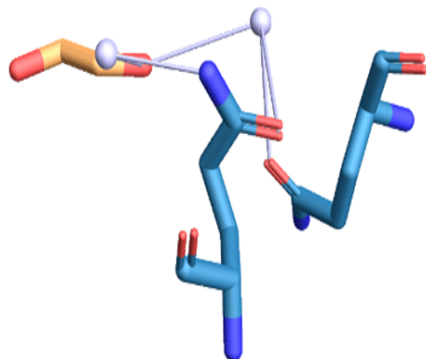


Figure. 57 Water Bridges MalasmoruponaqTM™ binding site(s) in 4YWI EDO (Ethylene Glycol) EDO-A-302 Interacting chains: A

Inde	Resid	AA	Dist.	Dist.	Donor	Water	Protein	Donor	Acceptor	Water
x	ue		A-W	D-W	Angle	Angle	donor	Atom	Atom	Atom
1	182	B GL	3.90	3.58	126.78	95.80	✗	3881 [O3]	3347 [O2]	4218
		N								
2	182	B GL	3.41	2.94	170.59	82.41	✓	3348 [Nam]	3881 [O3]	4236
		N								
3	223	B GL	3.27	3.58	126.78	106.13	✗	3881 [O3]	3658 [O2]	4218
		N								

EDO-B-305

Interacting chains: B

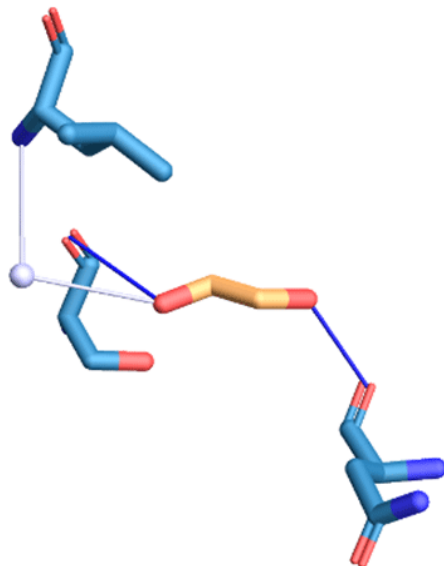


Figure. 58 Hydrogen Bonds from the MalasmoruponaqTM™ binding site(s) in 4YWI. EDO (Ethylene Glycol)EDO-A-302Interacting chains: A

Inde	Resid	AA	Distance H-A	Distance D-A	Donor Angle	Protein donor	Sidech ain	Donor Atom	Acceptor Atom
1	14B	AS	2.26	2.66	103.51	✗	✗	3887 [03]	2027 [02]
2	19B	SER	2.49	3.40	157.38	✗	✗	3885 [03]	2063 [02]

Water Bridges

Inde	Resid	AA	Dist. A-W	Dist. D-W	Donor Angle	Water Angle	Protein donor	Donor Atom	Acceptor Water Atom	
1	23B	LE	3.58	3.84	106.04	93.55	✓	2087 [Nam]	3885 [03]	4232

SO4 (sulfate) SO4-A-301 Interacting chains: A

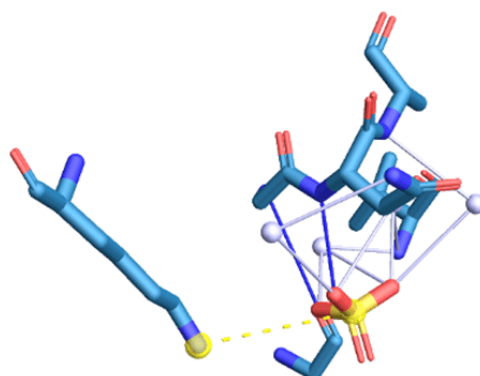


Figure. 59 Hydrogen Bonds from the MalasmoruponaqTM™ binding site(s) in 4YWI. MalasmoruponaqTM™ small molecule EDO (Ethylene Glycol)EDO-A-302Interacting chains: A

Inde	Resid	AA	Distance H-A	Distance D-A	Donor Angle	Protein donor	Sidech ain	Donor Atom	Acceptor Atom
1	232A	GLY	3.48	4.05	118.66	✓	✗	1796 [Nam]	3853 [03]
2	233A	AS	2.14	3.08	159.73	✓	✗	1800 [Nam]	3852 [02]

Water Bridges

Inde	Resid	AA	Dist. A-W	Dist. D-W	Donor Angle	Water Angle	Protein donor	Donor Atom	Acceptor Water Atom	
1	210A	GLY	3.06	2.78	124.99	73.62	✗	3853 [03]	1637 [02]	3981
2	212A	VA	3.59	2.98	162.35	101.49	✓	1644 [Nam]	3851 [02]	3981
3	212A	VA	2.66	3.99	125.98	103.29	✓	1644 [Nam]	3851 [02]	3921

4	212A VA L	4.00	3.99	125.98	81.84	✓	1644 [Nam]	3852 [O2]	3921
5	233A AS N	4.06	3.88	148.28	83.82	✓	1807 [Nam]	3852 [O2]	4075
6	234A AL A	3.67	3.67	105.79	108.78	✓	1808 [Nam]	3851 [O2]	4083

Salt Bridges

Index	Residue AA	Distance e	Protein positive	Ligand Group	Ligand Atoms
1	12A LYS	5.01	✓	Sulfate	3850, 3850

SO4-B-301 Interacting chains: B

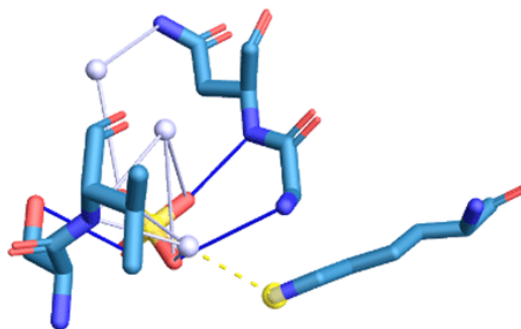


Figure. 60 Hydrogen Bonds from the MalasmoruponaqTM™ binding site(s) in 4YWI. MalasmoruponaqTM™ EDO (Ethylene Glycol)EDO-A-302 Interacting chains: A

Inde	Resid	AA	Distance H-A	Distance D-A	Donor Angle	Protein donor	Sidech ain	Donor Atom	Acceptor Atom
1	211B	SER	3.48	3.95	112.09	✗	✓	3871 [O3]	3574 [O3]
2	232B	GLY	3.32	3.93	121.57	✓	✗	3723 [Nam]	3868 [O2]
3	233B	AS	1.93	2.89	165.02	✓	✗	3727 [Nam]	3870 [O3]

Water Bridges

Inde	Resid	AA	Dist.	Dist.	Donor	Water	Protein	Donor	Acceptor	Water
x	ue		A-W	D-W	Angle	Angle	donor	Atom	Atom	Atom
1	212B	VA	3.52	3.09	152.21	108.59	✓	3575 [Nam]	3869 [O2]	4141
		L								
2	212B	VA	2.61	3.09	152.21	71.12	✓	3575 [Nam]	3868 [O2]	4141
		L								
3	212B	VA	4.05	3.99	131.42	116.54	✓	3575 [Nam]	3868 [O2]	4185
		L								
4	212B	VA	3.73	3.99	131.42	81.77	✓	3575 [Nam]	3870 [O3]	4185
		L								
5	233B	AS	3.77	3.91	157.19	80.67	✓	3734 [Nam]	3869 [O2]	4290
		N								

Salt Bridges

Index	Residue AA	Distance e	Protein positive	Ligand Group	Ligand Atoms
1	12B LYS	4.99	✓	Sulfate	3867, 3867

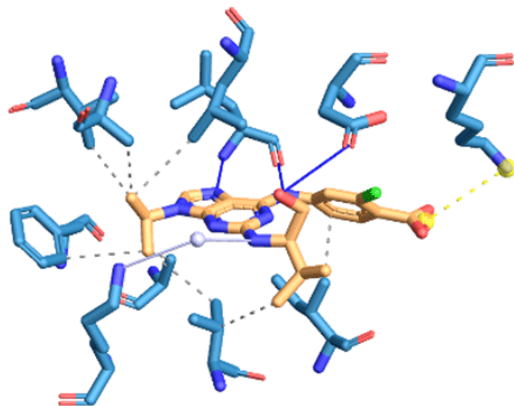


Figure. 61 MalasmoruponaqTM™ Hydrophobic Docking Interactions of the 2 MalasmoruponaqTM™ binding site(s) in 1V0P (cell division control protein 2 homolog). MalasmoruponaqTM™ small molecule PVB (purvalanol B)PVB-A-1287 Interacting chains: A

Index	Residue AA	Distance e	Ligand Atom	Protein Atom
1	10A	ILE 3.64	4324	85
2	18A	VAL 3.77	4340	139
3	18A	VAL 3.84	4336	138
4	30A	ALA 3.79	4340	239
5	63A	VAL 3.86	4341	506
6	79A	PHE 3.80	4340	642
7	132A	LEU 3.73	4341	1070
8	142A	ALA 3.42	4341	1150

Hydrogen Bonds from the

Inde	Resid	AA	Distance H-A	Distance D-A	Donor Angle	Protein donor	Sidech ain	Donor Atom	Acceptor Atom
1	82A	LEU	2.04	3.01	168.27	✓	✗	666 [Nam]	4320 [N2]
2	82A	LEU	1.80	2.76	161.73	✗	✗	4322 [NnII]	669 [O2]
3	85A	ASP	2.67	3.42	134.00	✗	✓	4339 [O3]	697 [O2]

Water Bridges

Inde	Resid	AA	Dist. A-W	Dist. D-W	Donor Angle	Water Angle	Protein donor	Donor Atom	Acceptor Atom	Water Atom
1	32A	LYS	3.76	3.70	149.40	83.69	✗	4333 [Npl]	256 [N3]	4470
2	32A	LYS	3.70	3.76	166.60	75.55	✓	256 [N3]	4333 [Npl]	4470

Salt Bridges

Index	Residue AA	Distance e	Protein positive	Ligand Group	Ligand Atoms
1	88A	LYS 4.20	✓	Carboxylate	4331, 4332

PVB-B-1287 Interacting chains: B

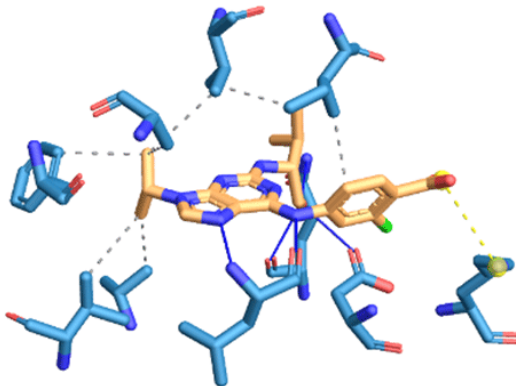


Figure. 62 MalasmoruponaqTM™ Hydrophobic Docking Interactions of the 2 MalasmoruponaqTM™ binding site(s) in 1V0P (cell division control protein 2 homolog). MalasmoruponaqTM™ SMALL MOLECULE PVB (purvalanol B) PVB-A-1287 Interacting chains: A

Index	Residue AA	Distance e	Ligand Atom	Protein Atom
1	10B	ILE 3.55	4354	2310
2	18B	VAL 3.82	4370	2364
3	18B	VAL 3.90	4366	2365
4	30B	ALA 3.96	4370	2464
5	63B	VAL 3.91	4371	2639
6	79B	PHE 3.67	4370	2746
7	142B	ALA 3.47	4371	3254

Hydrogen Bonds from the

Inde	Resid AA	Distance H-A	Distance D-A	Donor Angle	Protein donor	Sidech ain	Donor Atom	Acceptor Atom
1	82B	LEU 2.04	3.02	172.45	✓	✗	2770 [Nam]	4350 [N2]
2	82B	LEU 1.65	2.61	162.72	✗	✗	4352 [Npl]	2773 [O2]
3	85B	ASP 2.20	3.04	147.91	✓	✓	2801 [O3]	4369 [O3]
4	129B	GLN 2.56	3.17	120.07	✓	✓	3151 [Nam]	4369 [O3]
5	129B	GLN 2.16	2.85	127.08	✗	✗	4369 [O3]	3146 [O2]

Salt Bridges

Index	Residue AA	Distance e	Protein positive	Ligand Group	Ligand Atoms
1	88B	LYS 4.28	✓	Carboxylate	4362, 4361

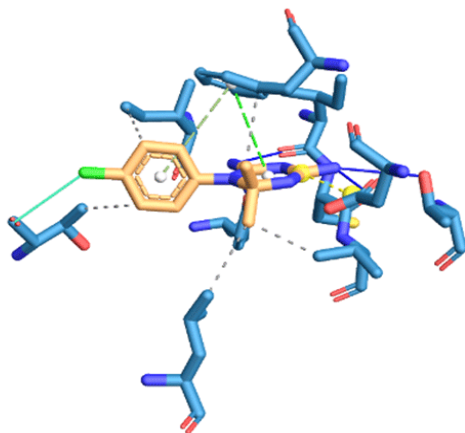


Figure. 63 MalasmoruponaqTM™ Hydrophobic Docking Interactions of the 6 MalasmoruponaqTM™ binding site(s) in 3UM6 (bifunctional dihydrofolate reductase-thymidylate synthase). small molecule 1CY (cycloguanil) 1CY-A-609 Interacting chains: A

Index	Residue AA	Distance e	Ligand Atom	Protein Atom
1	16A	VAL 3.60	9057	126
2	46A	LEU 3.79	9057	361
3	58A	PHE 3.59	9058	463

Index	Residue AA	Distance e	Ligand Atom	Protein Atom
4	108A	THR 3.77	9061	792
5	164A	ILE 3.62	9063	1266

Hydrogen Bonds from the

Inde	Resid	AA	Distance H-A	Distance D-A	Donor Angle	Protein donor	Sidech	Donor Atom	Acceptor Atom
1	14A	ILE	2.03	2.97	158.95	✗	✗	9056 [Npl]	110 [O2]
2	15A	CYS	1.99	2.98	179.32	✗	✗	9055 [Npl]	118 [O2]
3	170A	TYR	2.91	3.32	108.18	✓	✓	1306 [O3] [Npl]	9056
4	185A	TH R	3.12	3.66	117.13	✓	✓	1441 [O3] [Npl]	9055

π-Stacking

Index	Residue AA	Distance e	Angle	Offset	Type	Ligand Atoms
1	58A	PHE	4.97	74.30	1.93 T	9059, 9060, 9061, 9062, 9063, 9064
2	58A	PHE	4.30	29.55	1.25 P	9049, 9050, 9051, 9052, 9053, 9054

Halogen Bonds

Index	Residu	AA	Distance e	Donor Angle	Acceptor Angle	Donor Atom	Acceptor Atom
1	108A	THR	3.83	136.65	117.23	9065 [Cl]	789 [O2]

Salt Bridges

Index	Residue AA	Distance e	Protein positive	Ligand Group	Ligand Atoms	
1	54A	ASP	3.47	✗	Guanidine	9049, 9051, 9055

1CY-B-709 ★ Interacting chains: B

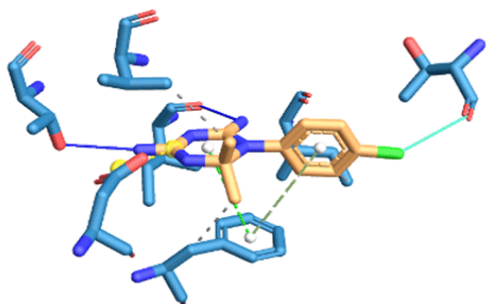


Figure. 64 MalasmoruponaqTM™ Hydrophobic Docking Interactions in 3UM6 (bifunctional dihydrofolate reductase-thymidylate synthase)

Index	Residue AA	Distance e	Ligand Atom	Protein Atom
1	16B	VAL 3.49	9142	4641
2	58B	PHE 3.47	9143	4977
3	164B	ILE 3.70	9148	5774

Hydrogen Bonds from the

Inde	Resid AA	Distance H-A	Distance D-A	Donor Angle	Protein donor	Sidech chain	Donor Atom	Acceptor Atom
1	14B	ILE 1.88	2.85	167.78	✗	✗	9141 [Npl]	4625 [O2]
2	185B	TH R	2.67	3.21	115.52	✓	5949 [O3]	9140 [Npl]
3	185B	TH R	2.63	3.21	117.28	✗	9140 [Npl]	5949 [O3]

π-Stacking

Index	Residue AA	Distance e	Angle Offset	Type	Ligand Atoms
1	58B	PHE 4.70	16.00	1.56 P	9134, 9135, 9136, 9137, 9138, 9139
2	58B	PHE 5.18	83.11	1.94 T	9144, 9145, 9146, 9147, 9148, 9149

Halogen Bonds

Index	Residu AA	Distance e	Donor Angle	Acceptor Angle	Donor Atom	Acceptor Atom
1	108B	THR 3.23	144.12	126.76	9150 [Cl]	5297 [O2]

Salt Bridges

Index	Residue AA	Distance e	Protein positive	Ligand Group	Ligand Atoms
1	54B	ASP 3.49	✗	Guanidine	9134, 9140, 9136

NDP (NADP)NDP-A-610 🌟 Interacting chains: A

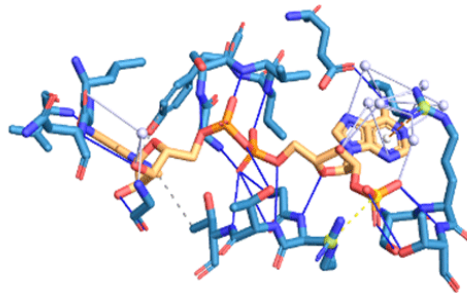


Figure. 65 MalasmoruponaqTM™ Hydrophobic Docking Interactions in 3UM6 (bifunctional dihydrofolate reductase-thymidylate synthase)

Index	Residue AA	Distance e	Ligand Atom	Protein Atom
1	108A	THR 3.92	9108	792
2	170A	TYR 3.96	9107	1304

Hydrogen Bonds from the

Index	Resid AA	Distance H-A	Distance D-A	Donor Angle	Protein donor	Sidech ain	Donor Atom	Acceptor Atom
1	16A	VAL 2.20	3.00	136.31	✓	✗	121 [Nam]	9105 [O2]
2	40A	LEU 2.08	3.05	168.06	✗	✗	9106 [Nam]	318 [O2]
3	42A	ASN 3.26	3.68	108.25	✓	✗	327 [Nam]	9097 [O3]
4	44A	GLY 2.62	3.45	143.43	✗	✗	9099 [O3]	347 [O2]
5	105A	GLY 3.60	4.01	107.60	✓	✗	764 [Nam]	9068 [O3]
6	105A	GLY 3.46	4.06	122.68	✗	✗	9068 [O3]	767 [O2]
7	106A	AR 2.01 G	2.93	154.39	✓	✗	768 [Nam]	9072 [O3]
8	107A	TH 2.75 R	3.65	152.83	✓	✗	779 [Nam]	9069 [O3]
9	107A	TH 2.99 R	3.41	107.67	✓	✓	784 [O3]	9088 [O3]
10	108A	TH 2.61 R	3.31	128.31	✓	✗	786 [Nam]	9068 [O3]
11	128A	SER 1.95	2.85	153.20	✗	✓	9113 [O3]	959 [O3]
12	129A	AR 2.05 G	2.96	153.12	✓	✗	960 [Nam]	9111 [O2]
13	130A	TH 3.61 R	3.90	100.35	✓	✓	976 [O3]	9112 [O3]
14	130A	TH 2.35 R	3.32	167.63	✓	✗	971 [Nam]	9111 [O2]
15	166A	GLY 2.27	3.05	135.22	✓	✗	1271 [Nam]	9068 [O3]
16	167A	SER 2.48	3.28	137.89	✓	✗	1275 [Nam]	9092 [O3]
17	168A	VAL 1.76	2.73	165.85	✓	✗	1281 [Nam]	9090 [O2]
18	169A	VAL 2.43	3.36	158.97	✓	✗	1288	9067

19	172A	GLU	1.86	2.80	157.39	✗	✓	9083 [Npl]	1323 [O3]
----	------	-----	------	------	--------	---	---	---------------	--------------

Water Bridges

Index	Residue AA	Dist. x ue	Dist. A-W	Dist. D-W	Donor Angle	Water Angle	Protein donor	Donor Atom	Acceptor Atom	Water Atom
1	41A	GLY	4.07	2.89	147.40	82.86	✗	9097	326 [O2]	9277 [O3]
2	44A	GLY	2.89	2.88	160.76	97.07	✓	344 [Nam]	9097 [O3]	9277
3	129A	AAR	2.62	2.54	141.49	77.08	✓	969 [Ng+]	9111 [O2]	9250
4	129A	AAR	3.95	2.62	156.70	79.23	✓	969 [Ng+]	9074 [O3]	9228
5	129A	AAR	3.48	3.97	115.01	97.32	✓	969 [Ng+]	9074 [O3]	9311
6	129A	AAR	4.10	3.38	124.63	104.49	✓	970 [Ng+]	9086 [N2]	9228
7	129A	AAR	3.73	2.88	131.52	112.55	✓	970 [Ng+]	9083 [Npl]	9296
8	129A	AAR	2.82	2.88	131.52	100.41	✓	970 [Ng+]	9084 [N2]	9296
9	129A	AAR	3.62	3.39	161.33	111.75	✓	970 [Ng+]	9083 [Npl]	9345
10	129A	AAR	3.35	3.39	161.33	90.70	✓	970 [Ng+]	9080 [N2]	9345
11	146A	VAL	3.26	2.87	165.38	89.57	✓	1109 [Nam]	9083 [Npl]	9404

π-Cation Docking Interactions

Index	Residue AA	Distance e	Offset charged	Protein	Ligand Group	Ligand Atoms
1	129A	ARG	3.61	1.25	✓	Aromatic 9081, 9082, 9084, 9085, 9086, 9087

Salt Bridges

Index	Residue AA	Distance e	Protein positive	Ligand Group	Ligand Atoms	
1	106A	ARG	4.17	✓	Phosphate 9110, 9110, 9076, 9111, 9112, 9113	

NDP-B-710 Interacting chains: B

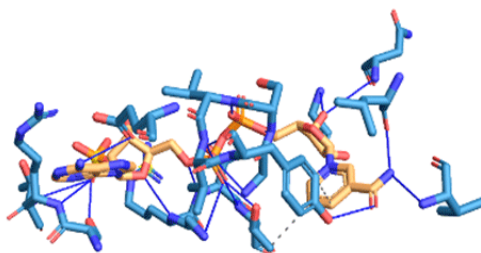


Figure. 66 MalasmoruponaqTM™ Hydrophobic Docking Interactions in 3UM6 (bifunctional dihydrofolate reductase-thymidylate synthase)

Index	Residue AA	Distance e	Ligand Atom	Protein Atom
1	108B	THR 3.91	9193	5300
2	170B	TYR 3.93	9192	5812

Hydrogen Bonds from the

Index	Resid AA	Distance H-A	Distance D-A	Angle	Protein donor	Sidech ain	Donor Atom	Acceptor Atom	
1	16B	VAL 2.95	3.80	145.52	✓	✗	4636 [Nam]	9191 [Nam]	
2	40B	LEU 2.49	3.47	179.05	✗	✗	9191 [Nam]	4833 [O2]	
3	42B	ASN 3.51	3.82	101.07	✓	✗	4842 [Nam]	9182 [O3]	
4	44B	GLY 3.18	3.57	105.69	✓	✗	4859 [Nam]	9182 [O3]	
5	44B	GLY 2.30	3.14	143.65	✗	✗	9184 [O3]	4862 [O2]	
6	105B	GLY 3.26	3.63	104.53	✓	✗	5272 [Nam]	9153 [O3]	
7	105B	GLY 2.99	3.62	123.83	✗	✗	9153 [O3]	5275 [O2]	
8	106B	AR G	2.32	3.25	158.45	✓	✗	5276 [Nam]	9157 [O3]
9	107B	TH R	3.21	3.55	102.41	✓	✓	5292 [O3]	9173 [O3]
10	107B	TH	2.87	3.75	148.49	✓	✗	5287	9154
11	108B	TH R	1.99	2.86	146.01	✓	✗	5294 [Nam]	9153 [O3]
12	108B	TH R	1.56	2.51	164.57	✓	✓	5299 [O3]	9153 [O3]
13	128B	SER	1.86	2.53	123.67	✗	✓	9198 [O3]	5467 [O3]

14	129B AR	2.52	3.40	148.65	✓	✗	5468	9198
		<i>G</i>					[Nam]	[03]
15	130B TH	2.64	3.58	159.31	✓	✗	5479	9198
		<i>R</i>					[Nam]	[03]
16	166B GLY	2.25	3.04	135.83	✓	✗	5779	9152
							[Nam]	[02]
17	167B SER	2.32	3.19	147.18	✓	✗	5783	9177
							[Nam]	[03]
18	168B VAL	1.79	2.72	156.18	✓	✗	5789	9175
							[Nam]	[02]
19	169B VAL	2.76	3.66	151.40	✓	✗	5796	9152
							[Nam]	[02]
20	170B TYR	2.21	3.02	145.02	✓	✓	5814	9190
							[03]	[02]
21	172B GLU	2.27	3.15	148.20	✗	✓	9168	5831
							[Npl]	[02]

Salt Bridges

Index	Residue AA	Distanc	Protein	Ligand	Ligand Atoms
		e	positive	Group	
1	106B ARG	4.40	✓	Phosphate	9195, 9195, 9161, 9196, 9197, 9198

UMP (22'-deoxyuridylic acid) UMP-A-611 Interacting chains: A, B

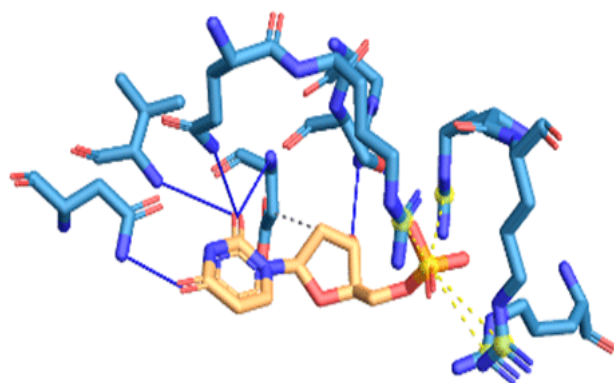


Figure. 67 MalasmoruponaqTM™ Hydrophobic Docking Interactions of the in 3UM6 (bifunctional dihydrofolate reductase-thymidylate synthase

Index	Residue AA	Distance e	Ligand Atom	Protein Atom
1	513A ASP	3.93	9123	3772

Hydrogen Bonds from the

Index	Residue AA	Distance H-A	Distance D-A	Donor Angle	Protein donor	Sidechain	Donor Atom	Acceptor Atom
1	509A GLN	3.14	3.66	114.21	✓	✓	3744 [Nam]	9120 [O2]
2	511A SER	1.68	2.57	150.47	✓	✓	3761 [O3]	9132 [O3]
3	511A SER	2.02	2.57	114.29	✗	✓	9132 [O3]	3761 [O3]
4	513A ASP	1.87	2.79	155.38	✓	✗	3768 [Nam]	9120 [O2]
5	518A VAL	3.58	3.93	103.51	✓	✗	3800 [Nam]	9120 [O2]
6	521A ASN	2.08	2.80	128.48	✓	✓	3832 [Nam]	9121 [O2]
7	551A HIS	1.90	2.83	159.92	✗	✓	9126 [O3]	4065 [N2]

Salt Bridges

Index	Residue AA	Distance e	Protein positive	Ligand Group	Ligand Atoms
1	345A ARG	4.13	✓	Phosphate	9130, 9130, 9129, 9131, 9132, 9133
2	470B ARG	4.27	✓	Phosphate	9130, 9130, 9129, 9131, 9132, 9133
3	471B ARG	4.69	✓	Phosphate	9130, 9130, 9129, 9131, 9132, 9133
4	510A ARG	4.26	✓	Phosphate	9130, 9130, 9129, 9131, 9132, 9133

UMP-B-711 Interacting chains: A, B

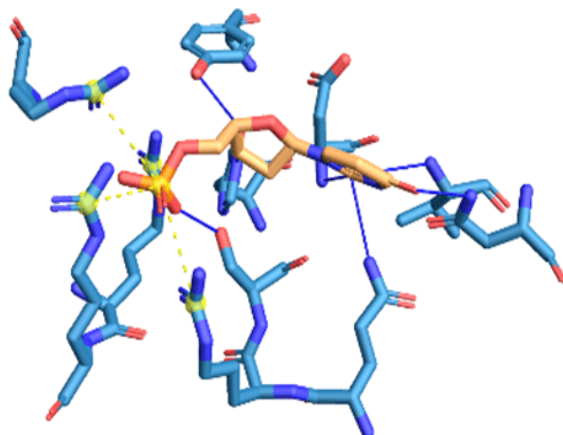


Figure. 68 MalasmoruponaqTM™ Hydrogen Bonds from the in 3UM6 (bifunctional dihydrofolate reductase-thymidylate synthase

Index	Residue AA	Distance H-A	Distance D-A	Donor Angle	Protein donor	Sidech chain	Donor Atom	Acceptor Atom
1	509B GLN	2.79	3.27	110.71	✓	✓	8252 [Nam]	9205 [O2]
2	511B SER	1.83	2.76	160.59	✓	✓	8269 [O3]	9217 [O3]
3	513B ASP	1.84	2.81	168.96	✓	✗	8276 [Nam]	9205 [O2]
4	518B VAL	3.54	4.00	111.10	✓	✗	8308 [Nam]	9205 [O2]
5	521B ASN	1.98	2.77	136.18	✓	✓	8340 [Nam]	9206 [O2]
6	551B HIS	1.86	2.81	169.17	✗	✓	9211 [O3]	8573 [N2]
7	553B TYR	2.09	2.94	149.59	✓	✓	8592 [O3]	9211 [O3]

Salt Bridges

Index	Residue AA	Distance	Protein positive	Ligand Group	Ligand Atoms
1	345B ARG	4.15	✓	Phosphate	9215, 9215, 9218, 9214, 9216, 9217
2	470A ARG	4.11	✓	Phosphate	9215, 9215, 9218, 9214, 9216, 9217
3	471A ARG	4.39	✓	Phosphate	9215, 9215, 9218, 9214, 9216, 9217
4	510B ARG	4.55	✓	Phosphate	9215, 9215, 9218, 9214, 9216, 9217

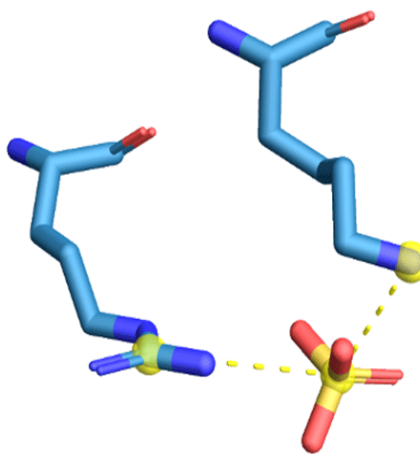


Fig.69 MalasmoruponaqTM™ 3 binding site(s) in 4IOD (malarial clp b2 atpase/hsp101 protein). SO4 (sulfate)
SO4-A-201 Interacting chains: A

Index	Residue	AA	Distance	Distance	Donor	Protein	Sidechain	Donor	Acceptor
			H-A	D-A	Angle	donor?		Atom	Atom
1	33A	ASN	2.09	3.01	154.54			1360 [Nam]	3522 [O3]

Index	Residue	AA	Distance	Distance	Donor	Protein	Sidechain	Donor	Acceptor
			H-A	D-A	Angle	donor?		Atom	Atom
2	34A	LYS	2.08	2.98	151.09			1368 [Nam]	3520 [O2]

Water Bridges

Index	Residue	AA	Dist.	Dist.	Donor	Water	Protein	Donor	Acceptor	Water
			A-W	D-W	Angle	Angle	donor?	Atom	Atom	Atom
1	32A	HIS	2.97	4.02	117.73	134.11		3521 [O3]	1356 [N2]	3788
2	36A	LYS	2.86	4.02	117.73	71.65		3521 [O3]	1393 [N3]	3788

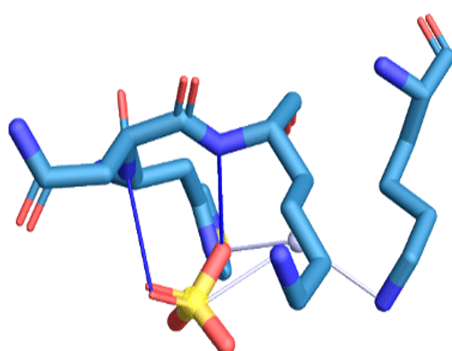
Salt Bridges

Index Residue AA Distance Protein positive? Ligand Group Ligand Atoms

1	32A	HIS	4.85		Sulfate	3518, 3518
---	-----	-----	------	--	---------	------------

SO4-B-201

Interacting chains: A, B



Hydrogen Bonds from the

Index	Residue	AA	Distance H-A	Distance D-A	Donor Angle	Protein donor?	Sidechain	Donor Atom	Acceptor Atom
1	75B	THR	2.75	3.50	134.63			528 [O3]	3515 [O2]

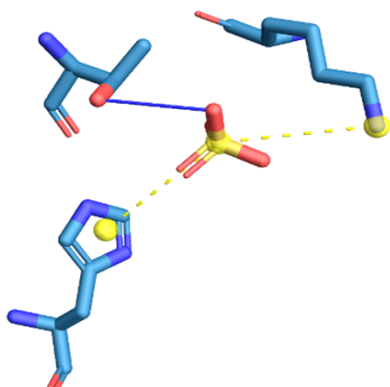
Salt Bridges

Index Residue AA Distance Protein positive? Ligand Group Ligand Atoms

1	32B	HIS	5.15		Sulfate	3513, 3513
2	108A	LYS	4.87		Sulfate	3513, 3513

SO4-C-201

Interacting chains: C



Salt Bridges

Index Residue AA Distance Protein positive? Ligand Group Ligand Atoms

1	147C	ARG	4.61		Sulfate	3523, 3523
2	151C	LYS	3.71		Sulfate	3523, 3523

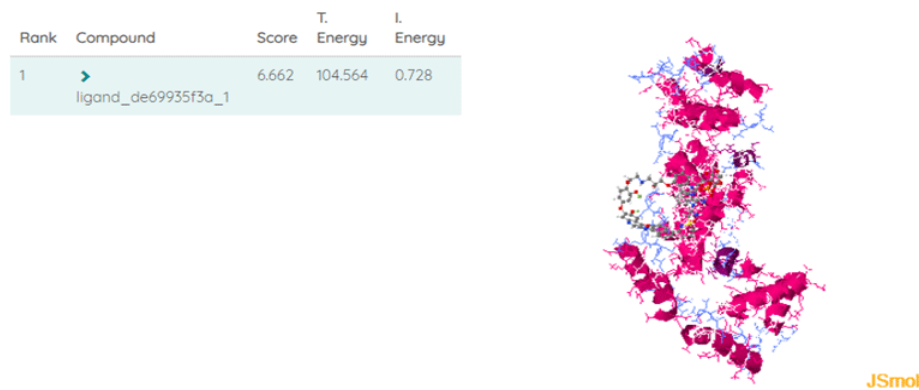


Fig. 70 MalasmoruponaqTM_5d25cb805d580 with (PDB:4F7F) Structure of *Anopheles gambiae* odorant binding protein 20 A novel mechanism of ligand binding and release in the odorant binding protein 20 from the malaria mosquito *Anopheles gambiae*.

MalasmoruponaqTM_File			Model	T.Energy	I.Energy	vdW	Coul	
NumRotors	RMSD	Score						
MalasmoruponaqTM_ligand_de69935f3a_1_run_1.log	0.728	24	0.000	6.662	1	104.564	0.728	-0.000
MalasmoruponaqTM_ligand_de69935f3a_1_run_1.log	0.729	24	10.514	6.662	3	104.565	0.729	-0.000
MalasmoruponaqTM_ligand_de69935f3a_1_run_1.log	0.729	24	9.833	6.662	4	104.566	0.729	-0.000

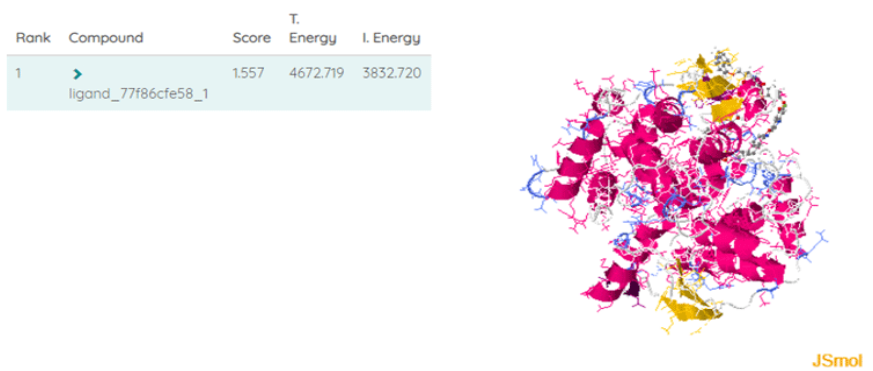
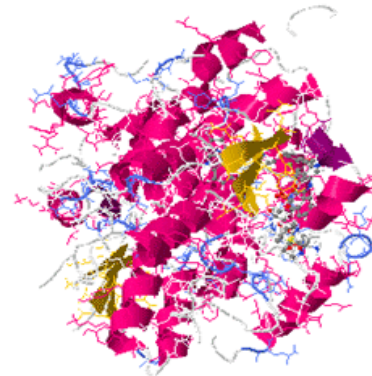


Figure. 71 3D Docking Docking Interactions of the MalasmoruponaqTM_5d25c9604090b_ with the 3zml_(PDB:3ZML)

MalasmoruponaqTM_	Model	T.Energy	I.Energy	vdW	Coul
NumRotors	RMSD	Score			
MalasmoruponaqTM_ligand_77f86cf58_1_run_17.log -46.595	26	0.000	1.557	1	4672.719
MalasmoruponaqTM_ligand_77f86cf58_1_run_17.log -24.685	26	2.330	2.526	3	4774.539
MalasmoruponaqTM_ligand_77f86cf58_1_run_17.log 5.789	21	4.871	1.550	8	5404.847
					4456.715
					4450.926

Rank	Compound	Score	T. Energy	I. Energy
1	▶ ligand_e9489e0982_1	-8.03	64.567	-17.901
2	▶ ligand_10a4743c6e_1	-7.516	56.237	-17.712
3	▶ ligand_a245d49ad0_1	-7.458	9.843	-22.256
4	▶ ligand_940ff43933_1	-7.257	61.300	-14.423
5	▶ ligand_182f64d74a_1	-7.068	72.286	-8.338
6	▶ ligand_1348dc9dcb_1	21.059	20325.073	19702.515



JSmol

Figure. 72a 3D Comparative Docking studies of the Docking Docking Interactions between the MalasmoruponaqTM AND Quinine, Quinidine, Proguanil, Atovaquone, Mefloquine, 3ZML with the 3zml_(PDB:3ZML)

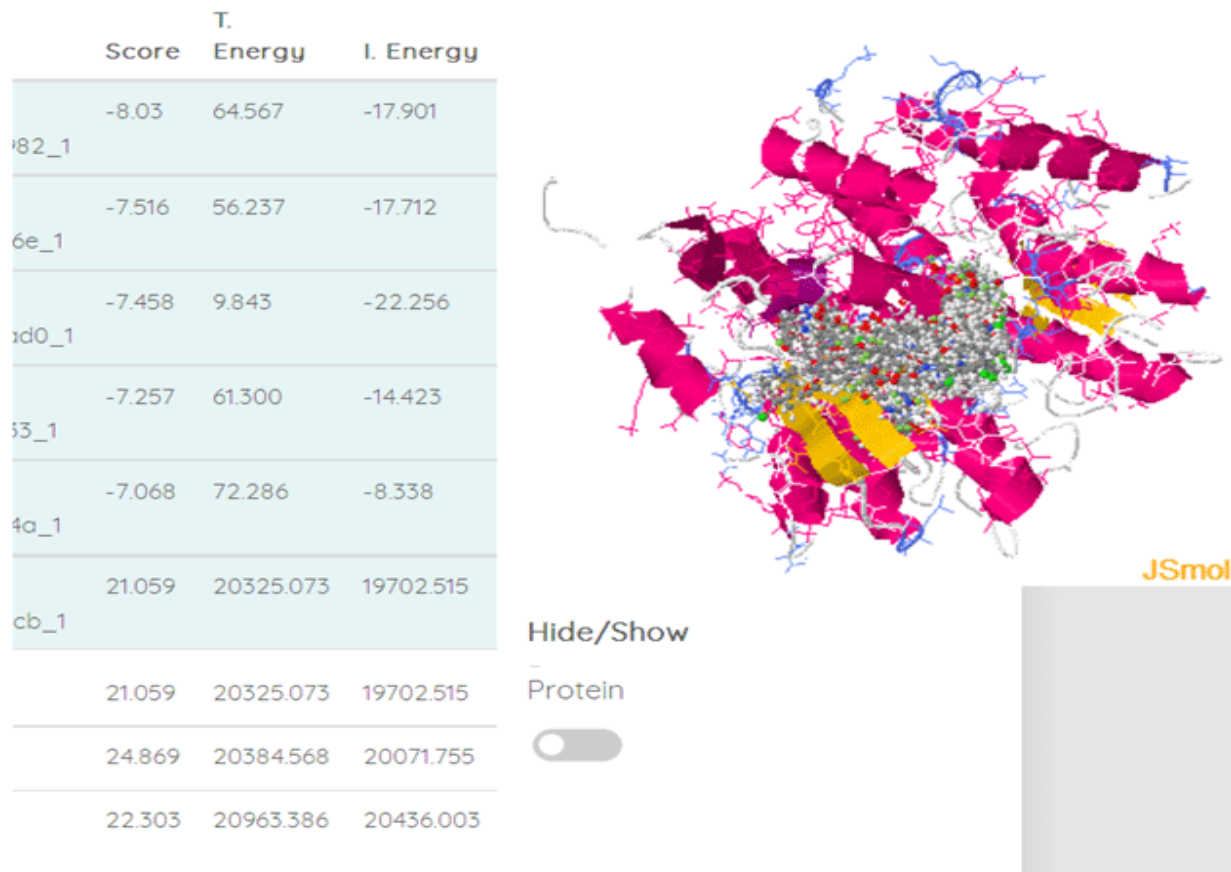


Figure. 72b 3D Comparative Docking studies of the Docking Docking Interactions between the MalasmoruponaqTM AND Quinine, Quinidine, Proguanil, Atovaquone, Mefloquine, 3ZML with the 3zml_(PDB:3ZML)



Figure. 73 MalasmoruponaqTM™_VS_FDAs_Spreadsheet1 Docking Energies.

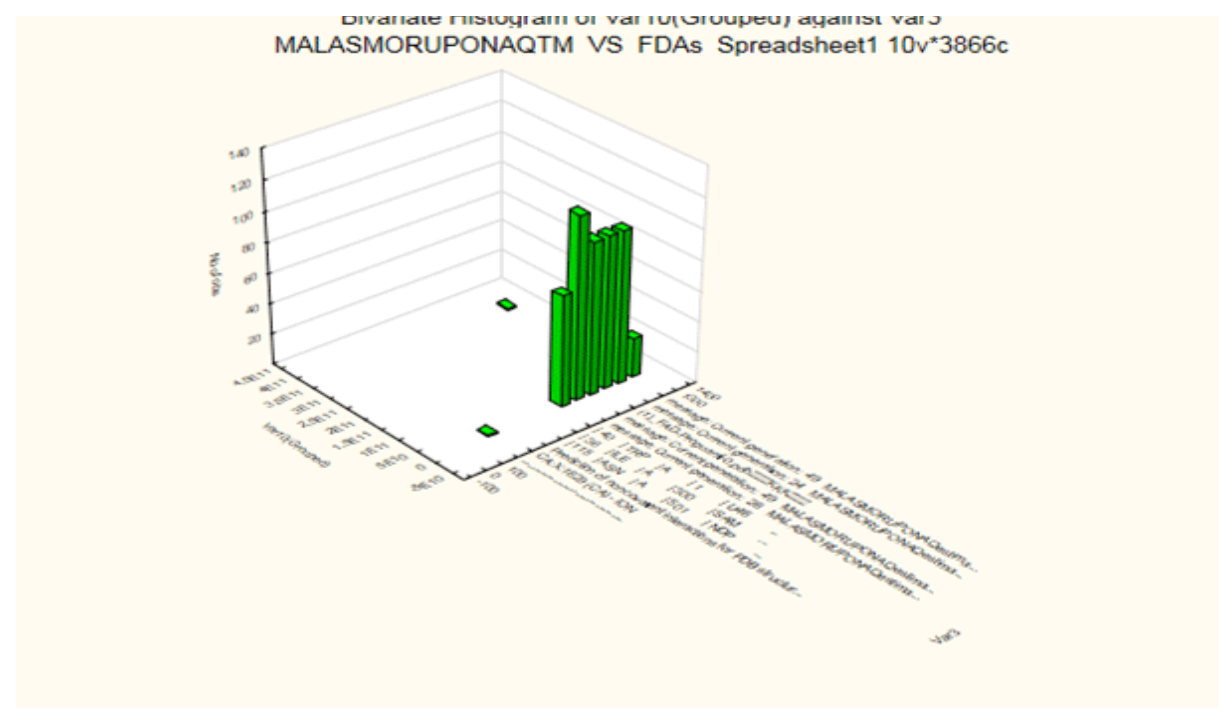


Figure. 74 MalasmoruponaqTM™_VS_FDAs_Spreadsheet1 10v*3866c

BiogenetoligandrolTMligandrolTM (Recoring Pharmacophoric Merging QM MMIDDD Algorithm)_Time_Predictions_4,3_Days_CellChangeTimes->{3.755534782528232^9}]]_
GridBoxAlignment->{ "Columns" -> {{Center}}, "ColumnsIndexed" -> {}, "Rows" -> {{Baseline}},
"RowsIndexed" -> {}}, GridBoxSpacings->{"Columns" -> { Offset[0.27999999999999997], {
Offset[0.7]}, Offset[0.27999999999999997]}, "ColumnsIndexed" -> {}, "Rows" -> { Offset[0.2], {
Offset[0.4]}, Offset[0.2]}, "RowsIndexed" -> {}}, "\[NoBreak]", ")"}]}], {
RowBox[{"\[ScriptCapitalB]", "\[LongEqual]", RowBox[{"(", "\[NoBreak]", GridBox[{
RowBox[{"cos", "(", "\[Psi]", ")"}], RowBox[{"sin", "(", "\[Psi]", ")"}], "0"}], {RowBox[{"-",
RowBox[{"sin", "(", "\[Psi]", ")"}]}]}], RowBox[{"+", 4, 3, Days, CellChangeTimes->{3.755534782528232*^9}]}], GridBoxAlignment->{ "Columns" -> {{Center}},
"ColumnsIndexed" -> {}, "Rows" -> {{Baseline}}, "RowsIndexed" -> {}},
GridBoxSpacings->{"Columns" -> { Offset[0.27999999999999997], { Offset[0.7],
Offset[0.27999999999999997]}, "ColumnsIndexed" -> {}, "Rows" -> {
Offset[0.2], { Offset[0.4], Offset[0.2]}, "RowsIndexed" -> {}}, "\[NoBreak]",
")"}]}], { RowBox[{"\[ScriptCapitalB]", "\[LongEqual]", RowBox[{"(", "\[NoBreak", GridBox[{
RowBox[{"cos", "(", "\[Psi]", ")"}], RowBox[{"sin", "(", "\[Psi]", ")"}], "0"}, {RowBox[{"-",
RowBox[{"cos", "(", "\[Psi]", ")"}], "0", "0", "1"}]}], GridBoxAlignment->{ "Columns"
-> {{Center}}, "ColumnsIndexed" -> {}, "Rows" -> {{Baseline}}, "RowsIndexed" -> {}},
GridBoxSpacings->{"Columns" -> { Offset[0.27999999999999997], { Offset[0.7],
Offset[0.27999999999999997]}, "ColumnsIndexed" -> {}, "Rows" -> {
Offset[0.2], { Offset[0.4], Offset[0.2]}, "RowsIndexed" -> {}}, "\[NoBreak]",
")"}]}]}, DefaultBaseStyle->"Column", GridBoxAlignment->{"Columns" -> {{Left}}},
GridBoxItemSize->{ "Columns" -> {{Automatic}}, "Rows" -> {{Automatic}}}, "Column"],
TraditionalForm]], "Output", CellChangeTimes->{3.755534782528232*^9}].

Conclusion

In this study we generated Docking Algorithms for the:

- Experimental quantum simulation of fermion-antifermion scattering via boson exchange in a trapped ion Docking Algorithms.
- Machine Learning and Computer Vision System for Phenotype Data Acquisition and Analysis Direct quantum process tomography via measuring sequential weak values of incompatible observables Docking Algorithms.
- Performance of Source Localization Docking Algorithms on the Extraction of gravitational waves in numerical relativity. Docking Algorithms in Feature Selection and Predictors of Falls with Foot Force Sensors Using KNN-Based Docking Algorithms.
- Numerical observation of emergent spacetime supersymmetry at

quantum criticality simple quantum voting scheme with multi-qubit entanglement Docking Algorithms.

•Multiscale Quantum Harmonic Oscillator Docking Algorithm for Multimodal Optimizationon Small Molecules as Rotating stars in relativity Improved Quantum Artificial Fish Docking Algorithm.

•Application to Distributed Network Considering Distributed Generation Artificial fish complete update and obtain the optimal value mainly through the following four behaviors: being random, preying, swarming, and following in the process of iterative calculation on Small Molecules as Rotating stars in relativity Improved Quantum Artificial Fish Docking Algorithm.

•Distributed Network Considering Distributed Generation Docking Algorithms on Mapping nonlinear gravity into General Relativity with nonlinear electrodynamics.

- Quantum Walks based Quantum Hash Function Docking Algorithms of a general model for metabolic scaling in self-similar asymmetric networks.
- Real-Coded Quantum Evolutionary Docking Algorithm Based on Hybrid Updating Strategy Docking Algorithms of an Analytical Framework for Studying Small-Number Effects in Catalytic Reaction Networks: A Probability Generating Function Approach to Chemical Master Equations.
- Estimation of Fractional-Order Chaotic Systems by Using Quantum Parallel Particle Swarm Optimization Docking Algorithm.
- The Spatial Chemical Langevin Equation and Reaction Diffusion Master Equations: moments and qualitative solutionschemical master equation: direct and closed-form solutions Novel Quantum-Behaved Docking Algorithms with Mean Best Position Directed for Numerical Optimization.
- Chemical Master Equation Closure for Computer-Aided Synthetic Biology: The Spatial Chemical Langevin Equation and Reaction Diffusion Master Equations: moments and qualitative solutions.
- Quantifying Magnetic Sensitivity Radical Pair Based Compass Quantum Fisher Information Docking Algorithms in Feature Selection and Predictors of Falls with Foot Force Sensors Using KNN parallel adaptive genetic Docking Algorithms for the controllability of arbitrary networks.
- Machine learning for electronic structure calculations Docking Algorithms in Feature Selection and Predictors of Falls with Foot Force Sensors Using KNN parallel adaptive genetic Docking Algorithms.
- Controllability of arbitrary networks Based Subect Docking Algorithms Docking Algorithms on the Performance of Source Localization Docking Algorithms.
- Discrete-Time Quantum Walk with Phase Disorder: Localization and Entanglement Entropy The Brainwave Nucleons Novel Quantum-Behaved Docking Algorithms with Mean Best Position Directed for Numerical Optimization Novel Quantum-Behaved Docking Algorithms.
- Mean Best Position Directed for Numerical Optimization Docking Algorithms.
- Experimental time-reversed adaptive Bell measurement towards all-photonic quantum repeaters Fast Gap-Free Quantum Docking Algorithm Enumerations.
- multivariate polynomial interpolation of Conformations and Sequences for Small Molecule Design Supercritical entanglement in local systems: Counter example to the area law for quantum matter Docking Algorithms.
- Complete 3-Qubit Grover search on a programmable quantum computer Docking Algorithms.
- Complete 3-Qubit Grover search on a programmable quantum computer Docking Algorithms for Supercritical entanglement in local systems: Counterexample to the area law for quantum matter Docking Algorithm.
- Time-of-Flight Three Dimensional Neutron Diffraction in Transmission Mode Implementation of controlled quantum teleportation with an arbitrator for secure quantum channels via quantum dots inside optical cavities.
- Adapting machine general-purpose earning techniques using inverse probability of censoring weighting and for the implementation of controlled quantum teleportation with an arbitrator for secure quantum channels via quantum dots inside optical cavities.
- Adapting machine general-purpose earning techniques using inverse probability of censoring weighting Docking Algorithm.
- Algebraic topology for biomolecules in machine learning based scoring and virtual screening.
- Quantum probability in decision making from quantum information neuronal «MalasmorupopnaqTMstates» Docking Algorithms.
- Machine learning: k-nearest neighbors on an Adaptive Weighted KNN Positioning Method Based on Omnidirectional Fingerprint Database and Twice Affinity Propagation Clustering.
- Absolute Binding Free Energy Calculations: On the Accuracy of Computational Scoring of Protein-MalasmoruponaqTM-ligand Docking Interactions.
- Proposed Indoor Localization Method Docking Algorithms to machine learning: k-nearest neighbors on an Adaptive Weighted KNN Positioning Method Based on Omnidirectional Fingerprint Database and Twice Affinity Propagation Clustering.
- Absolute Binding Free Energy Calculations: On the Accuracy of Computational Scoring of Protein-MalasmoruponaqTM-ligand Docking Interactions Constructing exact representations of quantum many-body

systems with deep neural networks Docking Algorithms_on Force-momentum-based self-guided Langevin dynamics: A rapid sampling method that approaches the canonical ensemble: neuronal version of Grover's quantum Docking Algorithm.

•-Quantum machine learning for electronic structure calculations neuronal version of Grover's quantum Docking Algorithm.

•-Electronic Nose Quantum_Noosphere_Improved Quantum Artificial Fish Docking Algorithm Application to Distributed Network quantum Quantum_Noosphere_Improved Quantum Artificial Fish Docking Algorithm Application to Distributed Network quantum classifiers.

•-Progressive sampling-based Bayesian optimization for efficient and automatic advanced machine learning Docking Algorithms Improvement of Performance, Stability and Continuity Molecular Dynamics Simulations by Modified Size-Consistent Multipartitioning Quantum Mechanical/Molecular Mechanical Modeling Method.

•-Generation of potential small multi-targeted molecules.

•-Investigation for their druggable small molecule likeness.

•-Ranking them according to their binding affinities within protein and DNA/RNA targetings.

•-Optimization of the generated hyper-molecules to energetically improve their multi-targeted binding characteristics.

•While we considered an Electronic Nose Quantum Noosphere Improved Quantum Artificial Fish Docking Algorithm Application to Distributed classifiers with a bounded working region, it is unclear what is the highest success probability that can be achieved by a general k-query Quantum machine learning for electronic structure calculations neuronal version of Grover's quantum Docking Algorithm without this restriction (and in particular, whether fewer than k queries could suffice to solve the Constructing exact representations of quantum many-body systems with deep neural networks Docking Algorithms on Force-momentum-based self-guided Langevin dynamics with high probability). Indeed, even for the Accuracy of Computational Scoring of Protein-MalasmoruponaqTM ligand Docking Interactions algorithm we proposed in, it remains open to understand what choice of the region S leads to the highest success probability in decision making from quantum information neuronal «MalasmoruponaqTM superposition states» Docking Algorithms. As mentioned, it would be useful to establish lower bounds on the query complexity of polynomial interpolation over infinite algebraic topology for biomolecules in machine learning based scoring and virtual screening

fields. Also, as stated in [20], for the univariate case over finite fields, the algorithm is time efficient since the function $Z^{-1}(z)$, i.e. finding a pre-image of elements in the range of Z, is efficiently computable using inverse probability of censoring weighting and for the Implementation of controlled quantum teleportation with an arbitrator for secure quantum channels via quantum dots inside optical cavities. However, for multivariate cases, it remains open whether there is an analogous efficiency analysis in Transmission Mode Implementation of controlled quantum teleportation with an arbitrator for secure quantum channels via quantum dots inside optical cavities. Here, we have discovered for the first time an in silico predicted and computer-aided molecular designed Inverse Molecular Design Docking Algorithm in a Model Binding Site as an In silico predicted and computer-aided molecular designed structure of peptide mimetic active pharmaco-agent (MalasmoruponaqTM™) against the gram positive bacteria *Staphylococcus aureus* for the depletion of its antibacterial defensin DEF-AAA for the deactivation of antimicrobial activity of the insect defensin from *Anopheles gambiae*. Furthermore, MalasmopuronaqTM small molecule could be used synergistically with dihydroartemisinin (DHA) antimalarial drug on its own or in combination with other artemisinins when used in areas for seasonal Intermittent Preventive Treatment (IPT) to reduce substantially the incidence, transmissios and prevent malaria in children. These findings not only are important for malarial PfNDH2 protein-based potential allosteric mechanism drug development but could also have broad implications for other NDH2-containing pathogenic microorganisms functions in Mtb to facilitate the anti-TB drug discovery approaches against the two homologous Ndh-2 enzymes in *Mycobacterium tuberculosis*. From the predicted host-pathogen PPIs, the MalasmoruponaqTM™ QMMIDDD small molecule from the present study targets into most of the host proteins within Malaria P. and Ebola EBOVpathogen structural proteins such as kinases, phosphatases, histone acetyltransferases, actin, histone deacetylases, tubulin, the viral proteins VP24-VP30-VP35-VP40, L (polymerase), bacterial and mammalian acetyl-CoA synthases, the ubiquitin ligase murine double minute 2, the glycoprotein (GP), the chaperonin heat shock protein 90, and histone by using an efficient and automatic advanced machine learning Docking Algorithms Improvements of Performance, Stability and Continuity Molecular Dynamics Simulations of a Modified Size-Consistent Multipartitioning Quantum Mechanical/Molecular Mechanical Modeling Method. The MalasmoruponaqTM™ QMMIDDD Small Molecule herbicide-like Derivatives is consisted of some of merged weighted harmonic electronegative groups with an electronegativity equilibration that allows the electronegativity of the prebonded hetero-atoms in the MalasmoruponaqTM™'s hyper-pharmacophoric fragments resulting to better binding properties than original molecule and more efficient antimalarial docking properties with better binding affinities as obtained. $7,\{[4,(2,\{[(2R),3,(42,2,3,4,4a,4b,5,6,7,8, decahydro,9\lambda^4,carbazol, 4,yloxy),2,hydroxypyropyl] amino}ethoxy],3, oxocyclohexyl]oxy\}$

19,[(42Z),1,[(2R),2,[(2S),2,amino,3[(3R),3,hydroxy,3,[(3R,4S,5R),4,hydroxy,5,[(42R),1,hydroxy,2,[(oxophospho),λ³,oxy]ethyl],2,oxooxolan,3,yl]propyl],1,3,diazinan,1,yl],2,(hydroxyamino)ethylidene],5,6-,dihydro,4H,1λ⁴,2,thiazin,3,yl],2λ³,oxa,10λ⁴,13λ⁴,diazapentacyclo[12.8.0.0^{3,12}.0⁴,9.0^{15,20}]docosa,1,9,10,12,13,pentaen,6,one dihydrofluoride is the best molecule which can be considered as drug molecule for in vivo analysis and validation involved in the infection process by targeting nuclear assembly proteins and thereby inhibiting the host cell to function properly for the development of anti-malarial agent for malarial treatment with better binding affinity and ADME properties. Here, We present the MalasmoruponaqTM™ QM MMID Small Molecule that targets into the structure of human KPNA5 C terminus in complex with eVP24 and PY-STAT1 binding domains within its non-classical nuclear localization signal (NLS) binding site on the KPNA5 that is necessary for the efficient PY-STAT1 nuclear transport. MalasmoruponaqTM™ QM MMID Small Molecule inhibits the eVP24, VP24, BDBV VP24 (bVP24), the RESTV VP24 (rVP24) and the three NPI-1 subfamily (KP-NAs KPNA1, KPNA5, KPNA6) to effectively compete with and inhibit the PY-STAT1 nuclear transport Docking Interactions on the VP24 stability.

MalasmoruponaqTM™ Targets the Unique NLS Binding Site on the three NPI-1 KPNAs. bVP2 and Karyopherin Alpha 5 to Selectively Compete the Nuclear Import of Phosphorylated STAT1 and eVP24 or rVP24 expression levels by exhibiting approximately some of 51,192261904761904 761904761904762 and 1,6937913016751191025049946211772 fold times to KPNA than either to Remdesivir Small Molecules T. and I. Energies respectively. In this paper it is shown that the MalasmoruponaqTM™ small molecule even in the form of its two fragmented compounds (MalasmoruponaqTM™_341139 and MalasmoruponaqTM™_937d73c677_1) binds within the (PDB: 4U2X) Ebola virus VP24 in complex with Karyopherin alpha 5 C-terminus and Ebola virus envelope protein MPER/TM domains (PDB:5T42) with some of -10.542 (score), 126.367(T.Energy), - 31.956(I.Energy) and -6.343 (score) -128.505 (T.Energy) and -27.128(I.Energy) respectively. Thus, the full potential of QM MMIDDD peptide-mimicking based anti-malarial drugs may be realized in the near future.

Acknowledgments

The authors would like to thank Grigoriadis George Pharmacist for scientific discussions.

Conflict of Interest

The authors declare that there is no conflict of interests regarding the publication of this paper.

References

- 1 Gelb MH (2007) Drug discovery formalaria: a very challenging and timely endeavor, Current Opinion in Chemical Biology 11(4): 440-445.
- 2.Wells TN (2013) “Discovering and developing new medicines for malaria control and elimination,” Infectious Disorders—Drug Targets 13(4): 292-302.
3. Le Roch KG, Chung DW, Ponts N (2012) Genomics and integrated systems biology in Plasmodium falciparum: a path to malaria control and eradication, Parasite Immunology 34(2-3): 50-60.
- 4 Snow RW, Guerra CA, Noor AM, Myint HY, Hay SI (2005) The global distribution of clinical episodes of Plasmodium falciparum malaria, Nature 434(7030): 214-217.
- 5 O'Meara WP, Mangeni JN, Steketee R, Greenwood B, (2010) Changes in the burden of malaria in sub-Saharan Africa, The Lancet Infectious Diseases 10(8): 545-555.
- 6 Foster S, Phillips M (1998) Economics and its contribution to the fight against malaria, Annals of Tropical Medicine and Parasitology 92(4): 391-398.
- 7 Barnes KI, Durrheim DN, Little F, et al. (2005) Effect of artemether-lumefantrine policy and improved vector control on malaria burden in KwaZulu-Natal, South Africa PLoS Medicine 2(11): 330.
- 8 Casadevall A, Pirofski LA (1999) Host-pathogen interactions: redefining the basic concepts of virulence and pathogenicity, Infection and Immunity 67(8): 3703-3713.
9. Casadevall A, Pirofski LA (2000) Host-pathogen interactions: basic concepts of microbial commensalism, colonization, infection, and disease, Infection and Immunity 68(12): 6511-6518.
- 10 Dyer MD, Murali TM, Sobral BW (2007) Computational prediction of host-pathogen protein-protein interactions, Bioinformatics 23(13): 159-166.
- 11 Mufunda J, Nyarango P, Usman A ,et al. (2007) Roll back malaria—an African success story in Eritrea, South African Medical Journal 97 (1): 46-50.
- 12 Franzosa EA, Garamszegi S, Xia Y (2012) Toward a three-dimensional view of protein networks between species, Frontiers in Microbiology 3: 428.
- 13 Zahiri J, Bozorgmehr JH, Masoudi-Nejad A (2013) Computa-

- tional prediction of protein-protein interaction networks: Docking Algorithms and resources, *Current Genomics* 14(6): 397-414.
- 14 Yosef N, Kupiec M, Ruppert E, Sharan R (2009) A complex-centric view of protein network evolution, *Nucleic Acids Research* 37(12): 88.
- 15 Uetz P, Glot L, Cagneyetal G (2000) A comprehensive analysis of protein-protein interactions in *Saccharomyces cerevisiae*, *Nature*, 403 (6770): 623-627.
- 16 Mendez-Rios J, Uetz P (2010) Global approaches to study protein-protein interactions among viruses and hosts," *Future Microbiology* 5(2) : 289-301.
17. Desai PV, Patny A, Gut J et al, (2006) Identification of novel parasitic cysteine protease inhibitors by use of virtual screening. 2. A available chemical directory, *Journal of Medicinal Chemistry* 49(5): 1576-1584.
- 18 Matthews LR, Vaglio P, Reboul J, et al. (2001) Identification of potential interaction networks using sequence-based searches for conserved protein-protein interactions or 'interologs', *Genome Research* 11(12): 2120-2126.
- 19 Qi Y, Tastan O, Carbonell JG, Klein-Seetharaman J, Weston J (2010) Semi-supervised multi-task learning for predicting interactions between HIV-1 and human proteins, *Bioinformatics* 26(18): 645-652.
- 20 Wuchty S (2011) Computational prediction of host-parasite protein interactions between *P. falciparum* and *H. sapiens*, *PLoS ONE* 6(11): e26960.
21. Krishnadev O, Srinivasan N (2008) A data integration approach to predict host-pathogen protein-protein interactions: application to recognize protein interactions between human and amalarial parasite, *In Silico Biology* 8(3-4): 235-250.
- 22 Lee SA, Chan CH, Tsai CH, Lai JM, Wang FS, et al. (2008) Ortholog-based protein-protein interaction prediction and its application to inter-species interactions, *BMC Bioinformatics* 9(12): S11.
- 23 Durmus Tekir S, Cakir T, Ardic E, Sayilarbas AS, et al. (2013) PHISTO:pathogen- host interaction search tool, *Bioinformatics* 29(10): 1357-1358.
- 24 Rapanoel HA, Mazandu GK, Mulder NJ (2013) Predicting and analyzing interactions between *Mycobacterium tuberculosis* and its human host, *PLoS ONE* 8(7): e67472.
- 25 Barale JC, Blisnick T, Fujioka H, et al. (1999) *Plasmodium falciparum* subtilisin-like protease 2, a merozoite candidate for the merozoite surface protein 1-42 maturase, *Proceedings of the National Academy of Sciences of the United States of America* 96(11) : 6445-6450.
- 26 Dow GS, Armson A, Boddy MR et al. (2002) Plasmodium: assessment of the antimalarial potential of triluralin and related compounds using a rat model of malaria, *Rattus norvegicus*, *Experimental Parasitology* 100(3): 155-160.
- 27 Fennell BJ, Naughton JA, Dempsey E, Bell A (2006) Cellular and molecular actions of dinitroaniline and phosphorothioamide herbicides on *Plasmodium falciparum*: tubulin as a specific antimalarial target, *Molecular and Biochemical Parasitology* 145(2): 226-238.
- 28 Mara C, Dempsey E, Bell A, Barlow JW (2011) Synthesis and evaluation of phosphoramidate and phosphorothioamidate analogues of amiprofosh methyl as potential antimalarial agents, *Bioorganic and Medicinal Chemistry Letters* 21(20): 6180-6183.
- 29 Garcia-Garcia J, Schleker S, Klein-Seetharaman J, Oliva B (2012) BIPS: BIANA Interolog Prediction Server. A tool for protein-protein interaction inference, *Nucleic Acids Research* 40: 147-151.
- 30 Huang da W, Sherman BT, Lempicki RA (2009) Bioinformatics enrichment tools: paths toward the comprehensive functional analysis of large gene lists, *Nucleic Acids Research* 37(1): 1-13.
- 31 Huang da W, Sherman BT, Lempicki RA (2009) Systematic and integrative analysis of large gene lists using DAVID bioinformatics resources, *Nature Protocols* 4(1): 44-57.
- 32 Mi H, Muruganujan A, Thomas PD (2013) PANTHER in 2013: modeling the evolution of gene function, and other gene attributes, in the context of phylogenetic trees, *Nucleic Acids Research* 41(1): 377-386.
- 33 Sastry GM, Adzhigirey M, Day T, Annabhimoju R, Sherman W (2013) Protein and MalasmoruponaqTM ligand preparation: parameters, protocols, and influence on virtual screening enrichments, *Journal of Computer-Aided Molecular Design* 27(3): 221-234.
- 34 Friesner RA, Banks JL, Murphy RB, Halgren TA, Klicic JJ, et al. (2004) Glide: a new approach for rapid, accurate docking and scoring. 1. Method and assessment of docking accuracy, *Journal of Medicinal Chemistry* 47(7): 1739-1749.
- 35 Friesner RA, Murphy RB, Repasky MP, Frye LL, Greenwood JR, et al. (2006) Extra precision glide: docking and scoring incorporating a model of hydrophobic enclosure for protein-MalasmoruponaqTM ligand complexes, *Journal of Medicinal Chemistry* 49(21): 6177-6196.

- 36 Gschwend DA, Good AC, Kuntz ID (1996) Molecular docking towards drug discovery, *Journal of Molecular Recognition* 9(2): 175-186.
- 37 Halgren TA, Murphy RB, Friesner RA, Beard HS, Frye LL, et al . (2004) Glide: a new approach for rapid, accurate docking and scoring. 2. Enrichment factors in database screening, *he Journal of Medicinal Chemistry* 47(7): 1750-1759.
- 38 Shelley JC, Cholleti A, Frye LL, Greenwood JR, Timlin MR, et al . (2007) Epik: a sotware program for pKprediction and protonation state generation for drug-like molecules, *Journal of Computer-Aided Molecular Design* 21(12): 681-691.
- 39 Chua HN, Sung WK, Wong L (2006) Exploiting indirect neighbours and topological weight to predict protein function from protein-protein interactions, *Bioinformatics* 22(13): 1623-1630.
- 40 Rawlings DJ, Fujioka H, Fried M, Keister DB, Aikawa M, et al. (1992) Alpha-Tubulin II is a male-speciic protein in *Plasmodium falciparum*, *Molecular and Biochemical Parasitology* 56(2): 239-250.
- 41 Gerald N , Mahajan B, Kumar S (2011) Mitosis in the human malaria parasite *Plasmodium falciparum*, *Eukaryotic Cell* 10(4): 474-482.
- 42 Kooij TWA, Janse CJ Waters AP (2006) Plasmodium post-genomics: better the bug you know *Nature Reviews Microbiology* 4(5): 344-357.
- 43 Mara C, Dempsey E, Bell A, Barlow JW (2013) Synthesis and evaluation of phenoxyoxazaphospholidine, phenoxyoxaza-phosphinane, and benzodioxaphosphininamine sulides and related compounds as potential anti-malarial agents, *Bioorganic and Medicinal Chemistry Letters* 23(12): 3580-3583.
44. E Lacey (1990) Mode of action of benzimidazoles, *Parasitology Today* 6 (4): 112-115.
- 45 MacDonald LM, Armonson A, Thompson AR, Reynoldson JA (2004) Characterisation of benzimidazole binding with recombinant tubulin from *Giardia duodenalis*, *Encephalitozoon inMalasmoruponaqTMinalis*, and *Cryptosporidium parvum*, *Molecular and Bio-chemical Parasitology* 138(1): 89-96.
46. Wallace AC, Laskowski RA, Thornton JM (1995) LIGPLOT:a program to generate schematic diagrams of protein-MalasmoruponaqTMligand interactions, *Protein Engineering* 8(2): 127-134.
- 44 Pugazhendhi D, Umamaheswari TS (2013) Insilico Methods in Drug Discovery - A Review, *International Journal of Advanced Research in Computer Science and Software Engineering* 3(5): 680-683.
- 45 Mandal S, Mandal SK (2009) Rational drug design. *European Journal of Pharmacology* 625(1-3): 90-100.
- 46 Jun Xu, Arnold Hagler (2002) Chemoinformatics and Drug Discovery, *Molecules* 7(8): 566-600.
- 47 Bharath EN, Manjula SN, Vijaychand A (2011) In silico drug design - tool for overcoming the innovation deficit in the drug discovery process 3(2): 6-10.
- 48 Dimasi JA, Hansen RW, Grabowski HG (2003) The price of innovation: new estimates of drug development costs 22:151-185.
- 49 Dror O, Shulman-Peleg A (2004) Predicting molecular interactions in silico: I. A guide to pharmacophore identification and its applications to drug design. *Current Medicinal* 11(1): 71-90.
- 50 Mishra P, Tripathi V, Yadav BS (2010) Insilco QSAR modeling and drug development process, 1(December) 37-40.
- 51 Mishra V, Kashyap S, Hasija Y (2015) Ligand based virtual screening for identifying potent inhibitors against viral neuraminidase: An in silico approach. *Journal of Taibah University for Science* 9(42): 20-26.
- 52 Nicolotti O, Benfenati E, Carotti A, Gadaleta D, Gissi A, et al. (2014) *Drug Discovery Today* 19(421): 1757-1768.
- 53 Potshangbam AM, Tanneer K, Reddy BM, Guruprasad L (2011) 3D-QSAR and molecular docking studies of 2-pyrimidinecarbonitrile derivatives as inhibitors against falcipain-3. *Bioorganic & Medicinal* 21(23): 7219-7223.
- 54 Sanschagrin P (2010) An Introduction to Molecular Docking What is Docking.
- 55 Chen YC (2015) Beware of docking! *Trends in Pharmacological Sciences* 36(2): 78-95.
- 56 Selzer D, Neumann D, Neumann H, Kostka KH, Lehr CM, et al. (2015) *European Journal of Pharmaceutics and Biopharmaceutics* 95: 68-76.
- 57 Tao L, Zhang P, Qin C, Chen SY, Zhang C (2015) Recent progresses in the exploration of machine learning methods as in-silico ADME prediction tools. *Advanced Drug Delivery Reviews* 86: 83-100.
- 58 Smith HJ, Hywel Williams "Chapter 8:Introduction to QSAR", *Introduction to the Principles of Drug Design*, 213-241.
- 59 Wolber G "Structure-Based 3D Pharmacophores: An Alternative to Docking Abstract & Outline."

- 60 Al-Balas QA, Amawi HA, Hassan MA, Qandil AM, Almaaytah AM, et al. (2013) Nizar M. Mhaidat4 Virtual Lead Identification of Farnesyltransferase Inhibitors Based on Ligand and Structure-Based Pharmacophore Techniques *Pharmaceuticals (Basel)* 6(6): 700-715.
- 61 Carr RA, Congreve M, Murray CW, Rees DC (2005) *Drug Discov. Today* 10(14): 987-992.
- 62 Tegar M, Purnomo H (2013) *Procedia Environmental Sciences* 17: 188-194.
- 63 Gupta CL, Akhtar S, Bajpai P (2014) In Silico Protein Modeling: possibilities and limitations 13: 513-515.
- 64 URL:<http://www.authorstream.com/templates/powerpoint-diagrams-drug-discovery-ppt-design-7332/>
- 65 URL:<http://www.intechopen.com/books/an-integrated-view-of-the-molecular-recognition-and-toxinology-from-analytical-procedures-to-biomedical-applications/computer-based-methods-of-inhibitor-prediction>
- 66 URL:<http://www.intechopen.com/books/an-integrated-view-of-the-molecular-recognition-and-toxinology-from-analytical-procedures-to-biomedical-applications/computer-based-methods-of-inhibitor-prediction>
- 67 Drews J (2000) Drug Discovery:a historical perspective, *Science* 287(5460): 1960-1964.
- 68 Ekins S, Ring BJ, Grace J, Mcrobie-Belle DJ, Wrighton SA (2000) Present and future in vitro approaches for drug metabolism. *J.Pharmacol. Toxicol. Methods* 44(1): 313-324.
- 69 Grigoriadis Ioannis, (2017) Evaluation of an Inverse Molecular Design Docking Algorithm in a Model Binding Site as An In silico predicted and computer-aided molecular designed HIV-1 protease CTLA-4 blockador for the increasement of the antigen-specific W191G mutant of cytochrome c peroxidase CD8+ T-cells to the inprevaccinated patients with melanoma using new cluster of Docking Algorithms for Large-Scale Protein-MalasmoruponaqTM™ligand Docking experiments Research Article – *Cancer Stud Ther J*
- 70 Grigoriadis Ioannis, (2017) Evaluation of an Inverse Molecular Design Docking Algorithm in a Model Binding Site in silico designed dosimetric autologous living vaccine consisting of with Multiple Wilms' Tumor 1 WT1- ConSynthetic-Restricted Peptide mimotopic Epitopes RMFPNAPYLP pulsed dendritic cells on a personalized Active Network analysis for asymptomatic or minimally symptomatic metastatic Pancreatic Cancer Research Article – *Cancer Stud Ther J*
- 71 Grigoriadis Ioannis, (2017) Quantum mechanically derived AMBER-compatible Algebraically in silico discovery of a multi-epitope mimic poly-pharmacophore to Multiple Peptides Derived from Cancer-Antigens as a promising anti-tumor pharmaco-agent for the maintance of a Specific T-cell Response in Long- term Vaccinated patients Advanced Biliary Tract Cancer using a parallel Cloud computing for protein-MalasmoruponaqTM™ligand binding site comparison for structural proteome-wide MalasmoruponaqTM™ligand-binding site comparisons Research Article – *Cancer Stud Ther J*
- 72 Grigoriadis Ioannis, (2017) Experimental simulation of Novel procedure quantum tunneling in small Computational Scaffolding systems on tumorigenic stem cell bacterial infected hybrids for the in silico rescaffolding and side-chain optimization on the neutrophil immune defense CAP37 protein Research Article– *Cancer Stud Ther J*.
- 73 Grigoriadis Ioannis (2017) Fast stochastic optimization of a quantum permutation Docking Algorithm with a single photon quuart Docking Algorithm on DC-tumor like high yield minimal magnetic signatures of electrotransfectioned ex vivo mediated hybrids for the generation of a computer-aided designed candidate drugable Toll-like receptor (Pam2IDG) peptide-domain agonistic agent Research Article – *Cancer Stud Ther J* human alcoholic brain". Experimental neurology 213:10-17.
74. White NJ, Pukrittayakameet S, Hien TT, Faiz M A, Mokuolu OA, et al. (2014) Malaria. *Lancet* 383(9918): 723-735.
75. Botte CY, Yamaryo-Botte Y, Rupasinghe TW, Mullin KA, MacRae JI, et al. (2013) Atypical lipid composition in the purified relict plastid (apicoplast) of malaria parasites. *Proc. Natl. Acad. Sci. USA* 110: 7506-7511. doi: 10.1073/pnas.1301251110.
76. Dechamps S, Shastri S, Wengelnik K, Vial HJ (2010) Glycerophospholipid acquisition in *Plasmodium* - a puzzling assembly of biosynthetic pathways. *Int. J. Parasitol* 40: 1347-1365. doi: 10.1016/j.ijpara.2010.05.008.
77. Vial H, et al. (2011) In Apicomplexan Parasites: Molecular Approaches toward Targeted Drug Development (ed Katja Becker) :137-162.
78. Vial HJ, Wein S, Farenc C, Kocken C, Nicolas O, et al. (2004) Prodrugs of bithiazolium salts are orally potent antimalarials. *Proc. Natl. Acad. Sci. USA* 101: 15458-15463.
79. Wein S, Taudon N, Maynadier M, Tran Van Ba C, Margout D, et al. (2017) High Accumulation and In Vivo Recycling of the New Antimalarial Albitiazolium Lead to Rapid Parasite Death. *Antimicrob Agents Chemother* 61: e00352-00317.

80. Wengelnik K, Vidal V, Ancelin ML, Cathiard AM, Morgat JL, et al. (2002) A class of potent antimalarials and their specific accumulation in infected erythrocytes. *Science* 295: 1311-1314.
81. Brancucci NMB, Gerd JP, Wang C, De Niz M, Philip N, et al. (2017) Lysophosphatidylcholine Regulates Sexual Stage Differentiation in the Human Malaria Parasite *Plasmodium falciparum*. *Cell* 171(1): 1532-1544.
82. Dechamps S, Wengelnik K, Berry-Sterkers L, Cerdan R, Vial HJ, et al. (2010) The Kennedy phospholipid biosynthesis pathways are refractory to genetic disruption in *Plasmodium berghei* and therefore appear essential in blood stages. *Mol. Biochem. Parasitol* 173: 69-80.
83. Sen P, Vial HJ, Radulescu O (2013) Kinetic modelling of phospholipid synthesis in *Plasmodium knowlesi* unravels crucial steps and relative importance of multiple pathways. *BMC systems biology* 7: 123.
84. Gonzalez-Bulnes P, Bobenck AM, Augagneur Y, Cerdan R, Vial HJ, et al. (2011) PG12, a phospholipid analog with potent antimalarial activity, inhibits *Plasmodium falciparum* CTP:phosphocholine cytidylyl transferase activity. *J. Biol. Chem* 286: 28940-28947.
85. Wein S, Maynadier M, Bordat Y, Perez J, Maheshwari S, Bette-Bobillo P, et al. (2012) Transport and pharmacodynamics of albitiazolium, an antimalarial drug candidate. *Br. J. Pharmacol* 166: 2263-2276.
86. Nagy GN, Marton L, Krámos B, Olah J, Revesz A, et al. (2013) Evolutionary and mechanistic insights into substrate and product accommodation of CTP:phosphocholine cytidylyl transferase from *Plasmodium falciparum*. *FEBS J* 280: 3132-3148.
87. Park YS, Sweitzer TD, Dixon JE, Kent C (1993) Expression, purification, and characterization of CTP:glycerol-3-phosphate cytidylyltransferase from *Bacillus subtilis*. *J. Biol. Chem* 268(22): 16648-16654.
88. Sundler R (1975) Ethanolaminephosphate cytidylyl transferase. Purification and characterization of the enzyme from rat liver. *J. Biol. Chem* 250: 8585-8590.
89. Veitch DP, Gilham D, Cornell RB (1998) The role of histidine residues in the HXGH site of CTP:phosphocholine cytidylyltransferase in CTP binding and catalysis. *Eur. J. Biochem* 255: 227-234.
90. Lee J, Johnson J, Ding Z, Paetzel M, Cornell RB (2009) Crystal structure of a mammalian CTP: phosphocholine cytidylyltransferase catalytic domain reveals novel active site residues within a highly conserved nucleotidylyltransferase fold. *J. Biol. Chem* 284: 33535-33548.
91. Cornell RB (2016) Membrane lipid compositional sensing by the inducible amphipathic helix of CCT. *Biochim. Biophys. Acta* 1861: 847-861.
92. Cornell RB, Ridgway ND (2015) CTP:phosphocholine cytidylyltransferase: Function, regulation, and structure of an amphitropic enzyme required for membrane biogenesis. *Prog. Lipid Res* 59: 147-171.
93. Contet A, Pihan E, Lavigne M, Wengelnik K, Maheshwari S, et al. (2015) *Plasmodium falciparum* CTP:phosphocholine cytidylyltransferase possesses two functional catalytic domains and is inhibited by a CDP-choline analog selected from a virtual screening. *FEBS Lett* 589: 992-1000.
94. Lee J, Taneva SG, Holland BW, Tielemans DP, Cornell RB (2014) Structural basis for autoinhibition of CTP:phosphocholine cytidylyltransferase (CCT), the regulatory enzyme in phosphatidylcholine synthesis, by its membrane-binding amphipathic helix. *J. Biol. Chem* 289(3): 1742-1755.
95. Ding Z, Taneva SG, Huang HKH, Campbell SA, Semenec L, et al. (2012) A 22-mer segment in the structurally pliable regulatory domain of metazoan CTP: phosphocholine cytidylyltransferase facilitates both silencing and activating functions. *J. Biol. Chem* 287: 38980-38991.
96. Huang HK, Taneva SG, Lee J, Silva LP, Schriemer DC, et al. (2013) The membrane-binding domain of an amphitropic enzyme suppresses catalysis by contact with an amphipathic helix flanking its active site. *J. Mol. Biol* 425: 1546-1564.
97. Ramezanpour M, Lee J, Taneva SG, Tielemans DP, Cornell RB (2018) An auto-inhibitory helix in CTP:phosphocholine cytidylyltransferase hijacks the catalytic residue and constrains a pliable, domain-bridging helix pair. *J. Biol. Chem* 293: 7070-7084.
98. Cornell RB, Kalmar GB, Kay RJ, Johnson MA, Sanghera JS, et al. (1995) Functions of the C-terminal domain of CTP: phosphocholine cytidylyltransferase. Effects of C-terminal deletions on enzyme activity, intracellular localization and phosphorylation potential. *Biochem. J* 310: 699-708.
99. Yang W, Boggs KP, Jackowski S (1995) The association of lipid activators with the amphipathic helical domain of CTP:phosphocholine cytidylyltransferase accelerates catalysis by increasing the affinity of the enzyme for CTP. *J. Biol. Chem* 270: 23951-23957.
100. Nagy GN, Marton L, Contet A, Ozohanics O, Ardelean LM, Revesz A, et al. (2014) Composite aromatic boxes for enzymatic transformations of quaternary ammonium substrates. *Angew. Chem. Int. Ed. Engl* 53: 13471-13476

101. Helmink BA, Braker JD, Kent C, Friesen JA (2003) Identification of lysine 122 and arginine 196 as important functional residues of rat CTP:phosphocholine cytidylyltransferase alpha. *Biochemistry* 42: 5043-5051.
102. D'Angelo I, Raffaelli N, DabustiV, Lorenzi T, Magni G, Rizzi M, et al. (2000) Structure of nicotinamide mononucleotide adenylyltransferase: a key enzyme in NAD(+) biosynthesis. *Structure* 8: 993-1004.
103. Maheshwari S, Lavigne M, Contet A, Alberge B, Pihan E, Kocken C, et al. (2013) Biochemical characterization of *Plasmodium falciparum* CTP:phosphoethanolamine cytidylyltransferase shows that only one of the two cytidylyl transferase domains is active. *Biochem. J* 450: 159-167.
104. Patridge KA, Weber CH, Friesen JA, Sanker S, Kent C, et al. (2003) Glycerol-3-phosphate cytidylyltransferase. Structural changes induced by binding of CDP-glycerol and the role of lysine residues in catalysis. *J. Biol. Chem* 278: 51863-51871.
105. Tian S, Ohtsuka J, Wang S, Nagata K, Tanokura M, et al. (2014) Human CTP:phosphoethanolamine cytidylyltransferase: enzymatic properties and unequal catalytic roles of CTP-binding motifs in two cytidylyl transferase domains. *Biochem. Biophys. Res. Commun* 449: 26-31.
106. Weber CH, Park YS, Sanker S, Kent C, Ludwig ML (1999) A prototypical cytidylyltransferase: CTP:glycerol-3-phosphate cytidylyltransferase from *bacillus subtilis*. *Structure* 7:1113-1124.
107. Park YS, Gee P, Sanker S, Schurter EJ, Zuiderweg ERP, et al. (1997) Identification of functional conserved residues of CTP:glycerol-3-phosphate cytidylyltransferase. Role of histidines in the conserved HXGH in catalysis. *J. Biol. Chem* 272: 15161-15166.
108. Peyrottes S, Caldarelli S, Wein S, Périgaud C, Alain Pellet, et al. (2012) Choline analogues in malaria chemotherapy. *Curr. Pharm. Des* 18(24): 3454-3466.
109. Marton L, Nagy GN, Ozohanics O, Lábas A, Krámos B, et al. (2015) Molecular Mechanism for the Thermo-Sensitive Phenotype of CHO-MT58 Cell Line Harbouring a Mutant CTP:Phosphocholine Cytidylyltransferase. *PLoS One* 10(6): e0129632.
110. Tellinghuisen J (2008) Isothermal titration calorimetry at very low c. *Anal. Biochem* 373: 395-397.
111. Turnbull WB, Daranas AH (2003) On the value of c: can low affinity systems be studied by isothermal titration calorimetry. *J. Am. Chem. Soc* 125: 14859-14866.
112. Piotto M, Saudek V, Sklenar V (1992) Gradient-tailored excitation for single-quantum NMR spectroscopy of aqueous solutions. *J. Biomol. NMR* 2: 661-665.
113. Pons JL, Malliavin TE, Delsuc MA (1996) Gifa V. 4: A complete package for NMR data set processing. *J. Biomol. NMR* 8: 445-452.
114. Walter TS, Diprose JM, Mayo CJ, Siebold C, Pickford MG, et al. (2005) A procedure for setting up high-throughput nanolitre crystallization experiments. Crystallization workflow for initial screening, automated storage, imaging and optimization. *Acta Crystallogr. D Biol. Crystallogr* 61: 651-657.
115. Kabsch W (1993) Automatic processing of rotation diffraction data from crystals of initially unknown symmetry and cell constants. *J. Appl. Crystallogr* 26: 795-800.
116. Kabsch W (2010) *Acta Crystallogr. D Biol. Crystallogr* 66: 125-132.
117. French S, Wilson K (1978) On the treatment of negative intensity observations. *Acta Crystallogr. Sect. A* 34: 517-525.
118. Evans P (2006) Scaling and assessment of data quality. *Acta Crystallogr. D Biol. Crystallogr* 62: 72-82.
119. Winn MD, Ballard CC, Cowtan KD, Dodson EJ, Emsley P, et al. (2011) Overview of the CCP4 suite and current developments. *Acta Crystallogr. D Biol. Crystallogr* 67: 235-242.
120. McCoy AJ, Grosse-Kunstleve RW, Adams PD, Winn MD, Storoni LC, et al. (2007) Phaser crystallographic software. *J. Appl. Crystallogr* 40: 658-674.
121. Emsley P, Cowtan K (2004) Coot: model-building tools for molecular graphics. *Acta Crystallogr. D Biol. Crystallogr* 60: 2126-2132.
122. Murshudov GN, Vagin AA, Dodson EJ (1997) Refinement of macromolecular structures by the maximum-likelihood method. *Acta Crystallogr. D Biol. Crystallogr* 53: 240-255.
123. Murshudov GN, Skubák P, Lebedev AA, Pannu NS, Steiner RA, et al. (2011) REFMAC5 for the refinement of macromolecular crystal structures. *Acta Crystallogr. D Biol. Crystallogr* 67: 355-367.
124. Adams PD, Afonine PV, Bunkóczki G, Chen VB, Davis IW, et al. (2010) PHENIX: a comprehensive Python-based system for macromolecular structure solution. *Acta Crystallogr. D Biol. Crystallogr* 66: 213-221.
125. DeLano WL (2002) The PyMOL Molecular Graphics System. <http://www.pymol.org>, DeLano Scientific, San Carlos, CA, USA.

126. Schüttelkopf AW, van Aalten DM (2004) PRODRG: a tool for high-throughput crystallography of protein-ligand S0907444904011679. complexes. *Acta Crystallogr Biol Crystallogr D60*: 1355-1363. doi: 10.1107/ Monte Carlo. *Phys Lett B* 195(2): 216-222.
127. Robert X, Gouet P (2014) Deciphering key features in protein structures with the new Endscript server. *Nucleic Acids Res* 42: W320-324. doi: 10.1093/nar/gku316.
128. Girolami M, Calderhead B (2011) Riemann manifold langevin and hamiltonian monte carlo methods. *J R Stat Soc: Series B (Stat Methodol)* 73(2): 123-214.
129. Wilkinson DJ (2006) Stochastic Modelling for Systems Biology Mathematical and Computational Biology, vol. 11. London, UK: Chapman & Hall/CRC.
130. Gelman A, Carlin JB, Stern HS, Rubin DB (2004) Bayesian Data Analysis, Texts in Statistical Science. London, UK: Chapman & Hall, CRC
131. Metropolis N, Rosenbluth AW, Rosenbluth MN, Teller AH, Teller E (1953) Equation of state calculations by fast computing machines. *J Chem Phys* 21(6): 1087-1092.
132. Kaderali L, Dazert E, Zeuge U, Frese M, Bartenschlager R (2009) Reconstructing signaling pathways from RNAi data using probabilistic Boolean threshold networks. *Bioinformatics* 25(17): 2229-2235.
133. Bois FY (2009) GNU MCSim: Bayesian statistical inference for SBML-coded systems biology models. *Bioinformatics* 25(11): 1453-1454.
134. Haario H, Laine M, Mira A, Saksman E (2006) Statistics and Computing. Switzerland: Springer. DRAM: Efficient adaptive MCMC.
135. Brooks S, Gelman A, Jones G L, Meng X-L (2011) Handbook of Markov Chain Monte Carlo. Handbooks of Modern Statistical Methods. London, UK: Chapman & Hall/CRC : 125.
136. Lawrence ND, Girolami M, Rattray M, Sanguinetti G (2010) Learning and Inference in Computational Systems Biology. Computational Molecular Biology. Cambridge, Massachusetts, London, England: The MIT Press.
137. Rannala B (2002) Identifiability of parameters in MCMC Bayesian inference of phylogeny. *Syst Biol* 51(5): 754-760.
138. Duane S, Kennedy AD, Pendleton BJ, Roweth D (1987) Hybrid 139. Radde N (2011) The role of feedback mechanisms in biological network models - a tutorial. *Asian J Control* 13(5): 597-610.
140. Calderhead B, Sustik M (2012) Sparse approximate manifolds for differential geometric mcmc. *Adv Neural Inf Process Syst* 26: 2888-2896.
141. Rao CR (1945) Information and accuracy attainable in the estimation of statistical parameters. *Bull Calc Math Soc* 37(3): 81-91
142. Calderhead B (2011) PhD thesis. University of Glasgow Differential geometric mcmc methods and applications.
143. Weckesser W (2008) Vfgen: A code generation tool. *JNAIAM* 3(1-2): 151-165.
144. Wolff U (2004) Monte Carlo errors with less errors. *Comput Phys Commun* 156(2): 143-153.
145. Schmidt H, Jirstrand M (2006) Systems biology toolbox for matlab: a computational platform for research in systems biology. *Bioinformatics* 22(4): 514-515.
146. Fritzsche-Guenther R, Witzel F, Sieber A, Herr R, Schmidt N, et al. (2011) Strong negative feedback from Erk to Raf confers robustness to mapk signalling. *Mol Syst Biol* 7(489): 1-13.
147. Brannmark C, Palmer R, Glad ST, Cedersund G, Stralfors P (2010) Mass and information feedbacks through receptor endocytosis govern insulin signaling as revealed using a parameter-free modeling framework. *J Biol C* 285(26): 20171-20179.
148. Anisimov VM, Cavasotto CN (2011) Quantum mechanical binding free energy calculation for phosphopeptide inhibitors of the Lck SH2 domain. *J. Comput. Chem* 32: 2254-2263.
149. Anisimov VM, Ziemys A, Kizhake S, Yuan Z, Natarajan A, et al. (2011) Computational and experimental studies of the interaction between phospho-peptides and the C-terminal domain of BRCA1. *J. Comput. Aided Mol. Des* 25(11): 1071-1084.
150. Aqvist J, Medina C, Samuelsson JE (1994) A new method for predicting binding affinity in computer-aided drug design. *Protein Eng* 7(3): 385-391.
151. Blomberg MR, Borowski T, Himo F, Liao RZ, Siegbahn PE (2014) Quantum chemical studies of mechanisms for metalloenzymes. *Chem. Rev* 114(7): 3601-3658.

152. Brandenburg JG, Grimme S (2014) Accurate modeling of organic molecular crystals by dispersion-corrected density functional tight binding (DFTB). *J. Phys. Chem. Lett* 5(11): 1785-1789.
153. Brooks BR, Brooks CL, Mackerell AD, Nilsson L, Petrella RJ, et al.(2009) CHARMM: the biomolecular simulation program. *J. Comput. Chem* 30(10): 1545-1614.
154. Cavasotto CN (2011) Handling protein flexibility in docking and high-throughput docking, in Virtual Screening. Principles, Challenges and Practical Guidelines, ed Sottriffer C (Weinheim: Wiley-VCH Verlag : 245-262.
155. Cavasotto C N (2012) Binding free energy calculations and scoring in small-molecule docking, in Physico-Chemical and Computational Approaches to Drug Discovery, eds Luque F. J., Barril X., editors. (London: Royal Society of Chemistry : 195-222.
156. Cavasotto CN (2012) Normal mode-based approaches in receptor ensemble docking. *Methods Mol. Biol* 819: 157-168.
157. Cavasotto CN, Orry A J (2007) Ligand docking and structure-based virtual screening in drug discovery. *Curr. Top. Med. Chem* 7(10): 1006-1014.
158. Cavasotto CN, Palomba D (2015) Expanding the horizons of G protein-coupled receptor structure-based ligand discovery and optimization using homology models. *Chem. Commun* 51 : 13576-13594.
159. Chaskar P, Zoete V, Rohrig UF (2014) Toward on-the-fly quantum mechanical/molecular mechanical (QM/MM) docking: development and benchmark of a scoring function. *J. Chem. Inf. Model* 54(11): 3137-3152.
160. Chaskar P, Zoete V, Rohrig UF (2017) On-the-fly QM/MM docking with attracting cavities. *J. Chem. Inf. Model* 57(1): 73-84.
161. Cho AE, Guallar V, Berne BJ, Friesner R (2005) Importance of accurate charges in molecular docking: quantum mechanical/molecular mechanical (QM/MM) approach. *J. Comp. Chem* 26(9): 915-931.
162. Cross J B, Thompson DC, Rai BK, Baber JC, Fan KY, Hu Y, et al. (2009) Comparison of several molecular docking programs: pose prediction and virtual screening accuracy. *J. Chem. Inf. Model* 49(6): 1455-1474.
163. De Benedetti PG, Fanelli F (2014) Multiscale quantum chemical approaches to QSAR modeling and drug design. *Drug Discov. Today* 19(12): 1921-1927.
164. Dewar MJS, Zoebisch EG, Healy EF, Stewart JP (1985) Development and use of quantum mechanical molecular models. 76. AM1: a new general purpose quantum mechanical molecular model. *J. Am. Chem. Soc* 107(3): 3902-3909.
165. Dixon SL, Merz KM J (1996) Semiempirical molecular orbital calculations with linear system size scaling. *J. Chem. Phys* 104: 6643-6649.
166. Ehrlich S, Goller AH, Grimme S (2017) Towards full quantum-mechanics-based protein-ligand binding affinities. *ChemPhysChem* 18(8): 898-905.